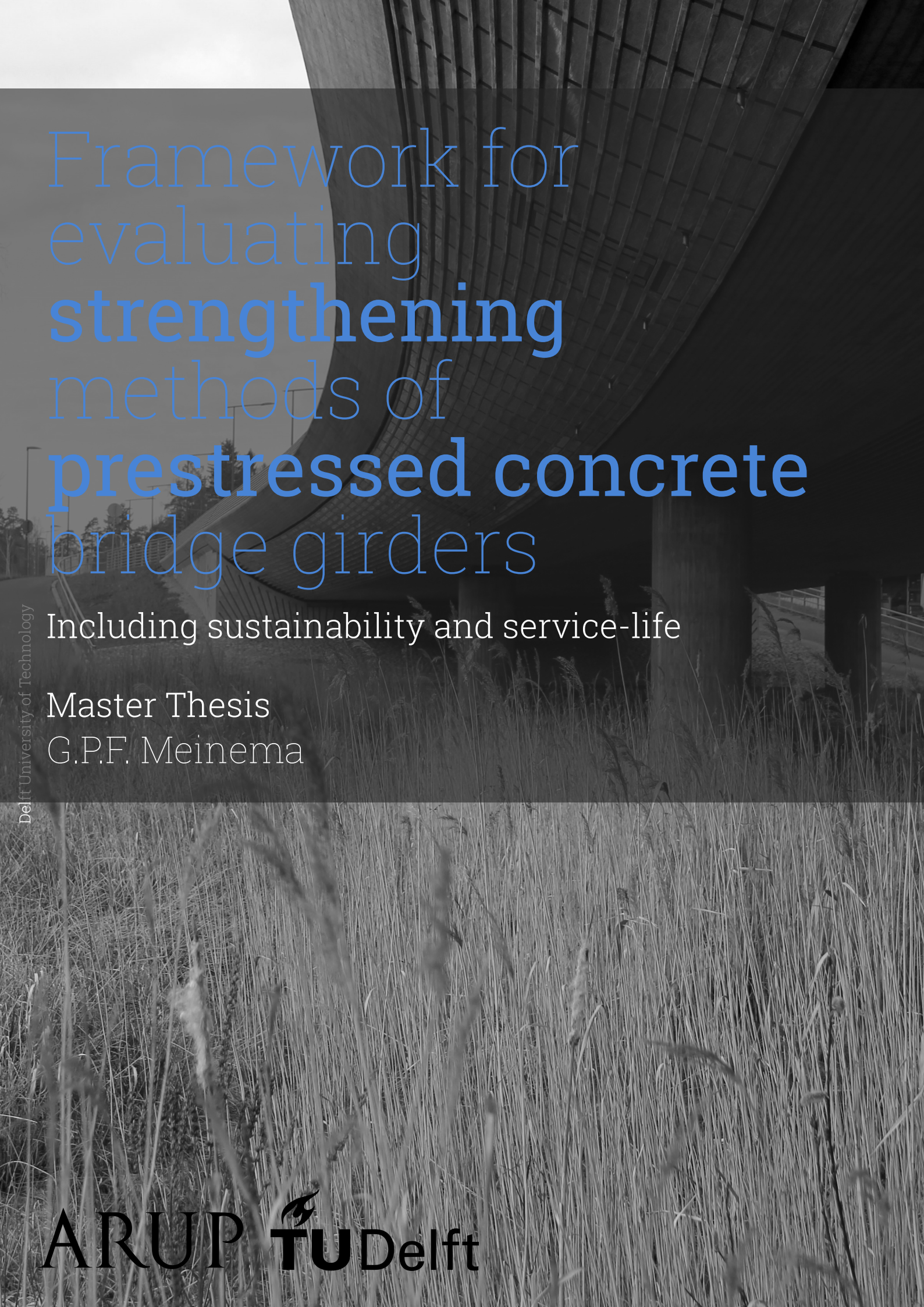

Framework for evaluating **strengthening** methods of **prestressed concrete** bridge girders

Including sustainability and service-life

Master Thesis

G.P.F. Meinema

Delft University of Technology

ARUP TU Delft

Framework for evaluating **strengthening** methods of **prestressed concrete** bridge girders

Including sustainability and service-life

by

G.P.F. Meinema

to obtain the degree of Master of Science

at the Delft University of Technology

to be defended publicly on Monday March 3, 2025 at 3:00 PM.

Student number:	4690281	
Project duration:	September, 2024 – February, 2025	
Thesis committee:	Dr. Ir. Y. Yang	TU Delft, chairman
	Dr. A.T. Gebremariam	TU Delft, supervisor
	Ir. K. Acosta	Arup, supervisor
	Dr. Ir. F. Molaioni	Arup, supervisor

Cover: By Harald Arlander [1]

An electronic version of this thesis is available at http://repository.tudelft.nl/.

TU Delft

Preface

Dear reader,

The enthusiasm for bridge engineering began during secondary school, where my fascination with bridges was started by a research project on timber cable-stayed bridges. This early interest eventually led me to start studying Civil Engineering, where my passion for bridge engineering grew.

Reflecting on my university years, I am especially thankful for the opportunity to take several courses in bridge engineering and for the experience of the bridge design course within the Faculty of Architecture. These moments have been important in shaping my understanding and enthusiasm for this field. Working on this MSc thesis has been a great experience. It has significantly improved my skills in writing, planning and efficiency, preparing me for the challenges as a structural engineer.

I would like to thank Arup, with special thanks to Kevin Acosta and Filippo Molaioni, for their supervision and guidance throughout this thesis. I would also like to thank Yuguang Yang and Abraham Gebremariam from TU Delft for their support and insights. I look forward to an exciting career and becoming a passionate bridge engineer.

Enjoy reading!

G.P.F. Meinema
Delft, February 2025

Abstract

In Europe, including the Netherlands, a significant Replacement and Renovation (R&R) challenge is expected between 2040 and 2060 for concrete bridges and viaducts due to ageing infrastructure reaching their end of service-life. Various options emerge when existing structures fail to meet current requirements, including accepting additional risk without mitigation measures, making minimal adjustments for a short period, or implementing longer-term modifications. Existing frameworks for assessing R&R decisions, include technical and cost aspects, although lack of sustainability criteria and performance prediction.

The research objective is to develop a decision-making framework for evaluating different strengthening methods versus replacement, considering factors such as (environmental) cost, service-life, structural performance prediction and reliability. The research includes a comparison method on different strengthening methods, external prestressing (EP), memory-steel (MS), carbon fibre reinforced polymer (CFRP) and ultra-high performance concrete (UHPC), versus total replacement. The study mainly focuses on shear deficiencies and strengthening for shear in precast pre-stressed T-beam bridges.

The research starts with a literature review on decision frameworks, structural deterioration mechanisms, T-beam assessment and strengthening methods. The literature review defines and elaborates on key performance indicators relevant to the study. The First Order Reliability Method (FORM) is used to determine failure probabilities by comparing demand versus capacity, providing insights into the current condition and expected lifespan of the structure. A multi-objective optimisation process is introduced to determine the most effective strengthening method based on the desired service-life extension. The goal of this optimisation process is to minimise (environmental) costs while maximising strength, subject to fabrication and physical constraints. A multi-criteria decision-making approach is applied, using the Analytical Hierarchy Process (AHP) to support complex decision-making where multiple variables and criteria must be prioritised. A parametric study is conducted to explore how (geometric) parameters influence decision outcomes.

The parametric framework enables the decision for optimal strengthening to be run multiple times, allowing trends and patterns to appear. Within the analysis, when accounting for varying spans, cross-sections, different states of current reliability and distinct deterioration phenomena for each strengthening method, CFRP consistently proves to be the best-performing and most frequently chosen option. This is due to its high strength-to-weight ratio, which helps minimise material costs and environmental impact. External prestressing excels mainly for larger spans and applying memory-steel is very unfavourable in any case when compared to other strengthening methods. Replacement ranks high in many cases but requires careful consideration, as the design is not fully optimised to each case and impact assessment remains less developed.

For complex geometries, the decision-making framework become less reliable, because strengthening and reliability calculations grow significantly more complex, which is not accounted for. A more integrated approach, considering the interaction between bending and shear, would improve the strengthening designs and could be further refined. Ultimately, while the framework provides a structured approach to decision-making, it should be seen rather as a supporting tool than a stand-alone decision-maker.

Contents

Nomenclature

Abbreviations

Abbreviation	Definition
AHP	Analytical Hierarchy Process
AP	Acidification Potential
APDf	Abiotic Depletion Potential for fuel
CFRP	Carbon Fibre Reinforced Polymer
CR	Consistency Ratio
EP	External Prestressing
EoL	End of Life
FORM	First Order Reliability Method
FRP	Fibre Reinforced Polymer
GGBFS	Ground Granulated Blast Furnace Slag
GWP	Global Warming Potential
LCA	Life-Cycle Analysis
LM1	Load Model 1
MCDM	Multi-Criteria Decision-Making
M,R&R	Maintenance, Rehabilitation and Reconstruction
MS	Memory-Steel
NC	Normal Concrete
RBK	Richtlijnen Beoordeling Kunstwerken
RC	Reinforced Concrete
RWS	Rijkswaterstaat
R&R	Replacement and Renovation
SMA	Shape Memory Alloy
UHPC	Ultra-High Performance Concrete
ULS	Ultimate Limit State

1

Introduction

1.1. Research context

Infrastructure construction in Europe peaked between 1960 and 1980, designed for an expected service-life of approximately 80 years. This is resulting in a significant Replacement and Renovation (R&R) challenge, expected between 2040 and 2060, particularly for bridges and overpasses [2, 3], as illustrated in Figure 1.1.

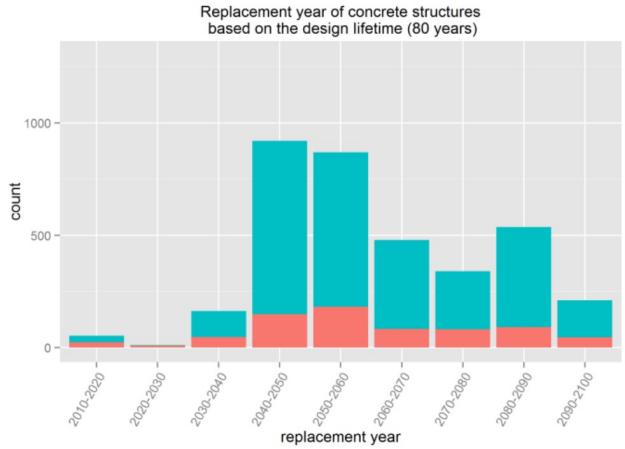

Figure 1.1: Replacement year of concrete structures based on the service-life of 80 years. Bridges in green. Overpasses in red [3].

A study by TNO [4] provides a national forecast for the replacement and renewal of civil infrastructure in the Netherlands. Currently, annual costs on infrastructure renewal already exceeds 1 billion Euros, with projections indicating a steady increase to 3-4 billion Euros by 2040–2050 and 4–6 billion Euros annually thereafter, peaking around 2080. Instead of complete renewal of the structure, strengthening of the existing structure could be considered, lowering cost projections. Aligning with circular economy principles such as the 10R strategies [5], which promote resource efficiency and environmental sustainability.

As infrastructure approaches the end of its service-life, increasing traffic loads and intensities since the 1960s have placed additional stress on existing bridges, affecting structural performance on the demand side. At the same time, socio-economic and socio-technical developments have led to evolving performance requirements [6], influencing functional aspects of infrastructures. On the capacity side, structural deterioration, such as reinforcement corrosion and prestress losses, significantly impacts bridge strength and plays a crucial role in reassessment efforts. However, these degradation processes are difficult to predict with certainty, adding complexity to maintenance and strengthening decisions.

Furthermore, evolving safety regulations further influence decision-making, where nowadays safety regulations are based on the desirable remaining service-life. This means that reduction factors may be introduced to adjust required reliability levels, adding even more complexity to the decision scenarios, since different End of Life scenarios can be considered for the same bridge.

To prevent a large number of bridges and viaducts from reaching a critical deterioration state, proactive measures should be taken now to manage the upcoming peaks in renovation and replacement demands. This study focuses on a structural analysis of precast pre-stressed T-beam bridges, as the T-beam is one of the most commonly used types in civil engineering construction, particularly in bridge construction [7]. In the Netherlands, about 70 constructions, using T-beams, were built between 1950 and 1970 [8]. An example of a T-beam structure is given in Figure 1.2.

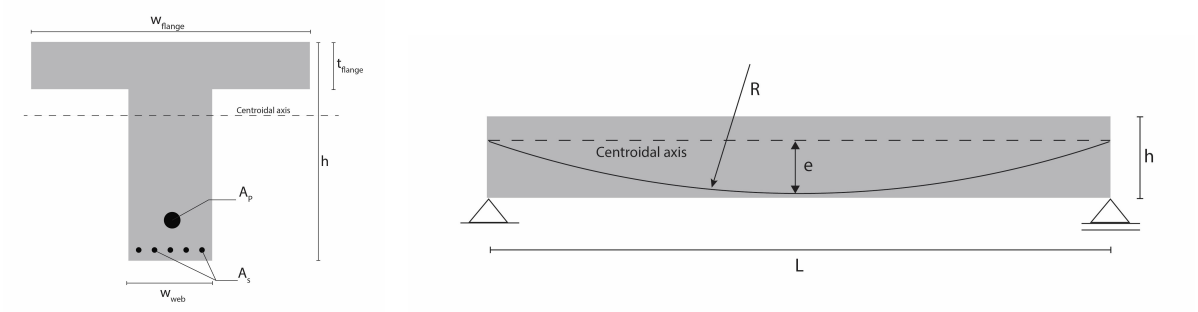

(a) Cross-section of T-beam.

(b) Parabolic tendon profile for T-beam.

Figure 1.2: Example T-beam.

The goal of applying a strengthening method is to increase the strength of a structure so it can withstand dynamic loads beyond its original design capacity in order to be sufficiently safe. Various strengthening techniques exist, but not all are equally suitable for T-beams. The selection of methods considered in this study is based on their practical applicability to T-beam bridges, availability of experimental data and existing strengthening prediction equations. The research includes a decision-making framework for different strengthening methods: External prestressing (EP), memory-steel (MS), carbon fibre reinforced polymer (CFRP) and ultra-high performance concrete (UHPC), versus total replacement.

The exact performance indicators used in the decision-making process often depend on the specific context and the preferences of stakeholders involved. Also, stakeholders prioritise criteria differently based on their experiences and perspectives, leading to potential conflicts in the decision-making process. Thereby, defining the performance of strengthening methods can be hard, making the comparison of strengthening methods and selection process complex. And while strengthening can extend service-life, the financial limit of renovating ageing infrastructure often becomes the primary deciding factor [6]. A full Life Cycle Analysis (LCA) further adds to this complexity, as it requires extensive data on transportation, manufacturing, installation and recycling processes. A decision-making framework could help address this challenge by supporting engineers in justifying their choices and providing a structured approach to evaluating strengthening methods based on specific preferences and requirements provided by the stakeholders.

Overall, the decision-making process for bridge maintenance and strengthening is very complex, involving evaluations of current structural condition, remaining service-life, cost considerations and the effectiveness of various strengthening methods. Many different design choices result in numerous possible outcomes, highlighting the necessity of a structured decision-making framework that integrates all relevant factors to determine the optimal strengthening strategy.

1.2. Research gap

Existing decision-making frameworks introduce valuable approaches, such as Life Cycle Performance metrics [9], functional performance models [10] and multi-criteria decision-making for concrete repairs [11]. However, these studies often focus on aspects such as traffic intensity, cost efficiency, or aesthetic considerations, rather than the structural performance and long-term sustainability of strengthening methods. Additionally, frameworks developed by Briseghella et al. [12], Raza et al. [13] and Borghese et al. [14] provide structured decision processes but are primarily applied to concrete bridge columns, limiting their direct applicability to prestressed concrete T-beams. Furthermore, sustainability consists of many performance indicators, the complexity of conducting a full sustainability assessment remains a challenge [15].

Other key gaps in literature are the definition of risk acceptance criteria and climate change related risks such as flooding, wildfires and severe storms, which can accelerate degradation. Where risk acceptance criteria determine acceptable reliability levels and associated risks. Improved methodologies are needed to predict the end of service-life by incorporating robustness into performance assessments [15]. Also, research on the impact of climate change on structural deterioration remains limited. Climate-related risks,

In conclusion, while many studies focus on the technical and cost aspect, they often overlook the environmental costs, circularity and extended service-life associated with different strengthening methods [16]. Existing literature does not sufficiently integrate risk acceptance criteria, robustness, climate change risks and sustainability requirements [17, 18]. Further research is required on functional requirements for bridge structures and defining functional end-of-life criteria [9].

1.3. Research objective

As mentioned earlier, various options emerge when existing structures fail to meet current requirements, including accepting additional risk without mitigation measures, making minimal adjustments for a short period, or implementing longer-term modifications. Within this decision, budget and extension of lifetime are very important considerations. Figure 1.3 tries to visualise this in a simplified manner.

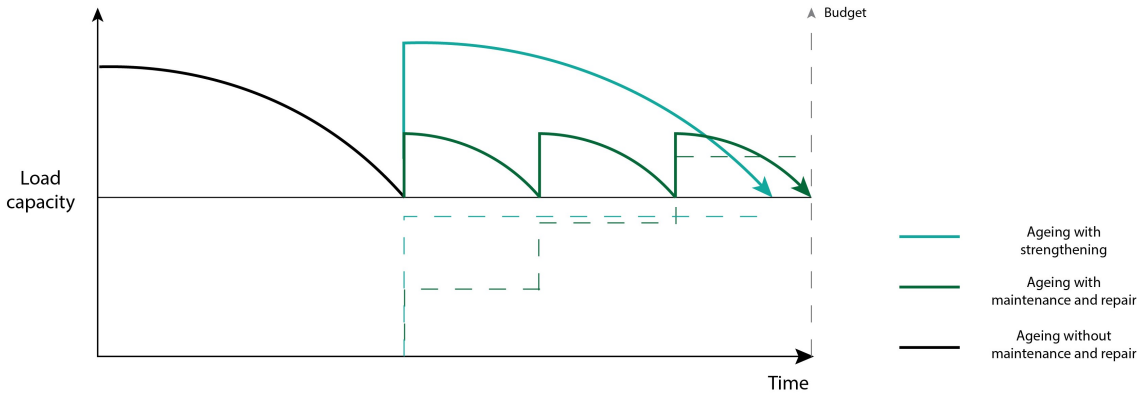

Figure 1.3: Two different strengthening strategies for service-life maintenance.

Different strengthening methods lead to varying degrees of load capacity improvement. Additionally, each method has distinct deterioration mechanisms that must be taken into account. Both the increase in strength and the rate of decay influence the effectiveness of extending the structure's lifespan, which can vary significantly.

The long-term effect must be considered. A one-time large investment in a durable strengthening solution may prove more cost-effective than frequent maintenance interventions over multiple decades. Although the optimal approach depends on the specific case, considering factors such as structural condition, financial constraints and sustainability goals, which vary between cases, this study aims to identify trends in decision-making for optimal strengthening across a wide range of scenarios.

The final objective of this research is to develop a framework that evaluates the environmental, social and economic sustainability of prestressed concrete bridge girder renovations, incorporating factors such as (environmental) cost, service-life, structural performance prediction and reliability. The research addresses the question of whether it is more safe and sustainable to renovate existing bridge beams for an extended period or to replace by new ones. It will be focused on addressing the following objectives within the context of prestressed concrete T-beam bridge renovation and replacement.

1. Investigate the effects of various strengthening methods on shear and bending performance in prestressed T-beams.
2. Analyse the advantages and limitations associated with each strengthening method.
3. Develop and optimise a decision-making process for strengthening, considering reliability, safety, service-life, circularity and sustainability.
4. Examine the influence of geometric properties, structural reliability and desired extension of lifetime on the selection of strengthening methods.
5. Assess the practicality and relevance of the proposed decision-making framework for real-life applications.

1.4. Research questions

This research addresses the urgent need for a complete framework to optimise the decision on bridge renovation and replacement in Europe, especially the Netherlands. As mentioned before, current literature lacks such a framework, particularly with the combination of strengthening prediction, sustainability criteria and service-life considerations. Therefore, the research question of this master thesis is:

*How to compare different **strengthening methods versus replacement** for prestressed concrete T-beams, which need strengthening, to improve the decision-making processes, while considering **sustainability and service-life?***

Based on the main research question, five sub-questions of the research are:

1. What are **common strengthening methods** for prestressed concrete T-beams and what is their **strengthening impact**?
2. How can **time dependent factors** for strengthening be included in the decision-making?
3. What **performance indicators** are considered in strengthening assessment?
4. How could assessment for **circularity** be integrated into the decision-making?
5. How could the **Analytical Hierarchy Process** be applied to decision-making for structural strengthening?

1.5. Research support

This thesis is performed in collaboration with Arup, under the guidance of supervisors Kevin Acosta and Filippo Molaioni. Both structural engineers, specialised in bridge structures. With over 75 years of expertise, Arup is globally recognised for its visionary approach to engineering and commitment to sustainable development. The firm has 18,500 designers, advisors and experts operating across 140 countries [19]. Arup's experience in infrastructure renovation, particularly in bridge strengthening, makes them an ideal partner for this research. Additionally, experts from Arup have contributed to this study by offering guidance on key aspects such as reliability, sustainability and circularity, further improving and supporting the research.

2

Literature review

The literature review aims to provide an overview of all key considerations in the complex decision-making process of comparing different strengthening methods versus replacement. This serves as a foundation for the research method, where these considerations are integrated to develop a framework that systematically brings them together and could serve as improvement on the existing decision-frameworks, discussed in Chapter 2.1.

The structural performance relates to the structural degradation of the bridge until a component fails or collapses. This performance highly depends on the deterioration of the structure, which can be caused by corrosion or loss of prestress, described in Chapter 2.7, influencing the capacity of the structure. Within the scope of the research, the structures capacity is defined by its shear and bending capacity, described in Chapter 2.3 and 2.4, respectively. Additionally, on the demand side, the increase in traffic intensity and associated loads can accelerate the deterioration of structures, described in Chapter 2.6. In order to quantify the deterioration it is directly related to the reliability index, described in Chapter 2.2.2. Reliability can be quantitatively assessed using methods such as the First-Order Reliability Method (FORM) [20].

Determining when exactly to maintain or strengthen is also significant to reduce both costs and environmental impact [21, 22]. This decision depends on each strengthening impact and design choices for strengthening, Chapter 2.8 states advantages and limitations for each strengthening method. Chapter 3.1 identifies this impact by doing a strengthening prediction, comparing theoretical and experimental results. The final decision-making is based on a combination of qualitative and quantitative criteria. The performance criteria outlined in Chapter 2.9 are categorised into sustainability, integrity and circularity. Chapter 2.9 offers a brief explanation of each criterion and its relevance to the decision-making process.

2.1. Existing decision-making frameworks

In building renovation issues, LCA is the common applied method for comparing impacts of replacement versus strengthening a structure [19]. This tool helps assess the environmental, societal and economic impacts, providing valuable insights into which option has the greater overall impact. While multiple LCA methods exist for buildings, relatively few are specifically designed for concrete bridges. In addition to LCA, numerous researchers have proposed frameworks to improve bridge strengthening decision-making, addressing various factors beyond environmental impact.

Xie [9] introduced the integration of Life Cycle Performance principles into infrastructure management through a ”Performance Age” metric, which adds an additional dimension to cost-based assessments for predicting the End of Life (EoL) of a structure. This method is based on the principle that a bridge does not necessarily reach the end of its life at its estimated technical age, provided it continues to perform better than its expected use. While this concept offers a useful addition for determining the EoL, it does not directly contribute to the decision-making process between strengthening and replacement.

Mooren [10] developed a dynamic model to assess a bridge's functional performance over time, aiding in intervention planning. However, this model is primarily focused on traffic data, specifically traffic intensity, rather than actual traffic loads, which are more directly linked to structural performance—the core focus of this thesis.

Furthermore, decision-making frameworks that integrate both economic and environmental criteria for concrete repairs remain limited [11]. Although Briseghella et al. [12] and Raza et al. [13] expanded decision frameworks by incorporating factors such as cost minimisation, construction time, traffic disruption and aesthetic preservation. Borghese et al. [14] build on the study of Briseghella et al. provide a valuable study with transparent performance indicators and a structured decision process. While these approaches are specifically applied to concrete bridge columns, making it somewhat different in scope, these studies still remain useful as inspiration for setting up a decision-making framework.

Despite these advancements in existing frameworks and reference studies, significant gaps remain in decision-making frameworks for prestressed concrete T-beams. No specific comparative studies exist for these structures and current frameworks lack a strong focus on the long-term sustainability and durability of strengthening methods. Additionally, there is insufficient attention given to the long-term performance of strengthening materials and their impact on structural reliability over time. Figure 2.1 gives an overview of what a decision-making framework should integrate.

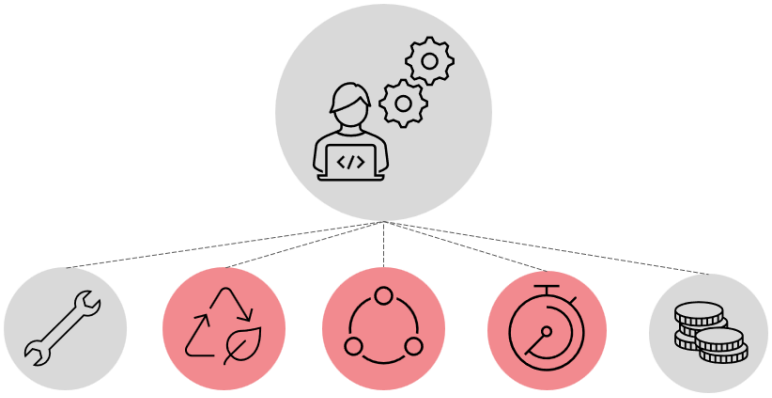

Figure 2.1: Overview of possible framework components.

2.2. Assessment of prestressed T-beams

Having the traffic load and structural deterioration in mind, assessment can be performed. The safety, or reliability, of existing concrete infrastructure structures is assessed using the Richtlijnen Beoordeling Kunstwerken (RBK) guidelines, which outline criteria for when existing structures, such as bridges, need evaluation. Key reasons for re-assessment include observed damage, increased traffic loads, or updates in design regulations. The assessment procedure is structured across three main stages and considers load factors, the remaining lifespan of the structure and the applicable traffic loads.

2.2.1. Assessment stages

- **Stage AI**: For structures that are to remain operationally safe, design traffic loads are applied following NEN-EN 1991-2 guidelines.
- **Stage AII**: The actual traffic loads are assessed based on current usage, with load factors and reference periods reflecting operational safety levels, per NEN 8701.
- **Stage AIII**: For structures approaching the threshold of safety, the actual traffic loads and load factors are applied with a focus on the rejection level of safety.

2.2.2. Reliability

The reliability of a bridge structure can be described as the likelihood that it satisfies specific demands under given conditions. Where beta (β) is the reliability index and is a measure for the safety of the system. To calculate the reliability, First Order Reliability Method (FORM) is a robust alternative to the computationally intensive Monte Carlo analysis, initially proposed by Hasofer and Lind in 1987, using only the mean and standard deviation of variables. First of all, for a bridge to be considered safe, the bearing capacity (R) must exceed the total applied load (S) acting on it. This is expressed by the performance function in Equation 2.1.

$$Z = R - S \tag{2.1}$$

Here, Z is the performance or limit state function, which differentiates safe and unsafe zones with respect to R and S. More generally, the performance function can be written as in Equation 2.2.

$$Z = g(x) \tag{2.2}$$

Where $g(x)$ depends on the n basic variables ($x_1, x_2, \ldots, x_n$) of the performance function. The performance function evaluates the structure's performance and can provide three outcomes $g(x) > 0$ which is the safe region, $g(x) = 0$ which is the limit state and $g(x) < 0$ which is the failure region. The probability of failure (p_f) is the likelihood of $Z < 0$, expressed in Equation 2.3.

$$p_f = 1 - \Phi(\beta) \tag{2.3}$$

Where the reliability index is defined as in Equation 2.4.

$$\beta = \frac{\mu_Z}{\sigma_Z} \tag{2.4}$$

$$\beta = \frac{\mu_R - \mu_S}{\sqrt{\sigma_R^2 + \sigma_S^2}} \tag{2.5}$$

In this equation, Φ is the cumulative distribution function of the standard normal variate and β is the safety index. FORM also generalises Z as in Equation 2.6.

$$Z = g(X_1, X_2, \ldots, X_n) \tag{2.6}$$

Where X_i are random variables. Using a Taylor series expansion around the mean, FORM approximates the mean (μ_Z) and variance (σ_Z^2) of Z as in Equation 2.7 and Equation 2.8, respectively.

$$\mu_Z \approx g(\mu_{X_1}, \mu_{X_2}, \ldots, \mu_{X_n}) \tag{2.7}$$

$$\sigma_Z^2 \approx \sum_{i=1}^{n} \sum_{j=1}^{n} \frac{\partial g}{\partial X_i} \frac{\partial g}{\partial X_j} \text{Cov}(X_i, X_j) \tag{2.8}$$

Here, Cov(X_i, X_j) is the covariance of X_i and X_j. The coefficient of variation (Cov) is defined in Equation 2.9. This is a normalised value of the standard deviation and can be found in the literature.

$$\text{Cov} = \frac{\sigma}{\mu} \tag{2.9}$$

Reliability threshold

The RBK not only defines load considerations but also outlines consequence classes and the minimum required safety levels, establishing acceptable reliability threshold values. Table 2.1 presents the reliability levels and load factors for different structural conditions, including new construction, renovation, operation and rejection.

Table 2.1: Levels of safety for existing bridges in RBK

Consequence class	β	γ_G	$\xi\gamma_G$	Traffic $\gamma_{Q,i}$
New construction	4.3	1.40	1.25	1.50
Renovation	3.6	1.30	1.15	1.30
Operation	3.3	1.25	1.15	1.25
Rejected	3.1	1.25	1.10	1.25

Another approach for setting a threshold value is considering human safety, using annual allowable individual risk as a key metric, typically expressed as a maximum probability of 10^{-5} per year. The values, for a 15-year reference period under simplified assumptions, are indicative and account for economic optimisation to extend the use of structures beyond their design life [23].

Table 2.2: Levels of safety for existing bridges in RBK

Consequence class	β, 1 year	β, 15 years
CC1b	2.3	1.1
CC2	3.4	2.5
CC3	4.0	3.3

Where the RBK specifies static reliability values, Kotes et al. [20] set the reliability threshold depending on current bridge age and the remaining lifetime planned for the structure, creating a more dynamic threshold value. Different reliability thresholds for different remaining lifetimes and bridge ages are provided in Table 2.3.

Table 2.3: Reliability indices (β) for different remaining lifetimes and bridge ages [20].

Remaining lifetime (years)	10	20	30	40	50	60	70	80	90
2	3.328	3.153	3.039	2.954	2.886	2.828	2.777	2.732	2.692
5	3.517	3.377	3.282	3.208	3.149	3.098	3.053	3.014	2.978
10	3.623	3.515	3.437	3.375	3.323	3.279	3.239	3.204	3.172
20	3.697	3.622	3.563	3.514	3.471	3.434	3.401	3.371	–
30	3.727	3.669	3.621	3.580	3.545	3.512	3.483	–	–
40	3.743	3.696	3.656	3.621	3.589	3.561	–	–	–
50	3.753	3.714	3.679	3.648	3.620	–	–	–	–
60	3.760	3.726	3.696	3.668	–	–	–	–	–

2.2.3. Condition rating

Another way of assessing a structure is a condition-based approach, such as the National Bridge Inventory (NBI) ratings, which relies on inspection data to generate deterioration models. These models describe the likelihood of an element transitioning from one condition state to another over a given time period [24].A bridge is classified as structurally deficient if any critical component (deck, superstructure, substructure, or culverts) is rated 4 or lower [25]. This classification does not imply that the bridge is unsafe but indicates the need for significant repairs or weight restrictions to ensure safety. The condition ratings outlined in Table 2.4 apply to bridge decks, superstructures and substructures.

Table 2.4: Summary of bridge deck and culvert condition rating.

Rating Code	Description
N	Not applicable.
9	Excellent condition.
8	Very good condition: no problems noted.
7	Good condition: some minor problems.
6	Satisfactory condition: structural elements show some minor deterioration.
5	Fair condition: all primary structural elements are sound but may have minor section loss, cracking, spalling, or scour.
4	Poor condition: advanced section loss, deterioration, spalling, or scour.
3	Serious condition: loss of section, deterioration, or spalling have seriously affected primary structural components. Local failures are possible.
2	Critical condition: advanced deterioration of primary structural elements. Closing the bridge may be necessary.
1	Imminent failure condition: major deterioration or section loss affecting structural stability. Bridge is closed.
0	Failed condition: out of service, beyond corrective action.

Condition rating type of assessment is very subjective, often failing to incorporate time-variant bridge reliability into decision-making processes. Enright et al. [26] demonstrated a method to connect condition ratings with reliability classes using Bayesian techniques. Condition ratings ranging from 0 (critical) to 10 (excellent) can be mapped to reliability indices (β), with a rating of 8 corresponding to $\beta = 6$. Ratings above 8 reflect even higher reliability, such as $\beta \geq 7$ for a rating of 10, while a rating of 0 aligns with $\beta \leq 0.0$ (failure). Intermediate values are interpolated linearly. While the proposed scale is practical, it doesn't explicitly compute the reliability from inspection data using Bayesian updating or time-dependent models.

Table 2.5: Condition Ratings related to Reliability Indices (β)

Condition Rating	Reliability Index (β)
0	0.0
2	2.0
4	4.0
6	5.0
8	6.0
10	7.0

2.2.4. Decay of reliability

Various approaches to determine the decay of the reliability are discussed in the literature: Simplified negative trends, deterministic methods and the inclusion of shrinkage and creep effects, considering differences in span length and main construction types. These decays in reliability are investigated in this Chapter and compared with a self-made prediction in Chapter 3.3.2. This should give an indication on how realistic the modelled reliability curve is.

Simplified approach

In this section, a relatively simple approach is adopted to illustrate the gradual decline in structural resistance. After a defined initiation period for corrosion, resistance is presumed to decrease linearly over time. This linear reduction in resistance is expressed mathematically as in Equation 2.10.

$$c_R = \begin{cases} 1 & \text{for } t < c_{R,t_0}, \\ 1 - \Delta c_R (t - c_{R,t_0}) & \text{otherwise,} \end{cases} \tag{2.10}$$

Where c_{R,t_0} is the time to initiation and Δc_R is the annual decrease in resistance. Assumed to have a mean of 0.0025 and CoV of 0.1. De Vries [23] utilises a conditional probability approach, which acknowledges that structures remain sufficiently reliable and safe for a specified service-lifetime. This concept is illustrated in Figure 2.2, which presents the annual reliability trends under different scenarios.

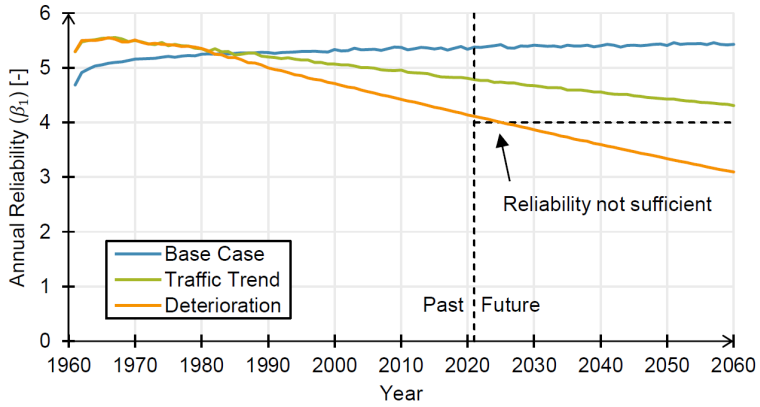

Figure 2.2: Conditional reliability curve [23].

The ”Base Case” represents an ideal scenario without significant external factors influencing reliability. The ”Traffic Trend” illustrates the impact of increased traffic loads on structural reliability. The ”Deterioration” curve reflects the reduction in reliability due to material degradation. The plotted reliability trends demonstrate that while the base case retains a relatively high reliability level over time, scenarios involving traffic growth and material degradation reveal declines. After a certain threshold (indicated by the dashed line on the graph), the reliability may no longer meet the required safety standards.

This conditional reliability framework considers a structure's intended service-life, emphasising long-term performance and safety. It should be noted that this model incorporates ongoing condition assessments, requiring the availability of actual assessment data from real-time monitoring, which is not currently accessible and therefore will not be applied. Nevertheless, it is worth recognising that such an approach could result in a different pattern of reliability decay over time.

Deterministic approach

The analysis of bridge deterioration is based on a condition-oriented approach that utilises a filtered dataset from the National Bridge Inventory (NBI). This dataset includes only concrete T-beam bridges with an Average Daily Traffic (ADT) ranging from 50,000 to 80,000 vehicles, aligning with the parameters of the case study to maintain relevance. The filtering ensures that the analysis focuses on a subset of bridges that experience comparable traffic volumes, enabling consistent and meaningful insights.

A deterministic approach was chosen for the analysis, emphasising simplicity while maintaining reliability. This methodology provides a straightforward and transparent framework for assessing bridge condition ratings. The first step involves organising the condition ratings of the selected bridges based on their age. The second step calculates the average condition rating for each age group. This averaging process reduces variability in the data and ensures that the results are not overly influenced by outliers or extreme values. By focusing on average trends, the analysis derives a representative picture of condition deterioration. The final step involves applying regression techniques to determine the trend that best describes the relationship between bridge age and condition ratings. Both linear and polynomial regression models were explored to evaluate their fit to the data.

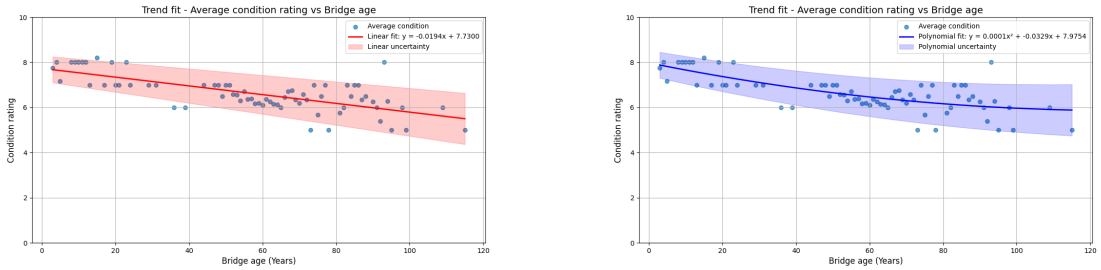

(a) Trend fit - Linear

(b) Trend fit - Polynomial

Figure 2.3: Comparison of linear and polynomial trend fits for average condition rating analysis

The linear model provides a straightforward relationship, which is easy to interpret and apply in practical contexts. However, the polynomial model may better account for variations in deterioration rates, particularly in cases where condition ratings deviate from a constant rate of decline.

Shrinkage and creep approach

Another method to validate reliability decay is by analysing the study of Fan et al. [27], incorporating shrinkage, creep, resistance degradation and vehicle load flows. This study provides a method for calculating time-varying reliability under traffic loads and shrinkage-creep effects.

Using a Monte Carlo approach, internal forces were evaluated with a 1% annual increase in vehicle load effects. The analysis, considering resistance degradation and load growth, showed a significant rise in failure probability due to shrinkage and creep. Creep effects depend on span length and the number of main girders, with smaller spans yielding safer reliability assessments.

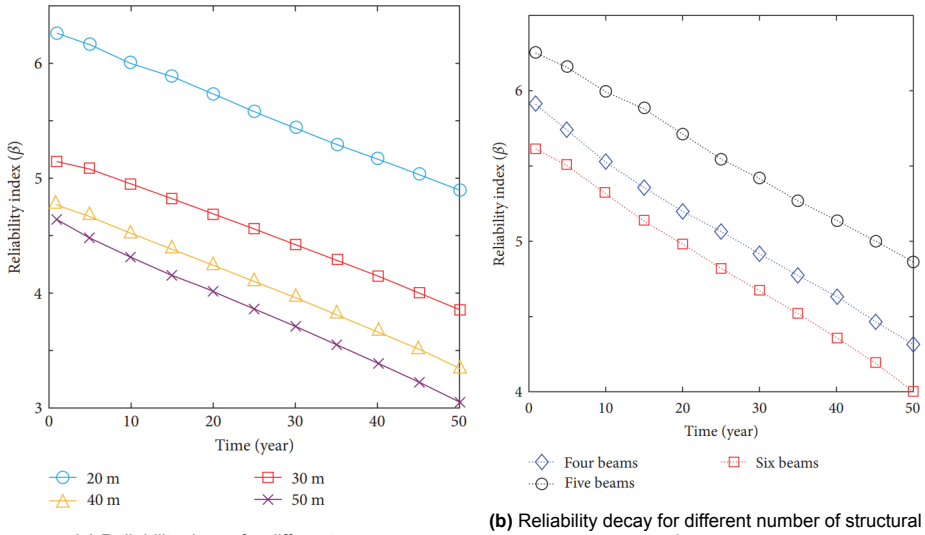

(a) Reliability decay for different spans.

(b) Reliability decay for different number of structural beams.

Figure 2.4: Reliability decay considering creep, shrinkage and traffic for varying spans and structural configurations [27].

2.2.5. End of Life

The end of life for an asset can occur for various reasons. A bridge is considered to have reached its life expectancy when it is either physically deteriorated or unable to provide its intended service. Functional performance, often referred to as service-life, describes the number of years a bridge component can continue to fulfil its intended function [28]. The expected bridge life is defined as the period until the bridge is replaced or taken out of service [24]. End of life can be indicated by either one of these:

- Reaching the reliability threshold.
- Insufficient functional performance.
- A condition rating (NBI) of 4.
- Unity check values significantly exceeding 1.0.

Determining the end of life helps prioritise interventions by establishing a foundation for design considerations, as the remaining and desired service life shape the initial framework for strengthening strategies.

2.3. Shear behaviour of prestressed T-beams

According to Ensink [8], an issue commonly observed is that the shear reinforcement in T-beams often falls short of current code requirements. Therefore, a complete understanding of these phenomena is essential for making an informed decision, ensuring safety and optimising strengthening design. Assessing shear strength according to Eurocode standards ensures that prestressed concrete beams meet safety requirements in both regions of shear behaviour and with or without shear reinforcement. Shear failure in beams can occur in various modes, including flexural shear failure, shear tension failure and shear compression failure. Each type of failure depends on the specific loading conditions, material properties and geometric parameters of the beam.

- Flexural shear failure: Occurs when the bending and shear stresses interact, causing cracking along the flexural plane. Which is not considered within this research.
- Shear tension failure: Develops when the tensile stresses in the web exceed the tensile strength of the concrete, leading to diagonal cracks.
- Shear compression failure: Results from high compressive stresses near the support regions, leading to crushing of the concrete.

2.3.1. Shear resistance without shear reinforcement

When considering shear resistance without shear reinforcement, Eurocode specifies different equations for regions based on the shear span-to-depth ratio.

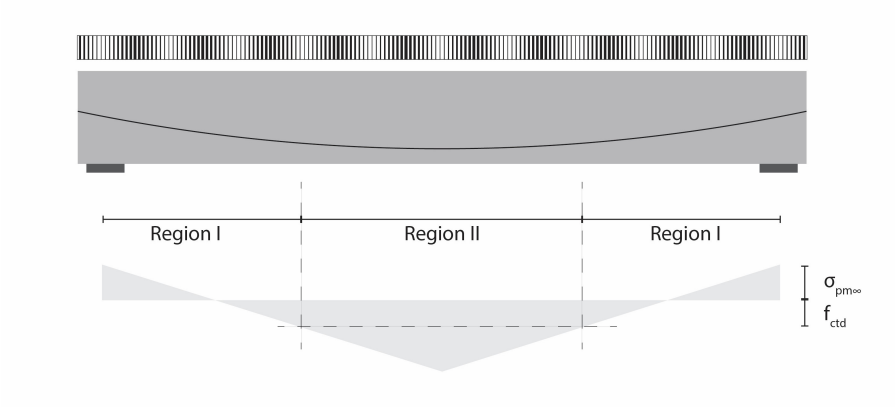

Figure 2.5: Shear resistance in region I and II.

Region I

In this region, the shear resistance $V_{Rd,c}$ is given by Equation 2.11.

$$V_{Rd,c} = \frac{I \cdot b_w}{S} \sqrt{f_{ctd}^2 + \alpha_l \sigma_{cp} f_{ctd}} \tag{2.11}$$

Where

$$f_{ctd} = \frac{\alpha_{ct} f_{ctk;0,05}}{\gamma_c} \tag{2.12}$$

$$\alpha_l = \frac{l_x}{l_{pt2}} \leq 1.0 \tag{2.13}$$

$$\sigma_{cp} = \frac{N_{Ed}}{A_c} \tag{2.14}$$

Region II
In this region, the shear resistance $V_{Rd,c}$ is governed by Equation 2.15.

$$V_{Rd,c} = \left(C_{Rd,c}k(100\rho_l f_{ck})^{1/3} + k_1\sigma_{cp}\right) b_w d \tag{2.15}$$

$$V_{Rd,c} \geq (v_{min} + k_1\sigma_{cp})b_w d \tag{2.16}$$

Where

$$C_{Rd,c} = \frac{0.18}{\gamma_c} \tag{2.17}$$

$$k = 1 + \sqrt{\frac{200}{d}} < 2.0 \tag{2.18}$$

$$\rho_l = \frac{A_{sl}}{b_w d} \leq 0.02 \tag{2.19}$$

$$\sigma_{cp} = \frac{N_{Ed}}{A_c} < 0.2 f_{cd} \tag{2.20}$$

$$v_{min} = 0.035 k^{3/2} f_{ck}^{1/2} \tag{2.21}$$

2.3.2. Shear resistance with shear reinforcement

When shear reinforcement is provided, the shear resistance is calculated using Equation 2.22.

$$V_{Rd,s} = \frac{A_{sw}}{S} z f_{ywd} \left(\cot(\theta) + \cot(\alpha)\right) \sin(\alpha) \tag{2.22}$$

The maximum shear resistance is limited by the compressive strength of the compressive struts. The maximum shear resistance of the compressive strut is given by Equation 2.23 (NEN-EN 1992-1-1).

$$V_{Rd,max} = \frac{\alpha_{cw} b_w z v_1 f_{cd} \left(\cot(\theta) + \tan(\theta)\right)}{1 + \cot^2(\theta)} \tag{2.23}$$

Where

$$\alpha_{cw} = \begin{cases} 1 + \frac{\sigma_{cp}}{f_{cd}} & \text{for } 0 < \sigma_{cp} \leq 0.25 f_{cd} \\ 1.25 & \text{for } 0.25 f_{cd} < \sigma_{cp} \leq 0.5 f_{cd} \\ 2.5\left(1 + \frac{\sigma_{cp}}{f_{cd}}\right) & \text{for } 0.5 f_{cd} < \sigma_{cp} \leq 1.0 f_{cd} \end{cases}$$

$$v_1 = \begin{cases} 0.6 & \text{for } f_{ck} \leq 60 \text{ MPa} \\ 0.9 - \frac{f_{ck}}{200} > 0.5 & \text{for } f_{ck} > 60 \text{ MPa} \end{cases}$$

The overall shear resistance of concrete prestressed beams with shear reinforcement is given by Equation 2.24.

$$V_{Rd} = \min\left\{V_{Rd,s}, V_{Rd,max}\right\} \tag{2.24}$$

2.4. Bending behaviour of prestressed T-beams

To calculate the bending moment resistance, the equilibrium model is used in combination with the bi-linear stress-strain diagram (Appendix A, Figure A.1). Which means all internal and external forces are in equilibrium. First, the height of the compressive zone is estimated by calculating the compressive forces. When the reinforcing steel yields, the total force in the reinforcing steel is $A_s f_{yd}$. If the prestressing steel is in the plastic state, its total force becomes $A_p f_{pd}$. For a compressive zone cross-section which is flanged, the compressive force in the concrete is given in Figure 2.6

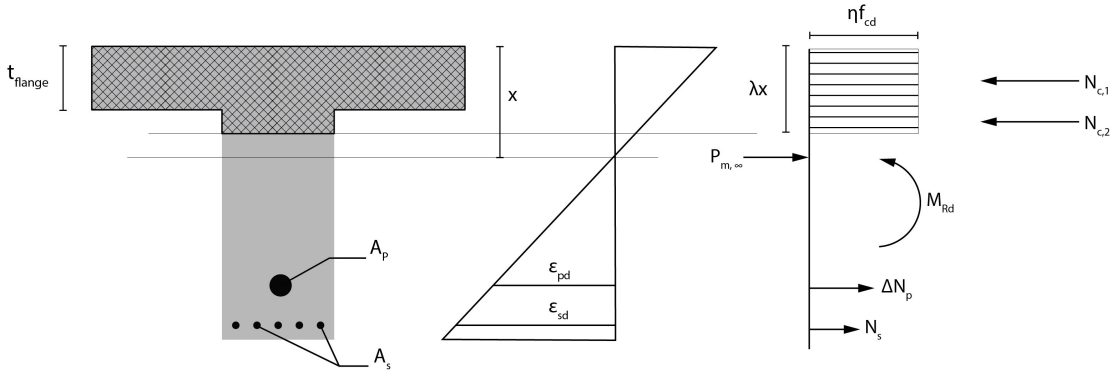

Figure 2.6: Bending moment resistance for flanged sections.

$$\eta = 1.0 \quad \text{for} \quad f_{ck} \leq 50\,\text{MPa} \tag{2.25}$$

$$\eta = 1.0 - \frac{(f_{ck} - 50)}{200} \quad \text{for} \quad 50 < f_{ck} \leq 90\,\text{MPa} \tag{2.26}$$

$$\lambda = 0.8 \quad \text{for} \quad f_{ck} \leq 50\,\text{MPa} \tag{2.27}$$

$$\lambda = 0.8 - \frac{(f_{ck} - 50)}{400} \quad \text{for} \quad 50 < f_{ck} \leq 90\,\text{MPa} \tag{2.28}$$

Using Figure 2.6, the height x_u of the compressive zone can be determined. The height x_u of the compressive zone must be checked to ensure it meets the requirement for the maximum allowable compressive zone height, as specified by the Dutch National Annex to EN 1992-1-1 5.5.

$$x_u \leq \frac{500}{f_{ck}} + \frac{f \cdot d}{f + \delta} \tag{2.29}$$

For $f_{ck} < 50$ N/mm²:

$$f = \frac{A_p \cdot f_{pm,\infty} - A_s \cdot f_{yd}}{A_s + A_p} \tag{2.30}$$

With the obtained height x_u of the compressive zone, the strains in both the concrete and the prestressing steel can be determined. The strain ε_s in the reinforcing steel follows from Equation 2.31.

$$\varepsilon_s = \frac{\varepsilon_{cu}}{x_u} (d_s - x_u) \tag{2.31}$$

Similarly, the increase in the strain of the prestressing steel $\Delta\varepsilon_p$ can be determined.

$$\Delta\varepsilon_p = \frac{\varepsilon_{cu}}{x_u}(d_p - x_u) \tag{2.32}$$

With the strains ε_s and $\Delta\varepsilon_p$, the stresses in the reinforcing steel σ_{su} and the prestressing steel σ_{pu} can be calculated. These stresses allow for determining the force in the reinforcing steel and the increase in the force in the prestressing steel.

$$N_s + \Delta N_p = A_s\sigma_{su} + A_p(\sigma_{pu} - \sigma_{p,\infty}) \tag{2.33}$$

Where N_s is the force in the reinforcing steel, ΔN_p is the increase in force in the prestressing steel, A_s is the area of the reinforcing steel and A_p is the area of the prestressing steel. It should be noted that the stress in the reinforcing steel will often be $\sigma_{su} = f_{yd}$. This check is performed in the parametric framework. Next, it should be verified whether Equation 2.34 is satisfied.

$$N_c + P_{m,\infty} = N_c \quad \Rightarrow \quad N = N_c - P_{m,\infty} \tag{2.34}$$

Three possible outcomes may arise.

- If $N_c < P_{m,\infty} - N$, the assumed height x_u of the concrete compressive zone is too large.
- If $N_c = P_{m,\infty} - N$, the assumed height x_u of the concrete compressive zone is correct.
- If $N_c > P_{m,\infty} - N$, the assumed height x_u of the concrete compressive zone is too small.

If the height x_u of the concrete compressive zone is assumed correctly, the calculation proceeds to the final step, which involves determining the moment resistance of the cross-section. In all other cases, a new height for the concrete compressive zone should be assumed. After a few iterations, the correct height of the concrete compressive zone will be found. With the correct height x_u of the concrete compressive zone, the magnitude of the bending moment resistance M_{Rd} can be determined.

$$M_{Rd} = N_s(d_s - x) + \Delta N_p(d_p - x) + N_c(x - \lambda x) \tag{2.35}$$

2.5. Structural safety

For the structural safety assessment, only Ultimate Limit State (ULS) is considered. The ULS is verified using the unity check comparing the design values of action effects to design resistance values. Load effects are determined using NEN 8700 and NEN 8701, while resistance calculations for concrete structures follow NEN-EN 1992-1-1 and RBK guidelines. The shear strength for existing prestressed beams is derived by combining shear reinforcement resistance and concrete shear resistance. where $V_{Rd,s}$ is calculated based on reinforcement specifications and $V_{Rd,c}$ is the concrete resistance.

$$V_{Rd} = V_{Rd,s} + V_{Rd,c} \tag{2.36}$$

$$\text{U.C.} = \frac{V_{Ed}}{V_{Rd}} \tag{2.37}$$

In addition to shear assessment, bending assessment is crucial for safety verification. Where $M_{Rd,s}$ is the contribution of reinforcement and $M_{Rd,c}$ the contribution of concrete. For prestressed sections, the bending capacity also considers the prestress force, adjusting for losses over time due to factors such as creep and shrinkage (NEN-EN 1992-1-1).

$$M_{Rd} = M_{Rd,s} + M_{Rd,c} \tag{2.38}$$

$$\text{U.C.} = \frac{M_{Ed}}{M_{Rd}} \tag{2.39}$$

2.6. Traffic loads

On the demand side of structural safety, the long-term durability and performance of structural infrastructure is significantly affected by increasing traffic loads, which can cause fatigue and weakening of structural components [29]. Therefore, it is essential to understand the loads that should be applied within the model and the extent to which these loads increase over time. This chapter focuses on describing these aspects in detail.

2.6.1. Load Model 1

Load Model 1 (LM1) is a method for assessing bridge live loading by dividing the carriageway into notional lanes and assigning characteristic loads to each lane, as defined by Eurocode. The model includes both tandem axle loads and uniformly distributed loads (UDL) to simulate traffic effects. The load components consist of tandem axle loads (TS), represented as concentrated forces and UDLs applied across the lane width. Double-axle concentrated loads, with each axle having a weight defined as in Equation 2.40.

$$\alpha_Q \times Q_k \tag{2.40}$$

Where α_Q is the adjustment factor, Q_k is the characteristic value of the axle load. Loads applied per square metre of a notional lane, defined as $\alpha_q \times q_k$. Where α_q is the adjustment factor, q_k is the characteristic value of the uniformly distributed load. The load values for the tandem system (TS) and UDL system for various lanes are given in Table 2.6.

Table 2.6: Load components for LM1.

Location	**Tandem system,** Q_k	**UDL system,** q_k
Lane 1	300	9
Lane 2	200	2.5
Lane 3	100	2.5
Other lanes	0	2.5
Remaining area (q_{rk})	0	2.5

The values of the adjustment factors α_{Q_i}, α_{q_i} and α_{q_r} should be selected based on the expected traffic and the route classification, given in Equation 2.41.

$$\alpha_{Q_1} \geq 0.8, \quad \text{and for } i \geq 2, \quad \alpha_{Q_1} \geq 1 \tag{2.41}$$

2.6.2. Load combinations

Eurocode 0 (NEN-EN-1990 2021) provides a semi-probabilistic approach, using characteristic values and partial safety factors to ensure adequate safety margins. For the Ultimate Limit State (ULS) Eurocode provides Equations 2.42 and 2.43. These combinations consider permanent loads, prestressing forces and variable actions to evaluate the most critical load scenarios.

$$\sum (\gamma_{Ga} \cdot G_{k,j}) - (\gamma_P \cdot P_k) + (\gamma_{Q_1} \cdot \Psi_{0,1} \cdot Q_{k,1}) + \sum (\gamma_{Q_i} \cdot \Psi_{0,i} \cdot Q_{k,i}) \tag{2.42}$$

$$\sum (\gamma_{Gb} \cdot G_{k,j}) - (\gamma_P \cdot P_k) + (\gamma_{Q_1} \cdot \Psi_{1,1} \cdot Q_{k,1}) + \sum (\gamma_{Q_i} \cdot \Psi_{2,i} \cdot Q_{k,i}) \tag{2.43}$$

2.6.3. Increase of traffic loads

Bridge performance is significantly influenced by traffic load and intensity, both of which can increase over time. For the Netherlands, traffic load projections often rely on generalised equations derived from historical trends and models, as described in Equation 2.44.

$$L(t) = L_0(1 + r)^t \tag{2.44}$$

Where $L(t)$ is the traffic load at time t (e.g., year t), L_0 is the initial traffic load (at $t = 0$), r is the annual growth rate of traffic load (as a fraction) and t is the time in years. For traffic analysis, INWEVA (INtensiteiten op WEgVAkken) is used. The average number of heavy truck traffic per weekday and the 25% quantile is visualised in Figure 2.7.

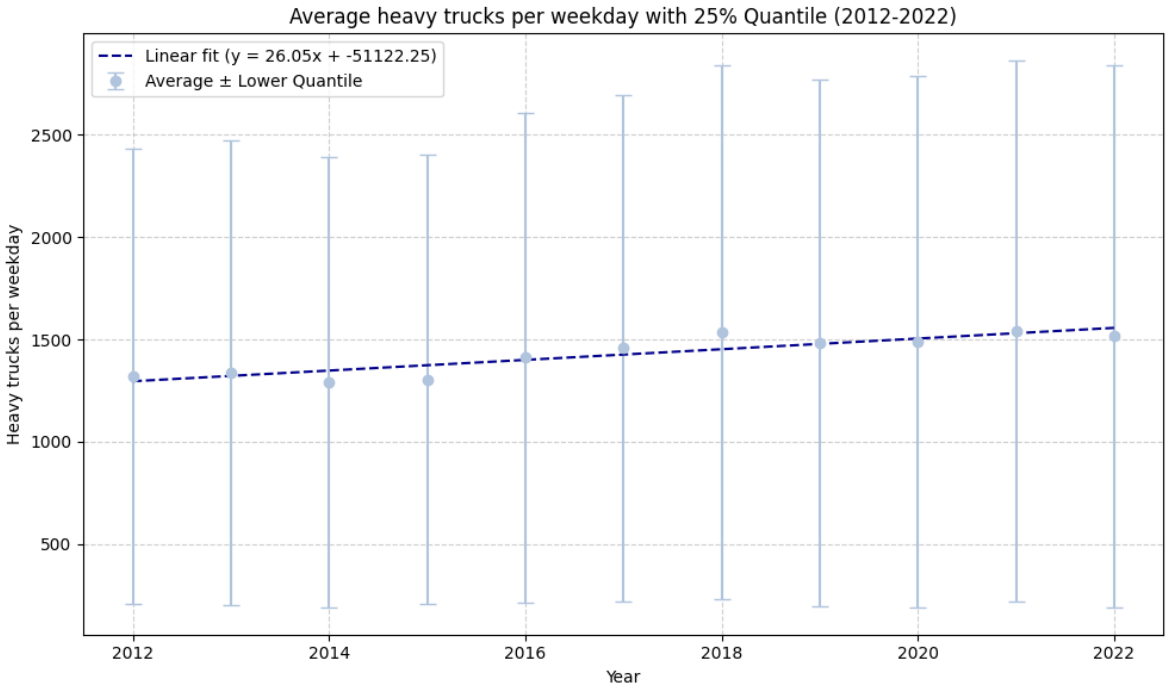

Figure 2.7: Average heavy truck traffic per weekday in the Netherlands.

2.6.4. Reduction of loads

The adjustment for the target remaining lifetime of a structure is achieved by using the reference table for reduction factors. For structures with lifetimes of less than 100 years, Table 2.7 provides appropriate values that can be interpolated if the exact reference period falls between the given entries. These reduction factors ensure a realistic assessment of structural reliability by adjusting the effects of applied loads for shorter service durations.

Table 2.7: Reduction for reference period below 100 years

Reference time y	20	50	100	200
100	1.00	1.00	1.00	1.00
50	0.99	0.99	0.99	0.99
30	0.99	0.99	0.98	0.97
15	0.98	0.98	0.96	0.96
1	0.95	0.94	0.89	0.88
0.08	0.91	0.91	0.81	0.81

In addition to the reference period, future trends in traffic loads are also considered, Table 2.8. Trend-based reduction factors account for anticipated changes in traffic growth and the frequency of heavy vehicles. These factors depend on the influence length of the bridge, which reflects the span contributing to the load effect, as well as the target year of the assessment. For example, by the year 2060, the reduction factors approach a value of 1.00, indicating no further reduction in load effects, whereas earlier years reflect lower values to account for expected increases in traffic.

Table 2.8: Trend reduction for year 2060

Influence length [m]	2010	2020	2030	2040	2050	2060
0	1.00	1.00	1.00	1.00	1.00	1.00
20	0.89	0.91	0.93	0.96	0.98	1.00
50	0.82	0.86	0.88	0.91	0.95	1.00
75	0.78	0.83	0.87	0.90	0.95	1.00
100	0.76	0.81	0.85	0.90	0.95	1.00
150	0.75	0.80	0.85	0.90	0.95	1.00
≥ 200	0.75	0.80	0.85	0.90	0.95	1.00

The final reduction factor is calculated by combining the reference period reduction factor with the trend-based factor. This is done by multiplying the two values, resulting in a single adjusted factor that is then applied to the line loads used in the design or assessment process. This combined factor ensures that the assessment reflects both the remaining service-life of the structure and future traffic trends, providing a balanced evaluation of structural demands.

When parameters such as reference time or influence length do not align exactly with the tabulated values, interpolation is performed. This ensures that reduction factors can be tailored for any combination of structural parameters and timeframes, enabling accurate application in a wide range of scenarios.

Reduction factors are integrated into the overall reliability assessment framework to ensure that the predicted reliability of the structure accurately reflects adjusted load effects. By using these factors the assessment aligns with Eurocode and national guidelines and structural interventions, such as strengthening, can be planned based on realistic projections of future loads and structural demands.

2.7. Structural deterioration

On the capacity side of structural safety, long-term durability and performance of structural infrastructure, is highly dependent on the material degradation, affected by phenomena such as corrosion and loss of prestress. Although many other deterioration mechanisms exist, the focus is on two well-documented phenomena in the literature.

2.7.1. Corrosion

Corrosion in reinforced concrete structures typically occurs in two distinct stages: the initiation stage and the propagation stage. The initiation stage is characterised by the diffusion of chloride ions through the concrete cover to reach the reinforcement bars. This diffusion process is often modelled using the one-dimensional Fick's law of diffusion. Tu et al. [30] and Vu et al. [31] offer detailed relationships describing this diffusion process, highlighting its dependency on various material and environmental factors. The corrosion initiation time, t_{ini}, expressed in years, can be predicted using Equation 2.45.

$$t_{ini} = \frac{t_{cov}^2}{4D_c}\left[\text{erf}^{-1}\left(1 - \frac{C_{cr}}{C_0}\right)\right]^2 \tag{2.45}$$

This equation accounts for the thickness of the concrete cover (t_{cov}), the diffusion coefficient of chloride ions (D_c), the constant chloride ion concentration on the concrete surface (C_0) and the threshold chloride concentration (C_{cr}). The relationship also incorporates the inverse of the error function (erf^{-1}), which quantifies the probability distribution of chloride ions within the concrete. The input parameters for t_{ini}, as summarised in Table 2.9, include the chloride concentration at the surface (C_s), the threshold

chloride concentration (C_{th}) and the diffusion coefficient (D_c), typically measured in mm^2/year. These variables depend on the environmental exposure conditions, concrete properties and service-life design requirements.

Table 2.9: Input data for the initiation time of corrosion [32].

Variable	Mean	Unit
C_s	5.3	%
C_{th}	0.5	%
D_c	8.83	$mm^2/year$

Once corrosion is initiated, the propagation stage begins, during which the steel reinforcement undergoes active corrosion. The rate of corrosion, characterised by the corrosion current density (i_{corr}), can be calculated using Equation 2.46. This equation reflects the influence of the water-to-cement ratio (w/c), concrete cover thickness (t_{cov}) and time elapsed since corrosion initiation ($t - t_{\text{ini}}$).

$$i_{\text{corr}}(t) = 0.85 \cdot \frac{37.5\left(1 - \frac{w}{c}\right)^{-1.64}}{t_{cov}} (t - t_{\text{ini}})^{0.29} \tag{2.46}$$

The propagation stage leads to the formation of pits in the steel reinforcement, which can compromise its load-carrying capacity. The radius of the corrosion pit at time t, denoted as $p(t)$, is calculated using Equation 2.47.

$$p(t) = 0.0116(t - t_{ini}) i_{\text{corr}} R \tag{2.47}$$

This equation incorporates the corrosion current density (i_{corr}) and a pit growth factor ($R = 3$), representing the ratio between maximum and average penetration depths. Where i_{corr} is the corrosion current density (μA/cm^2), $R = 3$ is the ratio between maximum and average penetration.

The geometric model proposed by Val and Melchers [33], provides a framework for computing the loss of effective cross-sectional area in reinforcement bars influenced by pitting corrosion. The remaining net cross-sectional area, $A_r(t)$, is defined by the piecewise function illustrated in Equation 2.48.

$$A_r(t) = \begin{cases} \frac{\pi D_0^2}{4} - A_1 - A_2, & p(t) \leq \frac{\sqrt{2}}{2} D_0 \\ A_1 - A_2, & \frac{\sqrt{2}}{2} D_0 < p(t) < D_0 \\ 0, & p(t) \geq D_0 \end{cases} \tag{2.48}$$

Where D_0 is the initial diameter of the reinforcement bar and A_1 and A_2 represent the areas of the remaining cross-section and the void created by the corrosion pit, respectively.

$$a = 2p(t)\sqrt{1 - \left(\frac{p(t)}{D_0}\right)^2}, \quad \theta_1 = 2\arcsin\left(\frac{a}{D_0}\right), \quad \theta_2 = 2\arcsin\left(\frac{a}{2p(t)}\right)$$

$$A_1 = \frac{1}{2}\left[\theta_1 \left(\frac{D_0}{2}\right)^2 - a\left(\frac{D_0}{2} - \frac{p^2(t)}{D_0}\right)\right], \quad A_2 = \frac{1}{2}\left[\theta_2 p^2(t) - a\frac{p^2(t)}{D_0}\right]$$

When the corrosion penetration depth ($p(t)$), exceeds the bar diameter (D_0), the remaining cross-sectional area becomes zero, identifying complete loss of the reinforcement bar's structural capacity. In addition to geometric degradation, pitting corrosion also reduces the mechanical properties of the reinforcement. The reduction in yield stress, $f_y(t)$, of the reinforcement at time t can be computed using Equation 2.49.

$$f_y(t) = (1 - 100\alpha_{\text{corr}} P_{\text{corr}})\, f_{y0} \tag{2.49}$$

Where f_{y0} is the initial yield (or ultimate) stress, P_{corr} is the percentage loss of cross-sectional area due to corrosion and $\alpha_{\text{corr}} = 0.0054$ is a coefficient specific to reinforcement bars. Figure 2.8 illustrates the geometry of pitting corrosion on a reinforcement bar.

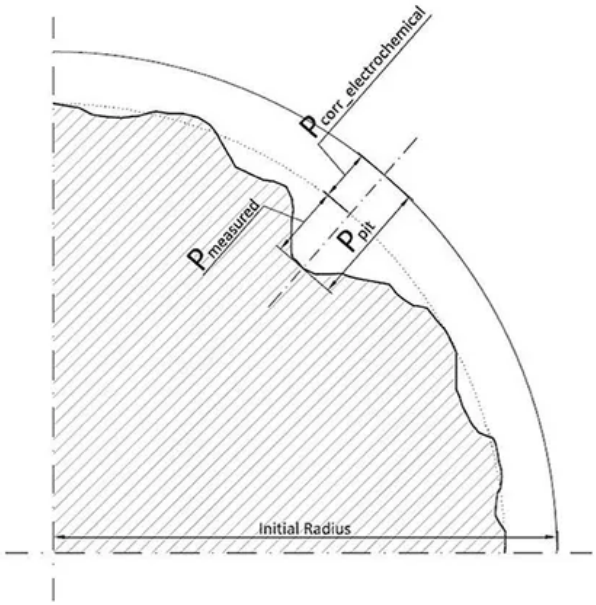

Figure 2.8: Pitting of the steel reinforcement [33].

2.7.2. Loss of prestress

Over time, the prestress in a structural element decays due to various factors. This phenomenon is mathematically described by Equation 2.50, which quantifies the proportional loss of prestress as a function of time.

$$\frac{\Delta\sigma_{pr}}{\sigma_{pi}} = 6.6\rho_{1000}e^{9.1\mu}\left(\frac{t}{1000}\right)^{0.75(1-\mu)} \times 10^{-6} \tag{2.50}$$

Where $\Delta\sigma_{pr}$ represents the loss in prestress, while σ_{pi} denotes the initial prestress applied, t is the time elapsed, expressed in hours, μ is a parameter that accounts for the wobbling effect, which is typically associated with deviations or irregularities in the tendon profile and ρ_{1000} is a factor related to the material properties and the structural configuration, evaluated at a reference point corresponding to 1000 hours. The loss of prestress occurs gradually due to the combined effects of factors such as creep, shrinkage of concrete and relaxation of the prestressing steel. The μ amplifies the impact of wobbling on the prestress loss, while the time dependency is included in hours.

2.8. Strengthening methods

Once the assessment of the concrete structure establishes its current condition, the next step is strengthening prediction, which aims to improve reliability and extend service-life. Traditional methods for strengthening concrete structures include reinforced concrete jacketing, steel jacketing, external post-tensioning and CFRP-wrapping. These techniques have been widely studied and applied in structural engineering [34, 35, 36, 37]. While steel and reinforced concrete jacketing improve strength and ductility, they also increase cross-sectional size and stiffness, which can be undesirable in some cases. Additionally, steel jacketing requires extra corrosion protection, adding to maintenance costs. Due to these drawbacks, this research focuses on more efficient and modern strengthening techniques, specifically external post-tensioning, memory-steel, CFRP-wrapping and UHPC.

Due to time constraints and the need to define a clear research scope, not all possible design options were considered. The selection of strengthening methods was primarily based on the availability of literature, established strengthening prediction equations and existing experimental results. In this chapter, the design considerations for each selected strengthening method are discussed, detailing their application, effectiveness and impact on structural performance.

2.8.1. External prestressing

Interest in external prestressing has increased in recent decades due to the need for strengthening structures under higher traffic loads and enabling repairs without closing bridges [38]. While external prestressing has benefits, such as ease of application, it also has drawbacks, including tendon corrosion and reduced clearance height beneath the structure [39]. An actual application is illustrated in Figure 2.9. Said et al. [40] demonstrated three external prestressing configurations, illustrated in Figure 2.10. Where the first two applications increase mostly the bending strength, while the third configuration increases the shear and bending strength.

Figure 2.9: External prestressing tendons set-up as applied by Freyssinet [41].

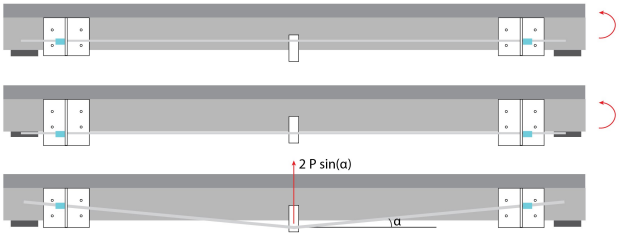

Figure 2.10: T-beam strengthening by applying external prestressing tendons.

The strengthening design using external prestressing in this thesis is anchored at the so-called 'tussenstorten' of the T-beam. Another way of anchoring these external tendons, is by applying steel anchorages, clamped or bolted onto the web of the beam. A straight tendon profile is applied in the middle section of the beam, while an inclined tendon profile is used at the outer ends, as illustrated in Figure 2.11. This configuration results in increased bending capacity in the central region of the beam and improved shear capacity at the ends. The strengthening design can vary in angle, thickness of the tendon diameter, the amount of prestress and type of steel tendon.

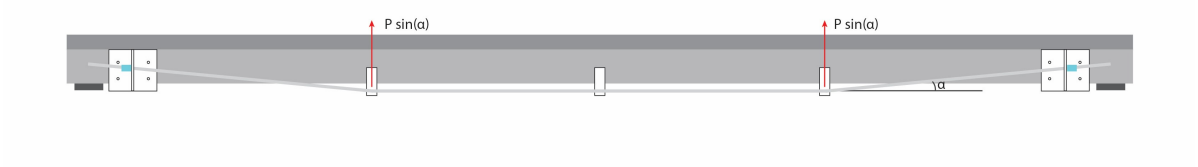

Figure 2.11: External prestressing tendons set-up for extended beams.

The prestressing force can vary but is limited. If the prestressing force becomes too high, it can lead to cracking in the top fibre. Also effects on the prestressing tendon within the concrete should be considered. Although, this effect is very hard to predict, since the prestressing cable is covered by the concrete.

Advantages

While external prestressing offers significant advantages, such as ease of application and minimal disruption to existing structures during implementation, it also comes with certain limitations. One of the primary benefits is its adaptability, allowing for repairs and strengthening without the need for extensive closures or intrusive work, which is particularly advantageous for bridges with high traffic demands.

Limitations

However, this strengthening method is not without challenges and limitations. Tendon corrosion remains a critical concern, particularly in aggressive environments, requiring effective protection measures to ensure long-term durability. Additionally, external prestressing can lead to a reduction in clearance height beneath the structure, which may restrict its use in certain applications. The prestressing force itself is subject to limitations, as excessive force can cause cracking in the top fibre of the concrete and may negatively impact the existing prestress within the concrete. These factors need careful design and monitoring to optimise the performance and service-lifetime of externally prestressed systems.

2.8.2. Memory-steel

Memory-steel strengthening uses Shape Memory Alloys (SMAs) which can return to their original shape after being deformed when heated, making them highly effective for retrofitting concrete structures [42]. Memory-steel stirrups, often in U-shaped ribbed bars, reduce deflection, crack width and internal steel stirrup stresses while increasing shear capacity [43]. Cladera [44] introduced a shear strengthening method using 12 mm U-shaped ribbed memory-steel bars combined with sprayed mortar. It is assumed the shotcrete has a thickness of about 30-50 mm. After the mortar cures, the bars are activated through resistive heating, inducing a prestress of about 300 N/mm², improving the structural performance by introducing compressive stresses in the RC beam's web. The mass-percentage rate used for the SMAs in this study is Fe-17Mn-5Si-10Cr-4Ni-1(V,C) (mass%).

The use of SMA strips as external reinforcement in RC T-girders delays the formation of shear cracks. Additionally, the delayed yielding of internal stirrups further retains the inherent shear capacity of the beam [43]. Retrofitting with U-shaped Fe-SMA strips has demonstrated an increase in shear strength of approximately 30% [44]. Prestressing of vertical stirrups has a negligible effect on increasing shear strength compared to conventional stirrups [42]. Therefore, using prestressing to enhance shear capacity is generally ineffective. However, the application of prestressing influences the displacement behaviour of the beam, contributing to reduced deflections.

Although SMAs have higher production energy costs than traditional reinforcement, they are more sustainable. Containing 10% chromium, memory steel uses abundant, sustainably sourced components. It avoids epoxy adhesives and synthetic Fibres, reducing environmental impact and is easily recyclable, promoting a circular economy [45].

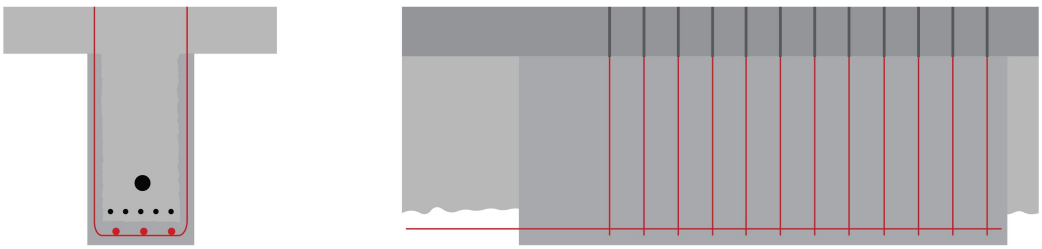

Figure 2.12: Strengthening a T-beam by applying Memory-steel.

(a) Roughening of the surface. **(b)** Applying memory-steel stirrups. **(c)** Sprayed grout layer.

Figure 2.13: Application of memory-steel [42].

The application of memory-steel is illustrated in a simplified way in Figure 2.14. The U-shaped ribbed memory-steel stirrups (Figure 2.13b) are guided around the existing, roughened concrete surface (Figure 2.13a) and over the additional longitudinal re-bar providing bending strengthening. They are then embedded in sprayed mortar (Sika MonoTop-412N) (Figure 2.13c) and grouted in the flange, providing anchorage over the neutral axis. The re-bar shear stirrups are electrically heated and activated from above, ensuring a secure connection with the existing concrete structure.

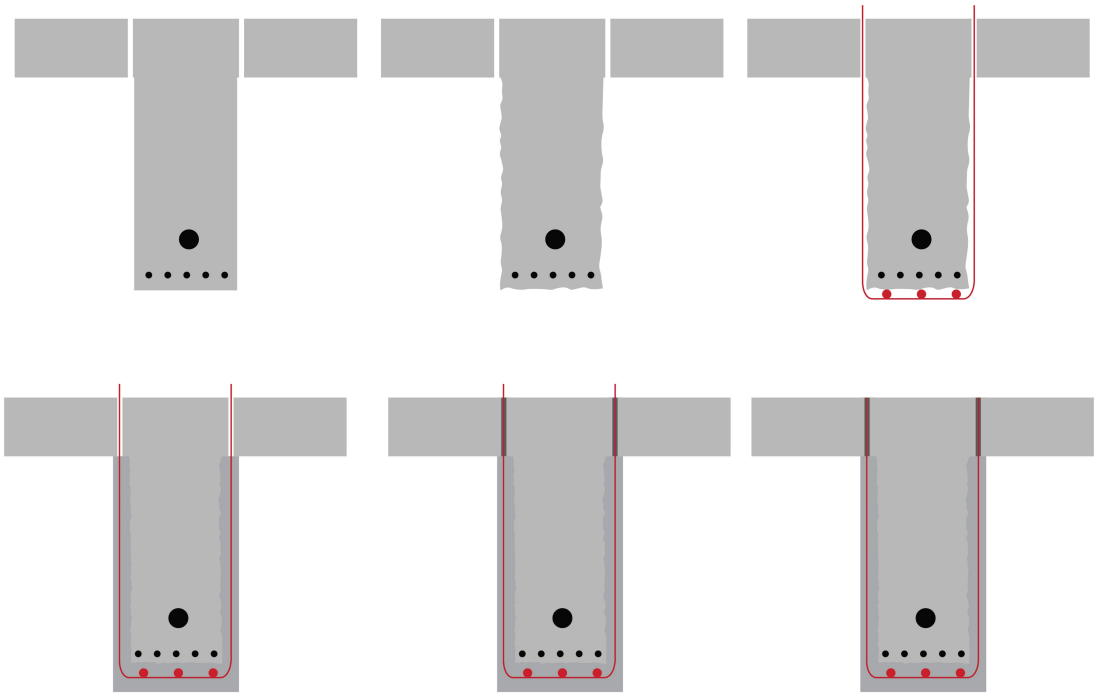

Figure 2.14: Application of Memory-steel step-by-step.

The increase in overall capacity can be attributed to the following factors: Firstly, an increase in the concrete area (A_c). Secondly, prestress introduced through the activation of memory steel (A_p). Thirdly, an increase in the area of shear reinforcement at anchorage points (A_{sw}). And finally, improved longitudinal reinforcement area, contributing to improved flexural capacity. Strengthening design and optimisation of the strengthening, can be done by changing the amount of stirrups, the amount of bars in longitudinal direction, the amount of prestress introduced by the activation and the spacing between the stirrups.

Advantages

The structural benefits of memory-steel arise from several factors. Starting with an increased concrete area, prestress introduced via activation, enhanced shear reinforcement area at anchorage points and improved longitudinal reinforcement area, which together contribute to greater shear and flexural capacity. This creates reduced deflections, improved aggregate interlock and the elimination of mechanical jacks and anchor heads.

Limitations

The use of memory-steel also presents challenges. The activation process is complex, requiring the removal of the deck layer and careful reliance on the bond between the memory-steel and mortar. Additionally, defining the exact prestressing force remains difficult, which can complicate the design and implementation process. SMAs are a less sustainable alternative to traditional reinforcement, as they use scarce materials and these materials have higher environmental impact.

Note: In this study, the tensile strengths of both the concrete and sika mortar in the tension area were disregarded, considering only the contributions of the steel rebar and Fe-SMA reinforcement. The compressive capacity of steel bars in the compression zone was also excluded from the analysis. The mortar layer primarily serves to facilitate the bond between the Fe-SMA strips and the T-girder, rather than contributing directly to the strength, as this section is subject mainly to bending.

2.8.3. Carbon Fibre Reinforced Polymer

CFRP has become a preferred solution for reinforcing bridges and buildings due to its lightweight nature, high strength, corrosion resistance and ease of application [46, 47]. It also offers sustainability benefits through construction efficiency and reduced environmental impact. However, debonding and poor performance in high temperatures and wet environments remain challenges [48]. The study of Liu et al. [49] applies Sikawrap Hex 230 C with Sikadur 300 epoxy and CFRP density was reported at 1800 kg/m³, with 55% carbon fibres and 45% epoxy resin in the composite [50]. Overall, CFRP represents a promising option for sustainable engineering, especially strengthening of concrete structures [50].

(a) Application of CFRP-wrapping.

(b) Different CFRP-wrapping lay-outs for a T-beam.

Figure 2.15: Illustrations of CFRP applications and lay-outs for T-beams.

To apply CFRP, an epoxy resin is first applied as an adhesive layer. The CFRP is then wrapped around the web of the beam. The CFRP can be anchored and applied in various configurations, as illustrated in Figure 2.15b.

Design parameters that can be adjusted to optimise the strengthening design include the number of sheets and their thickness. Additionally, the strength of the sheets varies depending on the manufacturer. Further strength enhancement can be achieved by anchoring the sheets into the web of the structure. Various CFRP strengthening designs are illustrated in Figure 2.16.

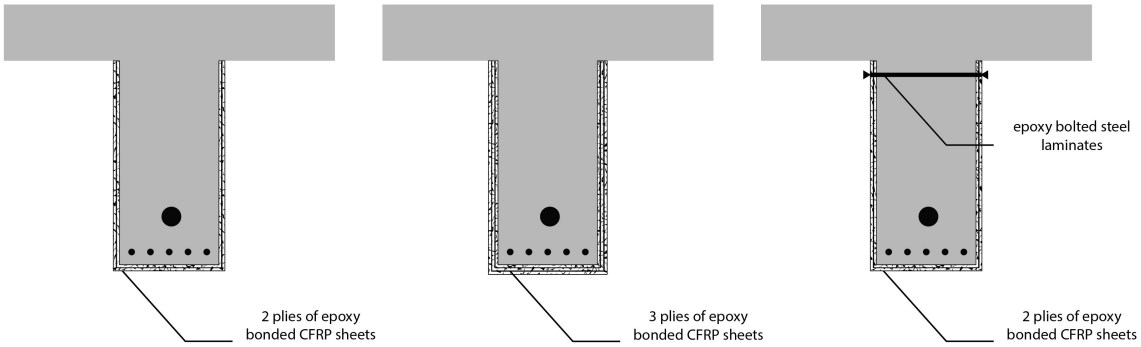

Figure 2.16: CFRP strengthening of a T-beam.

The application of CFRP (Carbon Fibre Reinforced Polymer) strips significantly improves the load-bearing capacity of reinforced concrete elements [51]. Increasing the size of CFRP strips leads to greater strength [52], although the use of epoxy bonding carries a risk of debonding, which can be mitigated by mechanical anchors [53]. Strengthening configurations have shown improvements in load capacity ranging from 13.6% to 36.4%, with U-jacketing being the preferred method for T-girders [54]. CFRP reinforcement can increase shear strength by 23% to 26%, with the use of mechanical anchors providing an additional boost of 7% to 48% [55, 56, 57]. The shear strength is affected by factors such as the number of strip layers and the spacing along the shear span [58].

Advantages

The high strength-to-weight ratio of CFRP makes it an ideal choice for retrofitting and strengthening projects, as it adds minimal additional weight to the structure while providing substantial strength gains. Its inherent corrosion resistance ensures durability, particularly in harsh environments, where traditional materials may deteriorate over time.

Limitations

Despite its advantages, CFRP has several limitations that must be considered. The use of epoxy bonding introduces a risk of debonding, which can compromise the effectiveness of the reinforcement. While mechanical anchors can mitigate this risk, they add complexity to the installation process. Furthermore, CFRP tends to perform poorly in wet or humid environments, where the epoxy may degrade over time, reducing long-term reliability. The installation process itself is complex, requiring skilled labour and precise application to ensure optimal bonding and alignment.

2.8.4. Ultra-High Performance Concrete

Ultra-High Performance Cementitious Composite (UHPC) is made of cement, reactive powders, fine aggregates (up to 1 mm), water, admixtures and a high volume of slender steel fibres [59, 60]. Where the fibres act as a sort of reinforcement. This layer can easily be applied using a spraying method, illustrated in Figure 2.17.

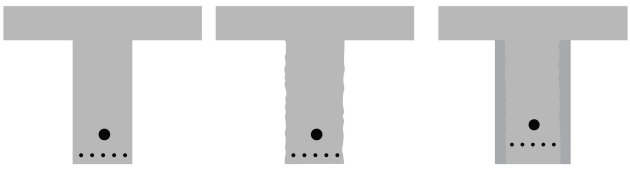

Figure 2.17: UHPC strengthening application method.

Figure 2.18: Application of UHPC strengthening [61].

Its structure differs significantly from NC offering improved performance and durability. Life Cycle Cost analysis indicates that UHPC has a longer lifespan, with spalling damage occurring after 80 years, compared to 40% damage in NC after 30 years [62]. Despite higher initial cement content and carbon emissions, the use of steel fibres and the material's longer service-life make UHPC a more sustainable option [63, 64]. Different configurations of UHPC strengthening are illustrated in Figure 2.19. Design parameters that can be adjusted to optimise strengthening include the mix composition of UHPC. However, in this study, the UHPC mix is considered constant, meaning both its compressive and tensile strength are assumed to remain unchanged. The thickness of the UHPC layer, however, is a variable parameter.

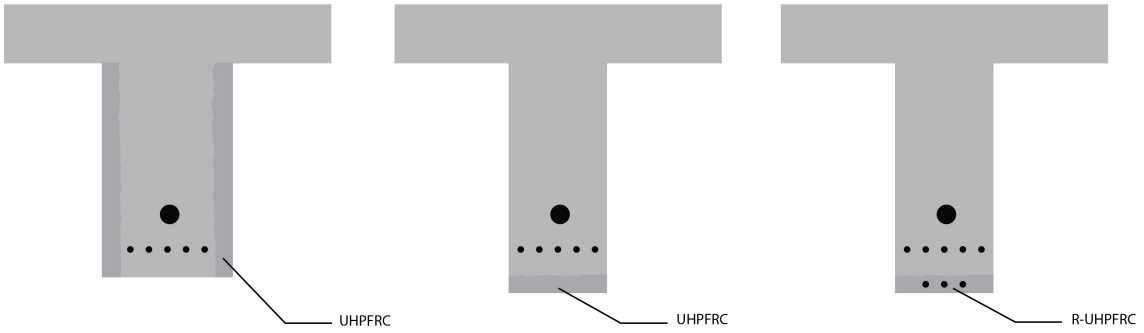

Figure 2.19: UHPC Strengthening of a T-beam.

UHPC enhances shear-deficient structures with increased shear capacity and stiffness. Lateral UHPC layers prevent height increase, while U-shaped jackets are used for added stiffness. However, relying solely on a bottom UHPC layer risks shear and separation failures [65]. UHPC's strength, durability and workability make it ideal for retrofitting [13], offering better cost-efficiency and service-life than NC. Challenges such as high costs, material variability and lack of standard design codes remain [66]. A possible composition of an UHPC mix, expressed as percentages by mass, is detailed in Table 2.10.

Table 2.10: Design mix ratio for UHPC (kg/m^3) [67].

Unit	Cement	Mineral powder	Silica fume	Sand	Water reducer (35%)	Water	Fibre
kg/m^3	820	180	100	1100	22	220	117.75
%	29.49	6.47	3.60	39.57	0.79	7.91	4.23

Advantages UHPC offers exceptional durability and strength, making it a preferred choice for retrofitting and strengthening shear-deficient structures. Its dense microstructure and inclusion of steel fibres provide superior resistance to cracking, spalling and environmental degradation, resulting in significantly extended service-life compared to Normal Concrete (NC). Resulting in less maintenance interventions required. Additionally, UHPC's ability to be applied through efficient methods, such as spraying, ensures a streamlined installation process, further enhancing its appeal for strengthening projects.

Limitations While UHPC offers numerous benefits, its high initial costs and significant carbon footprint due to its cement-intensive composition remain substantial design limitations. The lack of standardised design codes further complicates its application, often requiring tailored engineering solutions and expertise, which increases project complexity. Material variability is another concern, as achieving consistent properties in UHPC mixes can be challenging, particularly when sourcing specific components like silica fume and steel fibres.

2.9. Performance indicators

The assessment of strengthening methods focuses on the following LCA stages (NEN-EN 15804+A2): Production (A1, A3), encompassing raw material extraction and manufacturing processes. Construction (A5), which addresses the installation phase. Use (B1, B2, B3, B4, B5), including use, maintenance, repair, replacement and refurbishment activities. End of Life (C1, C2), covering deconstruction and transport processes. Also circularity is taken into account, which is covered by the Life Cycle stage (D), consisting reuse, recovery and recycling potential. An overview of considered LCA stages can be found in Appendix B, Figure B.1. Each strengthening method performance is evaluated using qualitative and quantitative indicators, focusing on sustainability, service-life, reliability, circularity and structural safety.

Sustainability is defined as meeting present needs without compromising future generations [68], including environmental, social and economic dimensions, with the environment as the most critical [69], as illustrated in Figure 2.20. Key examples include material costs, traffic hindrance and global warming power. Assessing circularity in concrete T-beams is key to identifying reuse opportunities, inspired by Coenen et al. [70]. Bridges, requiring significant materials, are often demolished due to functional changes rather than structural failure, making them ideal for increasing resource efficiency. Key examples include, scarcity, extensibility and disassembility. Safety is a prerequisite, not a criterion and must always be ensured. Strengthening should improve the damaged structure's safety by reducing failure probability through probabilistic calculations. Although, we group some of the criteria within the safety aspects and call this integrity. The integrity aspect focusses on functionality and reliability: Which are reduction in height, service-life extension and durability. Where the service-life extension should always match the desirable extension, set by the client, but this extension can differ based on the design input, which is described in Chapter 3.3.4.

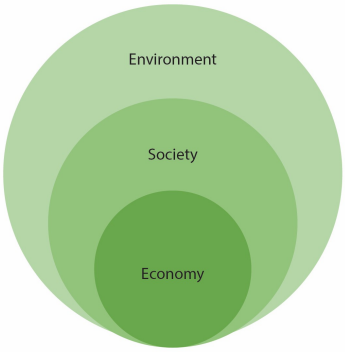

Figure 2.20: Representation of strong sustainability.

Indicators (I) were identified and bundled within Criteria (C) via a literature review of frameworks and LCAs, with input from Arup, RWS and TU Delft supervisors. All criteria align with the research objective and were selected based on the availability of information in the literature.

- **C1.** Environment
  - **I1.** Global warming potential (GWP) [kg CO_2]
  - **I2.** Acidification potential (AP) [kg SO_2]
  - **I3.** Abiotic depletion potential: fossil fuels (ADPf) [MJ]
- **C2.** Economy
  - **I4.** Material costs [Euro]
  - **I5.** Construction speed [-]
  - **I6.** Construction costs [-]
  - **I7.** Maintenance costs [-]
- **C3.** Society
  - **I8.** Human toxicity [kg 1,4 DB-eq]
  - **I9.** Traffic hindrance [-]
- **C4.** Functionality
  - **I10.** Reduction in height [m]
- **C5.** Reliability
  - **I11.** Service-life extension [years]
  - **I12.** Durability (related to corrosion) [-]
- **C6.** Resource availability
  - **I13.** Scarcity [-]
- **C7.** Adaptability
  - **I14.** Extensibility [-]
  - **I15.** Strengthenability [-]
- **C8.** Reusability
  - **I16.** Disassembility [-]
  - **I17.** Transportability [-]

Note: This list is far from complete and depending on the stakeholders, this list can be subject to change.

3

Research method

This chapter outlines the approach used to develop the decision-making framework. First, the strength increase achieved by various strengthening methods —EP, MS, CFRP and UHPC — is predicted and validated against experimental data (Chapter 3.1). If the predictions deviate from the experimental results, the model undergoes iterative refinement until acceptable values are reached. The validation process is detailed in Chapter 3.2, with an overview of the results provided in Chapter 3.2.5. The second part of the research method addresses time-dependent phenomena in structural assessments (Chapter 3.3). By incorporating reliability analysis, the approach enables the prediction of the structure's current state, its evolution over time and its End of Life. Multi-criteria decision-making is then applied to determine whether strengthening the T-beam or complete replacement is the optimal choice. Specifically, the Analytical Hierarchy Process (AHP) is employed as a mathematical tool to compare alternatives and identify the most effective strengthening solution (Chapter 3.5). Finally, all considerations are combined into the parametric framework, which is analysed (Chapter 4) and applied to a case study (Chapter 5). The overall approach is illustrated in Figure 3.1.

Figure 3.1: Visual of the research method.

3.1. Strengthening prediction

Analysing and predicting the shear and bending resistance of prestressed T-girders is challenging due to the complex interactions of various phenomena. This section aims to simplify the strengthening methods and their analytical calculation approaches, providing a structured estimation of their impact on shear and bending resistance. For each strengthening method, a corresponding analytical model is referenced and the predicted impacts are compared with experimental results from the literature. The primary focus is on shear strengthening, where strengthening is applied in the vertical direction. In contrast, bending strengthening is typically applied along the bottom of the web over the full length of the beam. These strengthening methods were selected for analysis due to the availability of extensive experimental data in the literature, specifically for their application to shear and bending enhancement in T-beams. This ensures that the analytical models can be validated against well-documented experimental findings.

3.1.1. External prestressing

The key factors influencing the strengthening effect of external prestressing include the increase in steel area within the cross-section, the magnitude of the applied stress and the method of anchoring the external prestressing. To model the increased shear capacity by external prestressing, the theory of Qi et al. [71] is applied. The model evaluates the shear strength of externally prestressed concrete beams with straight (Equation 3.1) and inclined tendons (Equation 3.2) by combining truss and arch action mechanisms.

$$V_{Rd,EP} = V_{\text{arch}} \tag{3.1}$$

$$V_{Rd,EP} = V_{\text{arch}} + V_{s,\text{arch}} \tag{3.2}$$

Where $V_{Rd,s}$ is given in Equation 2.22. The primary arch action can be calculated according to Equation 3.3.

$$V_{arch} = \frac{v f_{ck} b_w a_{arch}}{\sqrt{1 + (a/z)^2}} \tag{3.3}$$

Where v is the softening coefficient, f_{ck} is the cylinder compressive strength of concrete, b_w is the web width, z is the internal arm length and a_{arch} is the effective depth of the arch action. For beams with inclined tendons, the secondary arch contribution $V_{s,\text{arch}}$ is calculated through Equation 3.4

$$V_{s,arch} = \frac{F_p}{2} = A_p f_p \sin\alpha \tag{3.4}$$

Where A_p is the area of external tendons, f_p is the effective prestress in the tendons and α is the angle of tendon inclination. According to Wang et al. [72] the bending resistance of external prestressed specimens can be calculated, if the compression zone is less than the thickness of the flange, based on Equation 3.5. Where f_p should not exceed $0.7 * f_{pu}$, which is the characteristic strength of the steel. Where σ_{EP} is the prestress and A_{EP} is the prestressing area.

$$M_{Rd,EP} = A_{p,EP} \cdot \sigma_{p,EP} \cdot d_{EP} \tag{3.5}$$

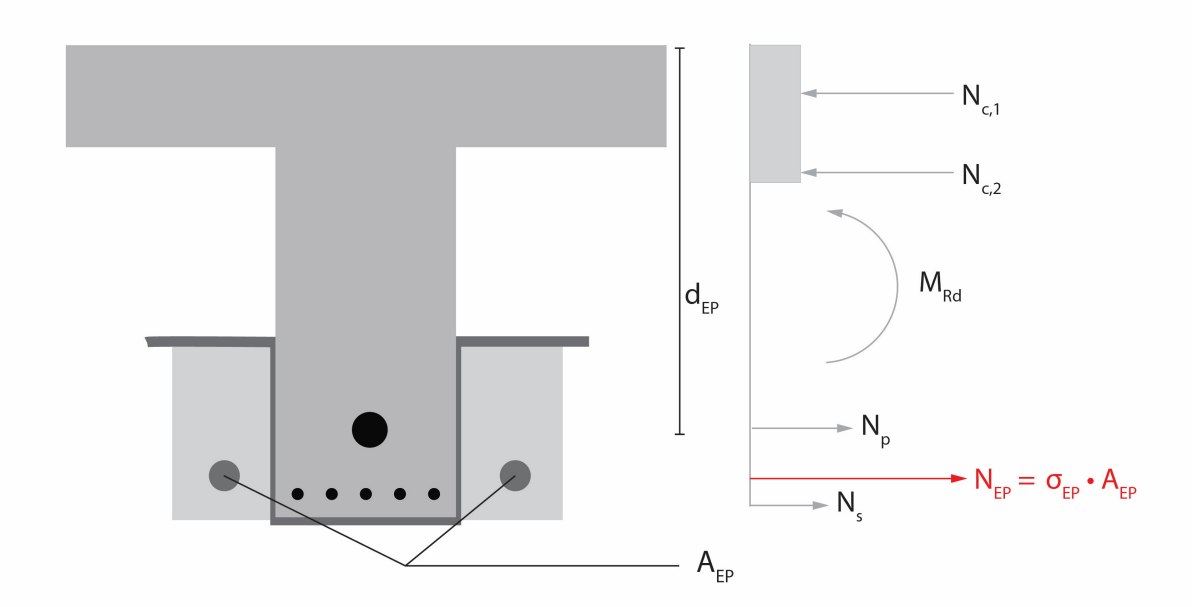

Figure 3.2: Bending strengthening calculation for external prestressing using the equilibrium method.

3.1.2. Memory-steel

For memory-steel strengthening, the ultimate limit state for shear design can be evaluated by disregarding the prestressing force in the shear reinforcement and using standard equations provided in codes and guidelines [42]. It is assumed that the shotcrete layer had pre-existing cracks due to shrinkage before activation. Therefore, the tensile strength of the shotcrete (f_{ct}) at the bottom is assumed to be zero and the shotcrete is considered to have no impact on the bending moment resistance. Resulting in Equation 3.6.

$$V_{Rd,\text{MS}} = \frac{2 \cdot \sigma_{p,\infty} \cdot A_{s,MS} \cdot z \cdot \cot(\theta)}{s} \tag{3.6}$$

Where $\sigma_{p,\infty}$ is the prestress after activating the Memory-steel, $A_{s,MS}$ is the area of the Memory-steel. The bending capacity is evaluated using the equilibrium model according to Shahverdi et al. [73], where the total moment capacity is influenced by the concrete area, ordinary steel reinforcement, the prestressed steel area (Equation 3.7) and the tensile contribution (Equation 3.8).

$$M_{\text{Rd,prestress}} = \sigma_{\text{MS}} \cdot A_{\text{MS}} \cdot d_{MS} \tag{3.7}$$

$$M_{\text{Rd,tensile}} = f_{\text{y,MS}} \cdot A_{\text{MS}} \cdot d_{MS} \tag{3.8}$$

$$M_{\text{Rd,MS}} = M_{\text{Rd,MS,prestress}} + M_{\text{Rd,MS,tensile}} \tag{3.9}$$

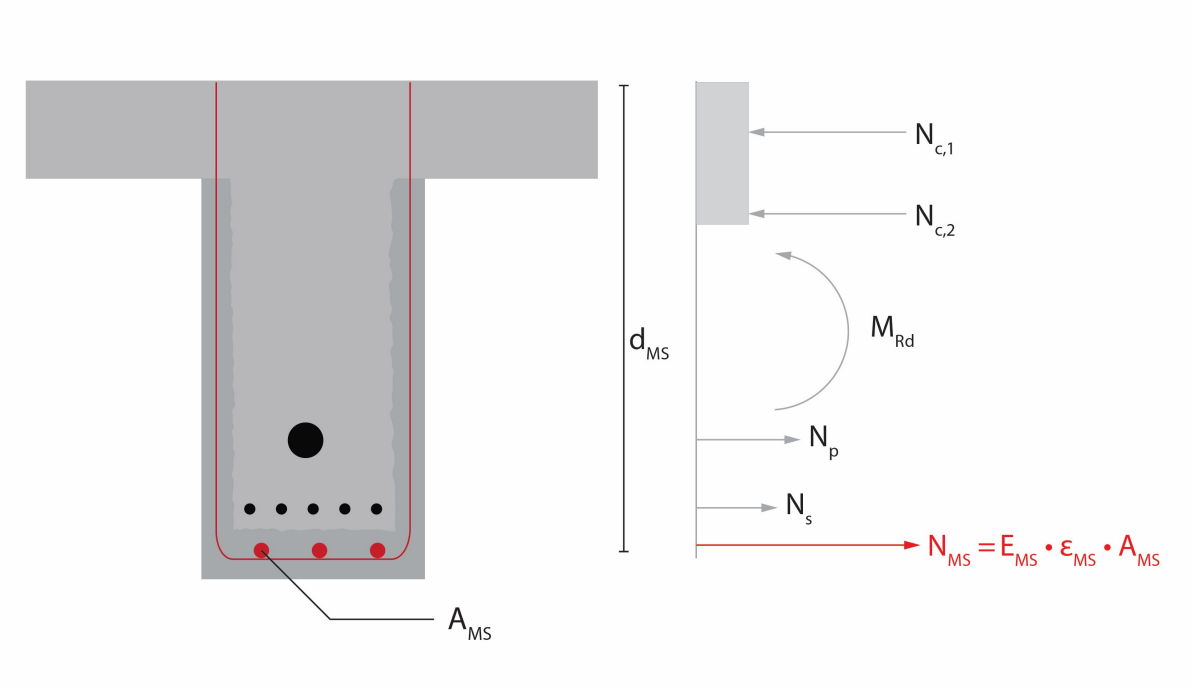

Figure 3.3: Bending strengthening calculation for memory-steel using the equilibrium method.

3.1.3. Carbon Fibre Reinforced Polymer

For CFRP strengthening, using U-jacketing and wrapping configurations, the Mörsch truss resisting mechanism is activated. The shear contribution of CFRP is calculated in Equation 3.13. Which depends on the effective length (3.10), debonding strength (3.11) and effective strength (3.12).

$$l_{eff} = \sqrt{\frac{E_{FRP} \cdot t_{FRP}}{2 \cdot f_{ctm}}} \tag{3.10}$$

$$f_{fdd} = \frac{0.80}{\gamma_{fd}} \cdot \sqrt{\frac{2 \cdot E_{FRP} \cdot \gamma_{Fk}}{t_{FRP}}} \tag{3.11}$$

$$f_{fed} = f_{fdd} \cdot \left(1 - \frac{1}{3} \cdot \frac{l_e \cdot \sin(\beta)}{\min(0.9 \cdot d, h_w)}\right) \tag{3.12}$$

$$V_{Rd,FRP} = \frac{1}{\gamma_{Rd}} \cdot 0.9d \cdot f_{fed} \cdot 2 \cdot t_f \cdot (\cot\theta + \cot\beta) \cdot \frac{w_f}{s_f} \tag{3.13}$$

Where d is the effective depth of the beam, f_{fed} the design effective strength of CFRP, $t_f$hickness of CFRP strip or sheet w_f, s_f the width and spacing of CFRP strips or sheets, θ the crack angle and β the angle of CFRP strip or sheet. Assuming a crack angle $\theta = 45°$ and vertically aligned CFRP strips or sheets ($\beta = 90°$). The anchorage of CFRP strips is improved by increasing the debonding strength, although this method has shown limited reliability. The increase in bending resistance can be calculated using the equilibrium model, as demonstrated by Picard et al. [74], Nguyen et al. [75] and Rasheed et al. [76], provided in Equation 3.4.

$$M_{Rd,FRP} = E_{FRP} \cdot \epsilon_{FRP} \cdot A_{FRP} \cdot d_{FRP} \tag{3.14}$$

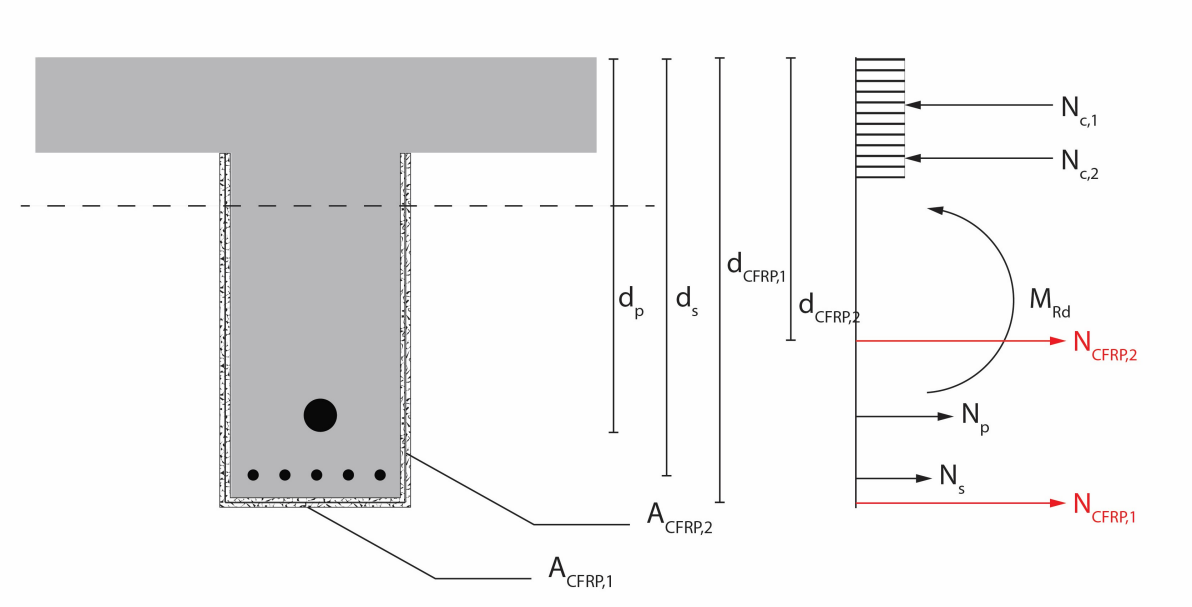

Figure 3.4: Bending strengthening calculation for CFRP using the equilibrium method.

3.1.4. Ultra-High Performance Concrete

Hong et al. [77] propose a model for the shear strength of UHPC-strengthened girders, assuming that only UHPC jackets on both sides resist shear. The UHPC at the bottom is not considered for estimating the shear strength of U-shaped-strengthened girders, with perfect bonding assumed between the existing concrete and UHPC, given in Equation 3.15.

$$V_{Rd,UHPC} = 0.5 \cdot \sqrt{f_{cd,UHPC}} \cdot t_{UHPC} \cdot d \tag{3.15}$$

Where $f_{cd,UHPC}$ is the compressive strength of UHPC, t_{UHPC} is the thickness of the UHPC-layer and d is the effective depth. The predicted moment strength (M_{pred}) for the side-strengthened beam is calculated using equilibrium conditions (Equation 3.16), also according to Hong et al. [77].

$$M_{Rd,UHPC} = A_{UHPC} \cdot f_{ct,UHPC} \cdot d_{UHPC} \tag{3.16}$$

Where A_{UHPC} is the area of the UHPC within the cross-section direction, $f_{ct,UHPC}$ is the tensile strength and d_{UHPC} the equivalent moment arm.

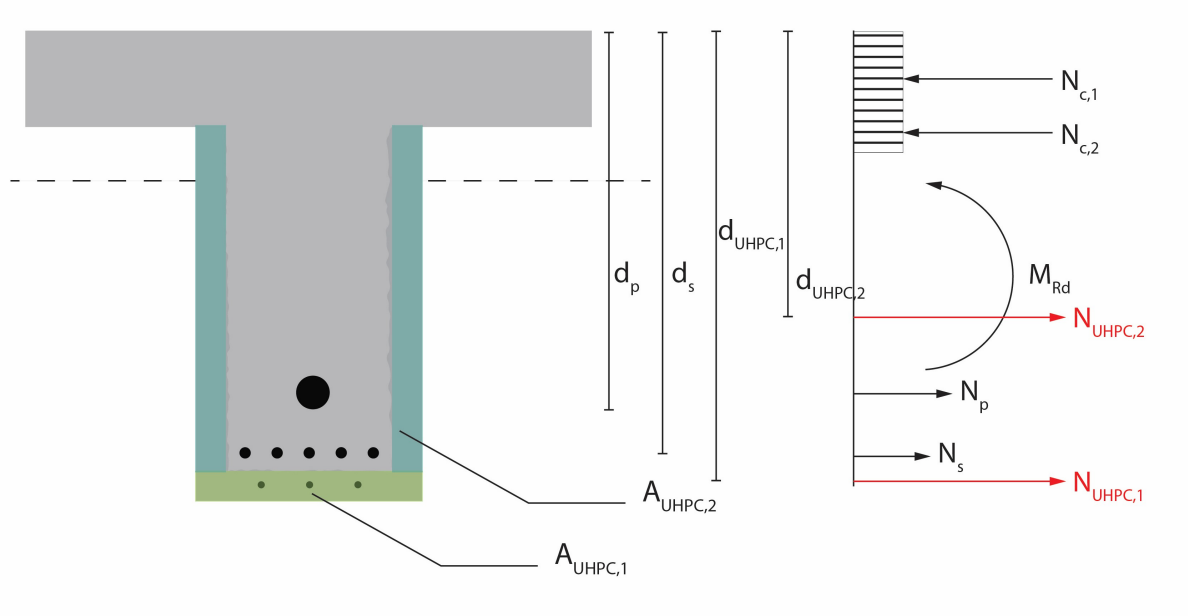

Figure 3.5: Bending strengthening calculation for UHPC using the equilibrium method.

3.2. Strengthening validation

For every strengthening method, the predictions for shear and bending resistance are assessed. Experimental shear or bending failure values are derived from the literature for each specimen and theoretical resistance values are calculated using the equations provided in Chapter 3.1. Bending resistance, M_{Rd}, is evaluated at mid-span, while shear resistance, V_{Rd}, is determined near critical shear locations, typically at the beam ends. The theoretical failure load, P_{th}, is used to calculate the theoretical bending failure M_{th} and theoretical shear failure V_{th} through static equations. In three-point bending tests, critical shear and bending resistances are determined using Equations 3.17 and 3.18.

$$V_{th} = \frac{P}{2} \tag{3.17}$$

$$M_{th} = \frac{P \cdot L}{4} \tag{3.18}$$

In four-point bending tests, the corresponding values are calculated using Equations 3.19 and 3.20.

$$V_{th} = \frac{P}{2} \tag{3.19}$$

$$M_{th} = \frac{P \cdot a}{2} \tag{3.20}$$

Validation confirms the expected failure modes (shear or bending) by comparing the theoretical failure loads for each mode. This comparison helps identify the likely failure mode for the beam and serves as a final check to validate the calculations.

As experimental data is used, safety factors are excluded from the calculations. The same validation approach is applied to assess shear strengthening. All experiments are discussed in the following sections of the report. For each strengthening method, the type of load test is indicated, along with a description of the modifications made to each beam. Note that not all reference specimens are T-beams.

3.2.1. External prestressing

To validate the increase in shear strength achieved through external prestressing, the study by Qi et al. [71] is used as the primary reference. In this study, externally prestressed T-beams were tested to failure to investigate the effects of key parameters such as prestressing level, shear span-to-depth ratio, shear reinforcement and the angle of external tendons on the shear behaviour and ultimate capacity of the beams. The experimental programme included several configurations: S-2, which served as the control beam without external tendons, S-8, incorporating straight external tendons, S-9, with external tendons inclined at an angle of 3.57 degrees and S-1, with external tendons inclined at an angle of 7.40 degrees. The experimental setup used to study the impact of inclined external tendons on shear behaviour is illustrated in Figure 3.6.

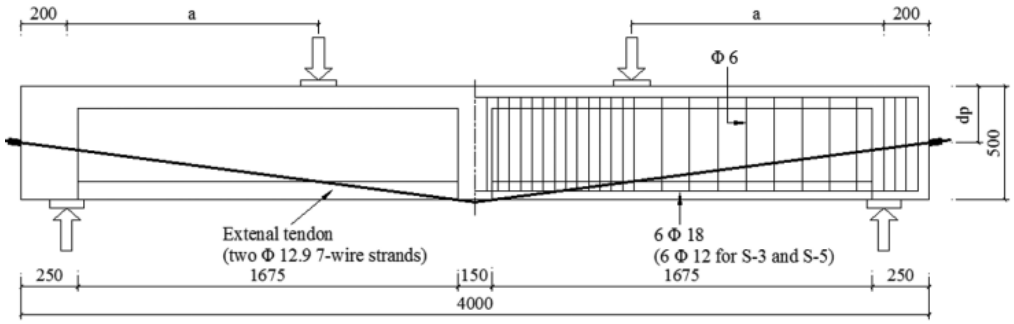

Figure 3.6: Experimental set-up for external prestressing with inclined tendons [71].

Table 3.1 presents the validation results for the increase in shear capacity due to external prestressing. The ratio of experimental to theoretical shear capacity (V_{exp}/V_{th}) ranges between 1.15 and 1.25, indicating that the predictions are conservative. Additionally, the theoretical failure load for shear is significantly lower than the corresponding value for bending, confirming that the failure observed in the experiment is governed by shear. This aligns with the failure modes reported by the authors, all classified as shear compression.

Table 3.1: Validation results of shear increase by external prestressing.

Specimen	V_{exp} [kN]	V_{th} [kN]	V_{exp}/V_{th} [-]	$P_{V_{th}}$ [kN]	M_{th} [kNm]	$P_{M_{th}}$ [kN]	Failure mode
S-2	261.0	210.5	1.15	210.5	672.1	1210.8	Shear compression
S-8	345.0	298.5	1.16	298.5	654.1	1189.3	Shear compression
S-9	360.6	315.8	1.14	315.8	672.1	1210.8	Shear compression
S-1	407.6	325.7	1.25	325.7	677.8	1232.4	Shear compression

To validate the increase of bending capacity achieved through external prestressing, the study by Saïd et al. [40] is used. The investigation focusses the influence of tendon depth (eccentricity) on bending behaviour, expressed as the depth ratio—the ratio of tendon depth to the height of the section. Four identical T-beams were tested to failure. The Control Beam (CB) is unstrengthened and served as a reference. The three strengthened beams (AT-1, BT-1, DT-1) were partially strengthened over 8% of the effective span using two external tendons. These tendons were fixed at varying depths and configurations and prestressed to a constant stress of 600 MPa. All beams were subjected to two concentrated loads applied at third points to evaluate their bending performance. The experimental setup for the study is illustrated in Figure 3.7.

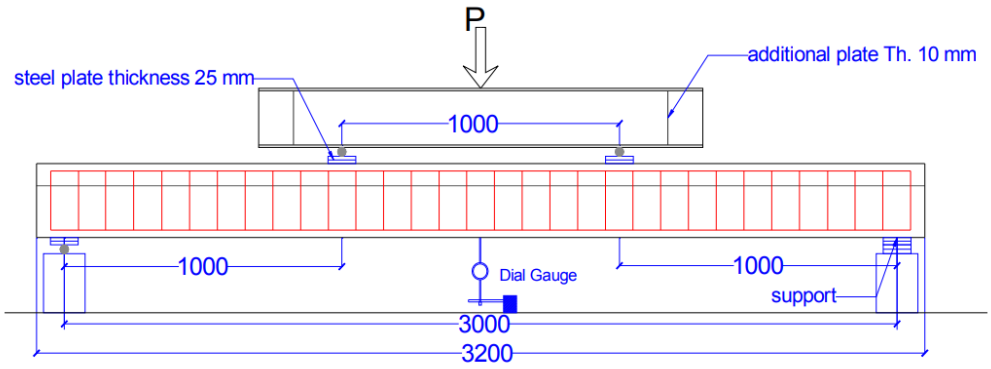

Figure 3.7: Experimental setup for bending tests with external prestressing [40].

The results of the bending capacity tests are summarised in Table 3.2. The M_{exp}/M_{th} ratios range from 0.80 to 1.09, demonstrating agreement between experimental and theoretical values. Furthermore, the theoretical applied failure loads for bending are lower, than for shear, indicating failure in bending. Matching the experimental outcomes, where most beams failed due to reinforcement yielding, except for DT-1, where failure occurred due to concrete crushing.

Table 3.2: Validation results of bending increase by external prestressing.

Specimen	M_{exp} [kNm]	M_{th} [kNm]	M_{exp}/M_{th} [-]	$P_{M_{th}}$ [kN]	V_{th} [kN]	$P_{V_{th}}$ [kN]	Failure mode
CB	31.5	53.3	0.80	106.6	131.0	262.0	Reinforcement yielding
AT-1	56.0	64.2	0.87	128.4	131.0	262.0	Reinforcement yielding
BT-1	66.5	70.4	0.95	140.8	133.0	266.0	Reinforcement yielding
DT-1	70.0	64.2	1.09	128.4	132.4	264.8	Concrete crushing

3.2.2. Memory-steel

The shear-strengthening capabilities of memory-steel were validated using the study by Czaderski et al. [42]. This research investigated the application of memory-steel in the form of U-shaped ribbed bars with a nominal diameter of 12 mm, combined with sprayed mortar. The memory-steel bars were activated through electric resistive heating, which induced a prestress of approximately 300 N/mm². The following beam configurations were tested: B1, the control beam without memory-steel, B3, strengthened with three unprestressed external memory-steel bars and B6, strengthened with five unprestressed external memory-steel bars. The experimental setup for studying the shear behaviour of memory-steel-strengthened beams is illustrated in Figure 3.8.

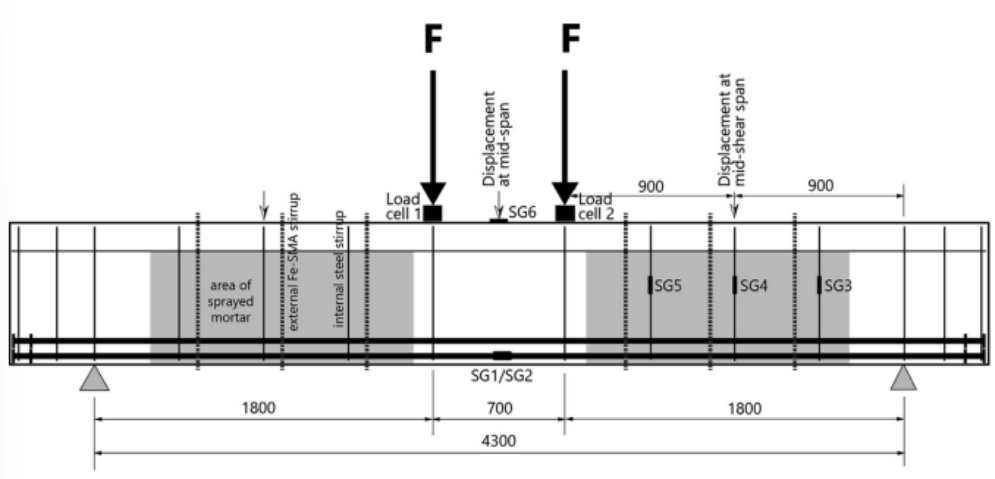

Figure 3.8: Memory-steel, experiment set-up for shear [42].

Validation results, presented in Table 3.3, with experimental-to-theoretical strength ratios (V_{exp}/V_{th}) exceeding 1.0 in most cases, which means the prediction is quite conservative. Also the theoretical failure load for shear is below the failure for bending, confirming the failure mode that is in shear compression.

Table 3.3: Validation results of bending increase by memory-steel.

Specimen	V_{exp} [kN]	V_{th} [kN]	V_{exp}/V_{th} [-]	$P_{V_{th}}$ [kN]	M_{th} [kNm]	$P_{M_{th}}$ [kN]	Failure mode
B1	156.7	161.3	0.97	322.6	482.1	535.7	Shear compression
B3	266.35	211.9	1.26	423.8	472.8	525.3	Shear compression
B6	291.5	301.8	0.97	603.6	503.8	559.8	Shear compression

The bending-strengthening performance of memory-steel is validated through the study by Shahverdi et al. [73], which explored ribbed Fe-SMA bars embedded in a shotcrete layer. The study involved four rectangular RC beams: A control beam (1), two strengthened with prestressed Fe-SMA bars embedded in shotcrete (10, 11) and one reference beam reinforced with conventional steel bars (9). The beams were subjected to bending tests, including activation and four-point bending to failure. The experimental setup for bending tests is illustrated in Figure 3.9. Beams strengthened with Fe-SMA bars exhibited higher cracking loads and reduced deflections, confirming the effectiveness of the technique. The strengthened beams demonstrated better bending behaviour and load-bearing capacity compared to the reference beam.

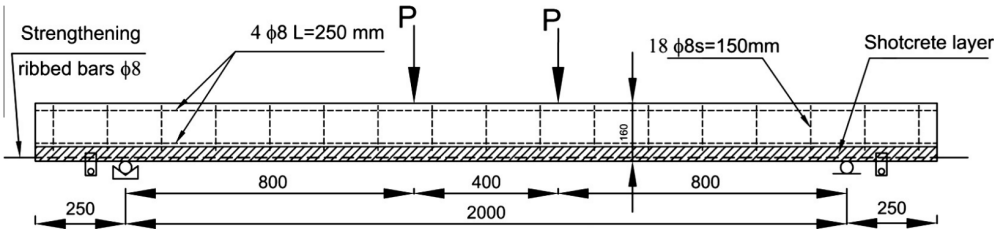

Figure 3.9: Memory-steel, experiment set-up for bending [73].

Table 3.4 summarises the bending test results. The experimental-to-theoretical moment ratios (M_{exp}/M_{th}) indicate a conservative strength prediction. Furthermore, the failure loads for bending are lower than those for shear, confirming that the failure mode observed is bending, which corresponds to steel yielding in the experiments.

Table 3.4: Validation results of bending increase by memory-steel.

Specimen	M_{exp} [kNm]	M_{th} [kNm]	M_{exp}/M_{th} [-]	$P_{M_{th}}$ [kN]	V_{th} [kN]	$P_{V_{th}}$ [kN]	Failure mode
1	7.8	7.1	1.10	8.8	18.9	18.9	Steel yielding
9	15.3	12.5	1.22	15.6	18.9	18.9	Steel yielding
10	17.0	13.4	1.27	16.8	18.9	18.9	Steel yielding
11	25.6	20.4	1.25	25.5	18.9	18.9	Steel yielding

3.2.3. Carbon Fibre Reinforced Polymer

The shear strengthening of reinforced concrete (RC) T-beams using epoxy-bonded CFRP is validated in the study by Chalioris et al. [78]. The tested beam configurations were as follows: the T beam, which served as the control beam without shear reinforcement, the TS beam, which included shear reinforcement, the T2J beam, strengthened with two CFRP sheets in a U-jacket configuration, the T3J beam, strengthened with three CFRP sheets in a U-jacket configuration and the T2J-A beam, which included two CFRP sheets in a U-jacket configuration with bolted steel anchorage. All beams were tested under four-point bending to evaluate their shear performance. The experimental setup for assessing the shear strengthening effect of CFRP is illustrated in Figure 3.10. The results demonstrated significant improvements in shear capacity for the CFRP-strengthened beams compared to the unstrengthened control beams.

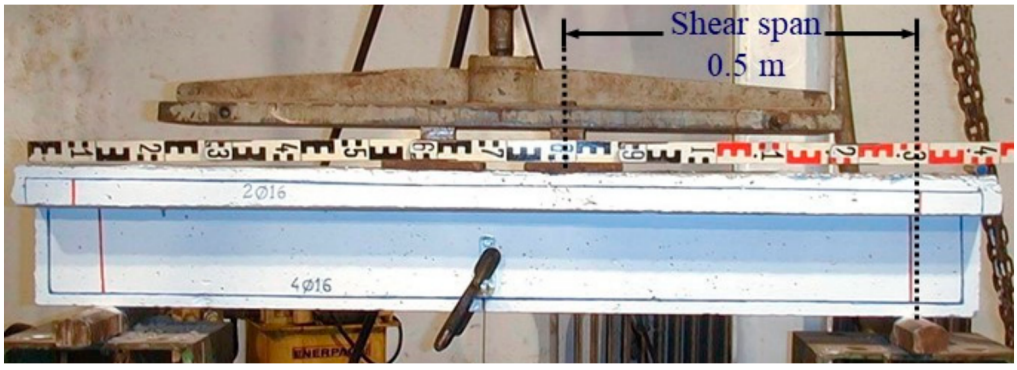

Figure 3.10: CFRP, experiment set-up for shear [78].

Table 3.5 summarises the results, presenting the ratio of experimental to theoretical shear capacity (V_{exp}/V_{th}), which demonstrates conservative predictions. Furthermore, the theoretical failure loads for shear are consistently lower than those for bending, confirming that the failure mode is in shear, consistent with the observed shear compression failure mode in the experiments.

Table 3.5: Validation results of shear increase by CFRP.

Specimen	V_{exp} [kN]	V_{th} [kN]	V_{exp}/V_{th} [-]	$P_{V_{th}}$ [kN]	M_{th} [kNm]	$P_{M_{th}}$ [kN]	Failure mode
T	58.8	46.9	1.25	93.8	251.1	1004.4	Shear compression
TS	93	75.6	1.23	151.2	260.2	1040.8	Shear compression
T2J	81.8	74.4	1.10	148.8	254.3	1017.2	Shear compression
T3J	101.3	88.1	1.15	176.2	248.2	992.8	Shear compression
T2J-A	101.0	94.9	1.06	189.8	249.5	998	Shear compression

The bending performance of CFRP-strengthened beams is evaluated in the study by Nguyen-Minh et al. [75]. This study investigated the effect of CFRP strengthening on the flexural behaviour of reinforced concrete beams. The tested beam configurations included the M0 control beam without CFRP strengthening, the M2CB beam strengthened with two CFRP sheets, the M4CB beam strengthened with four CFRP sheets and the M6CB beam strengthened with six CFRP sheets. The experimental setup for the bending tests with CFRP-strengthened beams is depicted in Figure 3.11.

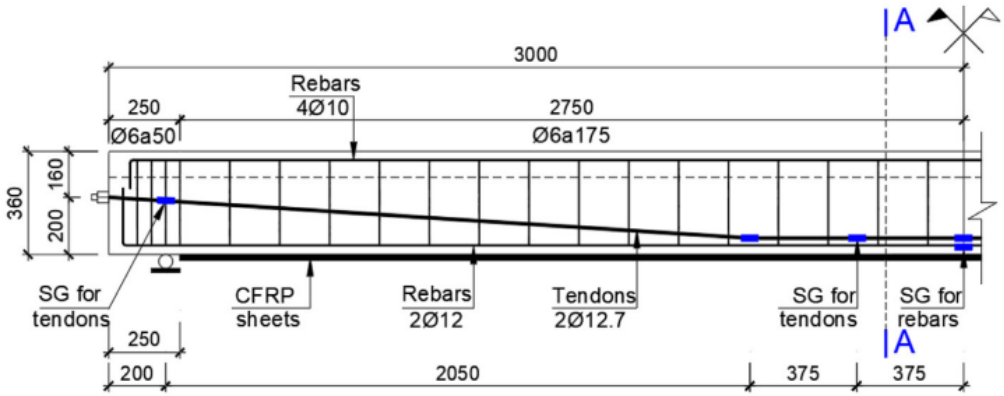

Figure 3.11: CFRP, experiment set-up for bending [75].

Table 3.6 summarises the results, presenting experimental and theoretical bending moments (M_{exp}, M_{th}) along with the observed failure modes. The experimental-to-theoretical ratios (M_{exp}/M_{th}) are below 1.0 in all cases, indicating unconservative predictions. Additionally, the debonding of the CFRP sheets is the governing failure mode in three out of four cases.

Table 3.6: Validation results of bending increase by external prestressing.

Specimen	M_{exp} [kNm]	M_{th} [kNm]	M_{exp}/M_{th} [-]	$P_{M_{th}}$ [kN]	V_{th} [kN]	$P_{V_{th}}$ [kN]	Failure mode
M0	135.6	159.6	0.85	170.7	112.1	224.2	Concrete crushing
M2CB	145.9	168.3	0.87	180.0	112.4	224.8	Debonding of CFRP
M4CB	154.3	177.0	0.87	189.3	111.8	223.6	Debonding of CFRP
M6CB	177.7	185.8	0.96	198.7	112.2	223.4	Debonding of CFRP

3.2.4. Ultra-High Performance Concrete

The shear-strengthening effects of UHPC layers on T-beams were validated in the study by Liu et al. [79]. This research investigated the performance of three T-beams strengthened with cast-in-place UHPC layers and one reference beam. All beams were tested under a three-point bending to evaluate their shear capacity. The experimental setup for shear strengthening with UHPC is illustrated in Figures 3.12. The beam configurations included the TS-R control beam without UHPC strengthening, the TS-W25 beam with 25 mm thick UHPC layers applied on both sides of the web, the TS-W50 beam with 50 mm thick UHPC layers on both sides of the web and the TS-W50-A beam, which also had 50 mm thick UHPC layers but with additional anchorage to the web.

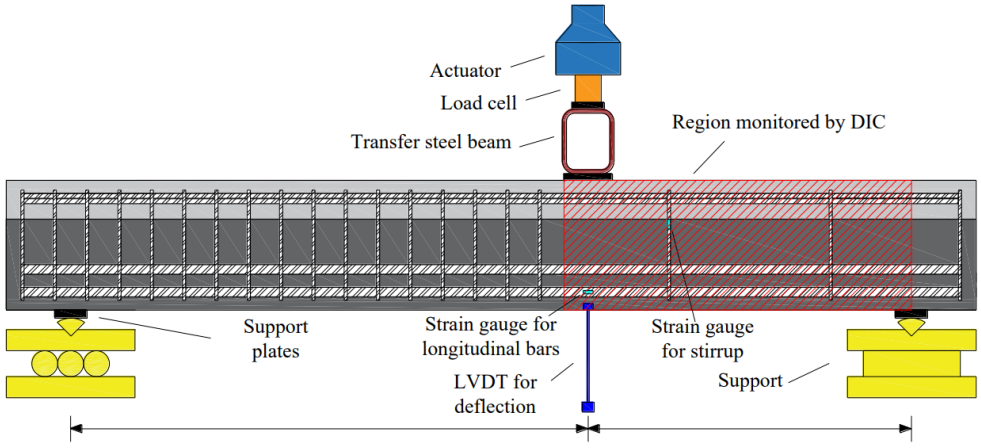

Figure 3.12: UHPC, experiment set-up for shear [79].

Table 3.7 summarises the shear test results, showing that the experimental and theoretical values are closely related, providing a reasonable prediction. The V_{exp}/V_{th} ratios generally indicate good agreement, demonstrating the effectiveness of the UHPC strengthening method. The TS-W50-A beam failed in bending-shear compression, which aligns with its failure loads for shear and bending, relating the combined influence of these mechanisms.

Table 3.7: Validation results of bending increase by memory-steel.

Specimen	V_{exp} [kN]	V_{th} [kN]	V_{exp}/V_{th} [-]	$P_{V_{th}}$ [kN]	M_{th} [kNm]	$P_{M_{th}}$ [kN]	Failure mode
TS-R	176.1	191.6	0.92	383.2	515.7	542.8	Shear compression
TS-W25	355.0	277.6	1.28	555.2	513.9	540.6	Shear compression
TS-W50	374.3	363.6	1.03	727.2	512.5	539.5	Shear compression
TS-W50-A	379.6	380.7	1.00	761.4	512.5	539.5	Bending-shear compression

The bending capacity improvement provided by UHPC is validated using the study by Li et al. [67]. The availability of experimental data on UHPC bending in the literature is limited, with only two specimens tested in this study. The specimens included an RC control beam without UHPC strengthening and an NC beam strengthened with a RUHPC layer applied to the bottom of the web. The experimental configuration for the bending tests is illustrated in Figure 3.13.

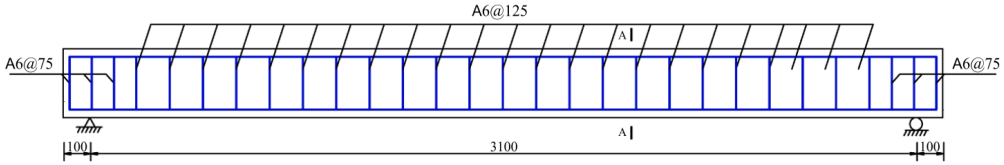

Figure 3.13: UHPC, experiment set-up for bending [67].

Drawing conclusions from the bending tests is challenging due to the limited number of specimens. Table 3.8 summarises the bending test results. The experimental-to-theoretical ratios (M_{exp}/M_{th}) fall within the range of 0.8–1.2, indicating reasonable alignment between experimental and theoretical values. Both specimens exhibited failure in bending, as predicted, which is consistent with the experimental observations.

Table 3.8: Validation results of bending increase by external prestressing.

Specimen	M_{exp} [kNm]	M_{th} [kNm]	M_{exp}/M_{th} [-]	$P_{M_{th}}$ [kN]	V_{th} [kN]	$P_{V_{th}}$ [kN]	Failure mode
RC	130.4	58.9	0.86	152.0	129.1	258.2	Bending failure
NC-RUHPC	75.6	62.5	1.21	161.3	150.0	300.0	Bending failure

3.2.5. Overview of validation

The comparison of experimental versus theoretical results shows that most values are within the range of 0.8–1.2. This uncertainty is governed by experimental results, which are taken into account within the FORM process. The uncertainty in predictions due to experimental results is thus incorporated into the analysis.

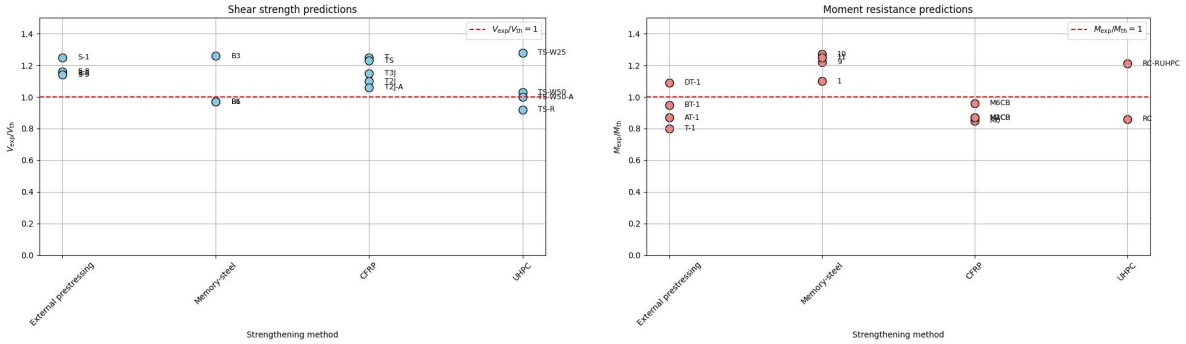

(a) Validation values for shear.

(b) Validation values for bending.

Figure 3.14: Validation values for shear and bending.

The comparison of experimental versus theoretical results shows that shear predictions are generally conservative, with most V_{exp}/V_{th} ratios exceeding or close to 1.0, particularly for CFRP and UHPC strengthening methods. In contrast, bending predictions tend to be slightly unconservative, with M_{exp}/M_{th} ratios below 1.0 for most cases, especially for CFRP and RC beams, though some configurations, such as UHPC, exhibit conservative results. These trends highlight the reliability of theoretical shear predictions and the need for refinement in bending resistance models, especially for CFRP-strengthened beams. All in all, the strengthening predictions perform quite well, but careful consideration is needed when interpreting the results.

3.3. Design of strengthening methods

Following validation of strengthening, the design of the strengthening methods can be developed. The design process is informed by several key factors. Input from the literature provides strengthening principles that align with those demonstrated in the previous chapter. Additionally, the design should be based on the evaluation that considers shear and bending demands, identifying specific locations where an increase in shear or bending capacity is necessary. Lastly, it should consider current reliability and the extension of service-lifetime by strengthening.

3.3.1. Current reliability

The reliability index β provides a probabilistic measure of structural safety, taking into account the variability and influence of resistance and load effects. By assessing the structures current reliability, we can define its condition state, which is the starting point of the strengthening design. The current reliability is calculated using FORM, according to Equation 3.21.

$$\beta = \frac{\mu_R - \mu_S}{\sqrt{\sigma_R^2 + \sigma_S^2}} \tag{3.21}$$

The mean resistance, μ_r, in Equation 3.21 is the sum of the shear resistances of the steel ($V_{Rd,s}$) and concrete ($V_{Rd,c}$). These values are influenced by the statistical parameters summarised in Table 3.9. The variability in resistance, σ_r (Equation 3.23), accounts for uncertainties in key structural parameters. Steel reinforcement area (A_{sl}) includes variations due to construction tolerances and manufacturing precision. Concrete compressive strength (f_{ck}) reflects natural variability in concrete properties. T-beam cross-sectional area (A_c) incorporates geometric imperfections or deviations from nominal dimensions. Reduction of diameter (d_s) captures potential wear, corrosion, or other degradation factors. Prestress level (σ_p) varies with material properties, aging effects and installation inconsistencies. Each term in σ_r is scaled by its corresponding coefficient of variation (CoV) to effectively model the uncertainty introduced by these parameters.

$$\mu_r = V_{Rd,s} + V_{Rd,c} \tag{3.22}$$

$$\sigma_r = \sqrt{(A_{sl} \cdot A_{sl,\text{cov}})^2 + (f_{ck} \cdot f_{ck,\text{cov}})^2 + (A_c \cdot A_{c,\text{cov}})^2 + (d_s \cdot d_{s,\text{cov}})^2 + (\sigma_p \cdot \sigma_{p,\text{cov}})^2} \tag{3.23}$$

The mean load effect, μ_s, combines the contributions of dead loads ($V_{Ed,g}$) and live loads ($V_{Ed,q}$), representing the average applied load on the structure. The variability in load effects, σ_s, is described as the square root of the sum of variances for dead and live loads, scaled by their respective CoVs. Dead loads ($V_{Ed,g}$) are typically less variable due to their predictable nature, such as the self-weight of materials. Live loads ($V_{Ed,q}$), on the other hand, exhibit higher variability influenced by traffic intensity and dynamic factors.

$$\mu_s = V_{Ed,g} + V_{Ed,q} \tag{3.24}$$

$$\sigma_s = \sqrt{(V_{Ed,g} \cdot V_{Ed,g,\text{cov}})^2 + (V_{Ed,q} \cdot V_{Ed,q,\text{cov}})^2} \tag{3.25}$$

An overview of statistical parameters is given in Table 3.9. The Table can be classified into five categories, (1) Initial structure, (2) External Prestressing, (3) Memory-steel, (4) CFRP and (5) UHPC. Some parameters are not considered as a random variable. Since these are usually nominal values and subject to a lot of quality control. All non-normal distributions are translated to normal distributions.

Shear and moment loads are divided into live and dead loads, with live loads following a Type I extreme value distribution and dead loads following a normal distribution. Live load means are derived from traffic analysis and Load Model 1. Parameters in category (1) depend on framework inputs, so exact means are not provided. The compressive strength of concrete is modelled with a normal distribution and a CoV of 0.10, reflecting typical material variability. Diameter reduction follows a log-normal

distribution, representing the variability due to corrosion. For prestress, different parameters are considered based on the age of prestressed cables (< 5 years or > 30 years). Strengthening parameters are drawn from literature and serve as initial design values but may change during optimisation.

Table 3.9: Summary of variables, distributions and references.

Variable	Symbol	Distribution	Mean	CoV	Reference
Shear live load	$V_{Ed,q}$	Type I extreme value	$\mu_{V,q}$	0.18	[80]
Shear dead load	$V_{Ed,g}$	N	$\mu_{V,g}$	0.10	[80]
Moment live load	$M_{Ed,q}$	Type I extreme value	$\mu_{M,q}$	0.18	[80]
Moment dead load	$M_{Ed,g}$	N	$\mu_{M,g}$	0.10	[80]
Compressive strength concrete	f_{ck}	N	$\mu_{f,ck}$	0.10	[80]
Dimensions of T-beam	A_c	N	μ_d	0.10	[30]
Reduction of diameter	d_s	LN	$\mu_{d,s}$	0.15	[81]
prestress (age <5 years)	$\sigma_{p,5}$	N	$\mu_{\sigma,p,5}$	0.4	[81]
prestress (age >30 years)	$\sigma_{p,30}$	N	$\mu_{\sigma,p,30}$	0.12	[81]
Reduction of diameter	d_p	LN	12.7	0.15	Assumed
External prestress	$\sigma_{p,EP}$	N	1067.6	0.12	Assumed
Reduction of diameter	d_{MS}	N	12	0.15	Assumed
Prestress of memory-steel	σ_{MS}	N	350	0.12	Assumed
Design effective strength	f_{FRP}	Weibull	1.5	0.02	[80]
Fibre orientation	β_{FRP}	N	$90°$	0.05	[80]
UHPC compression strength	f_{UHPC}	N	150.8	0.02	[28]
UHPC thickness	t_{UHPC}	N	40	0.05	[28]

For external prestressing, prestress values are assumed to follow a normal distribution with a CoV of 0.12, which is consistent with expected stress variations in new systems. Memory-steel includes parameters such as sprayed mortar thickness and strength. CFRP exhibits very low variability due to its fabrication method. UHPC is reflecting its superior reliability.

For each year, the reliability of the structure is calculated by considering key decaying mechanisms such as corrosion and loss of prestress (Appendix C.9, Appendix C.10). Increasing traffic loads further decay the reliability. The resulting decay curve, illustrated in Figure 3.15, illustrates how the reliability decreases annually. In this particular case, corrosion is expected to initiate after approximately 83 years, as indicated on the curve. Beyond this point, the rate of reliability decline accelerates due to the progressive impact of corrosion, as illustrated in Figure 3.16. The inclusion of corrosion introduces a critical inflection point, emphasising a higher rate of degradation compared to earlier years. To confirm the decay of reliability, each function contributing to the decay is plotted individually in Appendix D.

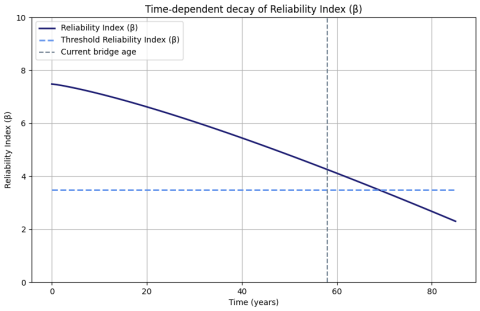

Figure 3.15: Reliability curve for shear over time.

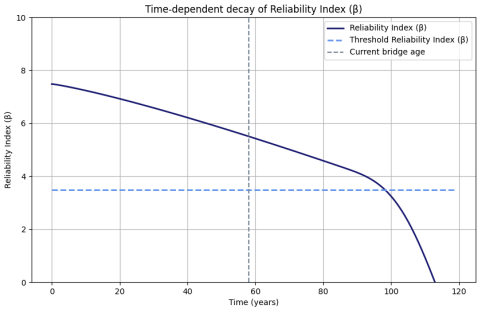

Figure 3.16: Reliability curve for shear over time, showing corrosion.

To assess the current condition of the structure, it is essential to determine its present reliability value. This is represented by the intersection of the grey dotted line with the reliability curve, marking the structure's current age. Additionally, the point at which the reliability curve meets the threshold value indicates when the structure's reliability no longer satisfies acceptable threshold values.

By examining the section of the curve between the current reliability point and the threshold value, it becomes possible to estimate the remaining service life of the structure. This decay provides crucial insights into the rate of reliability decline and gives a base point for strengthening or replacement strategies.

Reliability threshold

The stakeholder specifies the desired target for the remaining service life, which corresponds to the threshold value for reliability. Table 2.3 is used to interpolate and determine this threshold value, resulting in Figure 3.17. As the structure's service life increases and its remaining lifetime decreases, the targeted reliability level is gradually reduced. Consequently, the reliability threshold value can be adjusted over time, as illustrated in Figure 3.18.

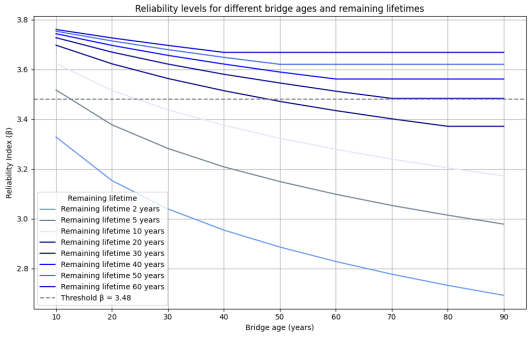

Figure 3.17: Reliability levels for concrete bridges over time.

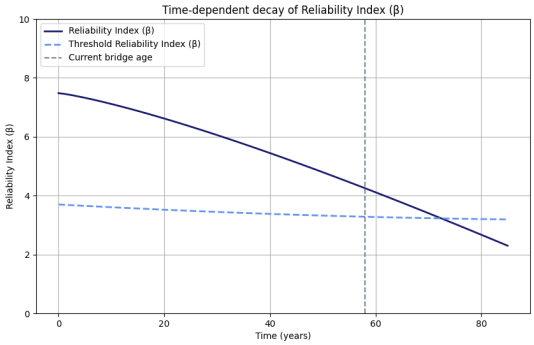

Figure 3.18: Reliability levels for concrete bridges over time, including a time-dependent threshold value.

3.3.2. Comparison in decay of reliability

The decay of reliability can be compared with those reported in the literature ([23], [26], [27], [82]). Each of these references examines the reliability decay of concrete T-beams. This comparison is presented in Figure 3.19. While direct comparison is challenging due to variations in structural characteristics and parameters, these studies provide valuable insights. A code snippet of the reliability curve can be found in Appendix C.11.

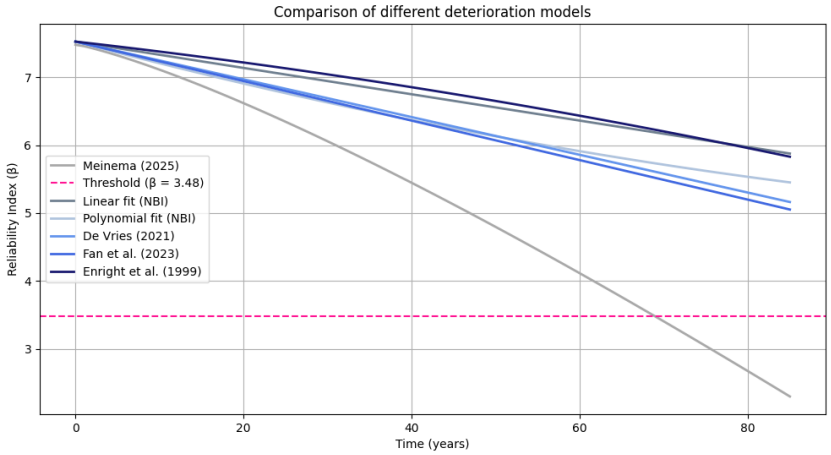

Figure 3.19: Comparison of decay rates for shear.

The comparison of the curves reveals that the decay rate obtained in this thesis decreases at an excessively high rate. Therefore, the reliability decay cannot be considered realistic. This difference is probably due to the simplified nature of the FORM method, which does not account for all factors influencing reliability. Furthermore, not all decaying mechanisms have been included in the analysis.

3.3.3. Increase of reliability by strengthening

When the threshold value is reached, strengthening measures are implemented. The objective is to design all strengthening methods to achieve a similar increase in reliability. However, achieving an identical reliability increase across all methods is challenging due to design constraints (Chapter 3.3.4). After strengthening—such as through external prestressing—the variability and mean of resistance are recalculated according to Equation 3.23 and Equation 3.27.

$$\mu_r = V_{Rd,s} + V_{Rd,c} + V_{Rd,EP} \tag{3.26}$$

$$\sigma_r = \sqrt{(A_{sl} \cdot A_{sl,\text{cov}})^2 + ... + (d_p \cdot d_{p,\text{cov}})^2 + (\sigma_{p,EP} \cdot \sigma_{p,EP,\text{cov}})^2} \tag{3.27}$$

3.3.4. Limitations of strengthening methods

For some strengthening methods, adjustments to the dimensions are possible, while for others, they are not, which imposes design limitations, influences reliability, and ultimately affects the extension of service life. Additionally, the rate of structural deterioration in the strengthened system varies depending on the method used. The limitations and varying deterioration characteristics of each strengthening method are discussed below.

For external tendons, the number of tendons can be 2, 4, 6, or 8. External prestressing is available in diameters of 12.7 mm, 15.2 mm, 15.7 mm, or 17.8 mm, and multi-strand configurations can be used with strand diameters of 12.7 mm and 15.2 mm. The jacking stress is limited to values between 1395 and 1488 MPa, while the service stress can reach approximately 1116 MPa. The eccentricities e_1 and e_2 are constrained, with e_1 ranging between 0 and 500 mm, and e_2 between 300 and 800 mm. These values depend on the height of the web, and e_2 must always be greater than e_1.

For memory-steel, the prestress can range between 0 and 350 MPa. Conventional stirrup diameters include 6, 8, 10, 12, 16, and 20 mm, while the spacing of the stirrups can vary between 0.1 and 1 metre, depending on the specific strengthening requirements.

In the case of CFRP, the strengthening can be applied with 1, 2, or 3 sheets. Several thickness options are available, including 0.111 mm, 0.13 mm, 0.167 mm, and 0.3 mm. The elastic modulus of CFRP varies between 120 and 300 GPa, depending on the manufacturer and material specifications.

For UHPC, the available compressive strength values include 120, 150, 180, 210, 240, 270, and 300 MPa. The thickness of the applied UHPC layer can range between 50 and 150 mm, allowing flexibility in design based on structural requirements.

External prestressing

A protective layer is applied to the external prestressing system, which is assumed to delay the onset of the corrosion propagation stage by 15 years. After this period, the corrosion process begins. While the strengthening system itself is protected, the existing structure remains exposed, allowing the corrosion process to continue. As a result, this strengthening method is limited by the initiation phase of corrosion. In addition to applying external prestressing, renovation work on the existing structure can be performed concurrently. It is assumed that the concrete and corrosion rate are restored when strengthening is applied. In the example below, the corrosion delay is extended by 20 years through this approach. This extension increases the corrosion initiation time, effectively postponing the end of the service life.

Resulting in the reliability function illustrated in Figure 3.20, the reliability index increases by approximately 3. This increase extends the service life by about 35 years. In this case, a prestressing steel diameter of 12 mm, with 2 bars and prestressing stress is 100 MPa are used.

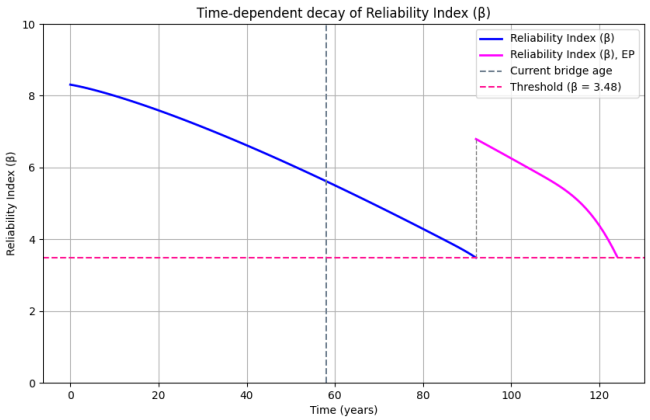

Figure 3.20: Reliability curve after strengthening, applying external prestressing.

Memory-steel

When combined with shotcrete, this delays the initiation of corrosion, providing a protective layer for the existing structure. However, as noted by Zhang [83], limited research has been conducted on the long-term service life of shotcrete. Therefore, a certain decay is assumed based on corrosion deterioration. Given the unique properties of shotcrete, different diffusion coefficients, critical chloride concentrations and water/cement ratios are considered. The shotcrete layer is assumed to have a thickness of approximately 30–50 mm, leading to the formulation expressed in Equation 3.28.

$$V_{Rd,MS}(t) = V_{Rd,MS,initial} - 0.0001 \cdot (t[i] - EoL_1)^6 \tag{3.28}$$

This results in the reliability function illustrated in Figure 3.21, which closely relates to the external prestressing curve. However, it requires a greater increase in reliability to achieve the same extension of service life. In this case, a long-term prestressing of 350 N/mm^2, a loss factor of 0.85 for relaxation, stirrup bars with a diameter of 10 mm and a stirrup spacing of 500 mm are used.

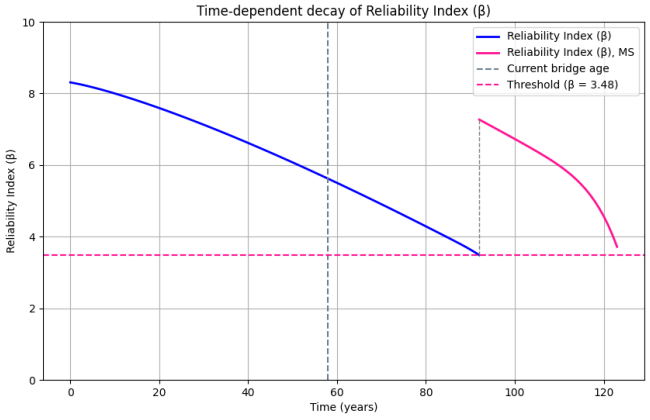

Figure 3.21: Reliability curve after strengthening, applying memory-steel.

Carbon Fibre Reinforced Polymer

CFRP systems provide protection for the existing structure. However, over time, moisture absorption can degrade the fibres [84], leading to a reduction in their strength and modulus of elasticity. Additionally, moisture ingress can result in the loosening of the epoxy resin and the connections within the CFRP wrapping. Despite the gradual degradation of its properties, CFRP should reach a long service life,

estimated at approximately 50 year [85]. The modulus of elasticity for CFRP deteriorates over time following an exponential decay (approximately 0.001/year) model. To model this deterioration, Equation 3.29 is used.

$$V_{Rd,FRP} = V_{Rd,FRP,initial} - 0.001 \cdot (t[i] - EoL_1 - 20)^5 \tag{3.29}$$

The resulting reliability function is illustrated in Figure 3.22. This approach extends the service lifetime by approximately 50 years but requires an increase of about 4 in the reliability index. This increase is significantly higher compared to external prestressing and memory-steel. In this case, a CFRP elastic modulus of 230×10^3 N/mm^2, a thickness of 0.13 mm for the CFRP sheets and a design strength of 517.82 MPa are used.

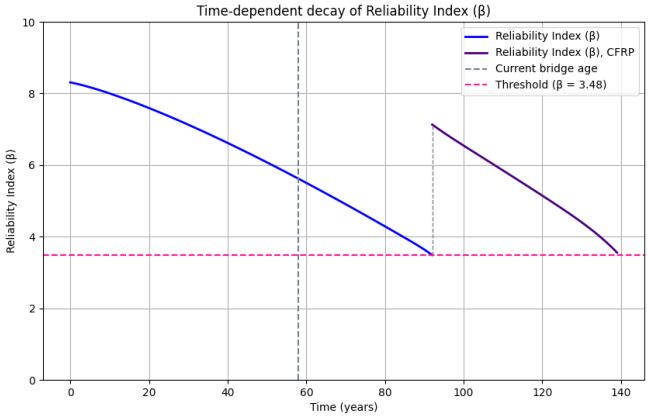

Figure 3.22: Reliability curve after strengthening, applying CFRP.

Ultra-High Performance Concrete

UHPC provides excellent protection for existing structures, particularly against chloride penetration and corrosion. Its diffusion coefficient is exceptionally low, measured at 1.3×10^{-13} m^2/s (equivalent to 3.15 mm^2/year), highlighting its strong resistance to chloride ingress. The surface chloride concentration is typically around 5.47 kg/m^3 and UHPC is characterised by a very low water-cement ratio, usually about 0.25, which further improves its resistance to chloride penetration. Corrosion at the rebar surface is expected to initiate when the chloride content reaches a critical threshold, following a process similar to that of normal concrete (NC). The initiation time for UHPC is calculated through Equation 3.30

$$t_1 = \frac{t_{UHPC} \cdot \left[\text{erf}^{-1}\left(1 - \frac{C_{th}}{C_0}\right)\right]^{-2}}{4D} \tag{3.30}$$

Assuming corrosion of the reinforcement within the existing structure can be delayed by 20 years, similar to external prestressing and applying the principles of chloride penetration for UHPC, the reliability function develops as illustrated in Figure 3.23. In this case, only a small increase in reliability is required to achieve the same extension of service life as with other strengthening methods. In this case, a design compressive strength of 150.8 MPa and a UHPC thickness of 30 mm are used.

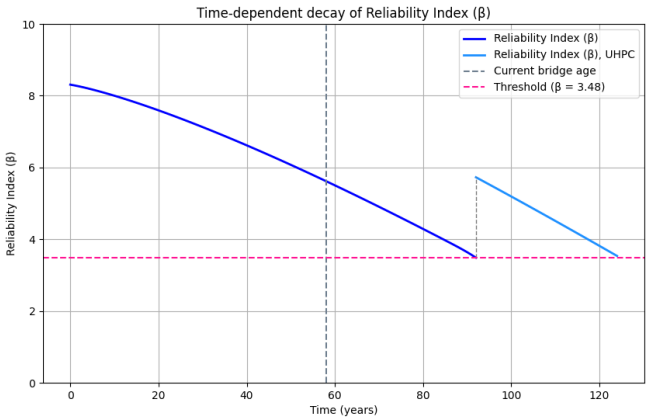

Figure 3.23: Reliability curve after strengthening, applying UHPC.

Reliability curve after strengthening

The design process incorporates the same extension of lifetime as defined by the stakeholder. All strengthening methods are required to achieve this targeted extension. By accounting for decay, the required reliability increase varies depending on the strengthening method. This process leads to the reliability functions as in Figure 3.24.

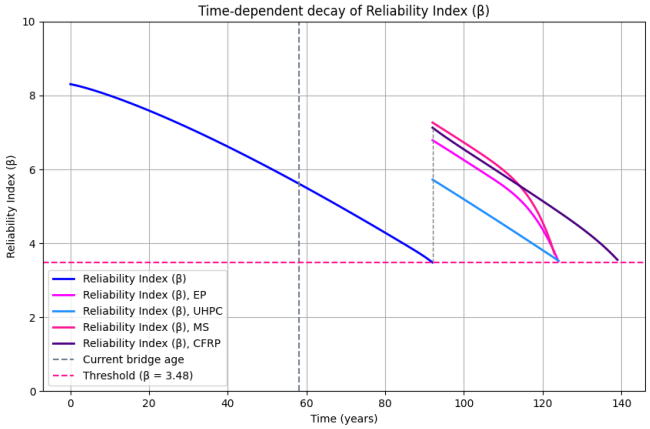

Figure 3.24: Reliability function for shear, including strengthening.

The figure demonstrates that certain methods require less reliability improvement to achieve the same lifetime extension due to differing deterioration mechanisms. This insight serves as the foundation for optimising strengthening parameters. Note: It should be discussed whether each parameter can realistically be adjusted as is done in this study, given the limitations imposed by fabrication and production processes. For example, changing the thickness of CFRP sheets, the strength of UHPC material, the prestress applied by memory steel or the rebar diameter of memory steel.

3.3.5. Optimisation of strengthening parameters

The initial strengthening parameters were derived based on their contribution to improving reliability, which can be considered a part of the optimisation process. However, further optimisation can be performed to maximise the increase in structural strength. A key step in this process is creating a correlation matrix for each strengthening method, which identifies how individual parameters influence the strengthening impact. For instance, as illustrated in Figure 3.25, the angle and quantity of external tendons are found to significantly affect the shear strength improvement in external prestressing. Adjusting these parameters is therefore highly effective in improving shear capacity.

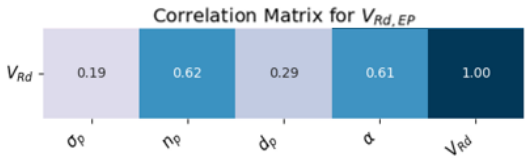

Figure 3.25: Correlation matrix for external prestressing.

Furthermore, multi-objective optimisation is conducted to maximise strength while simultaneously minimising environmental impact and costs. Assessment criteria without measurable units are excluded from this process, as they remain unchanged during optimisation. The objective function, designed to optimise a strengthening method by balancing these competing factors, is provided in Equation 3.31.

$$\text{Objective function} = -w_s \cdot V_{Rd} + w_c \cdot C + w_e \cdot E \tag{3.31}$$

Where w_s, w_c, w_e are weights assigned to strength, cost and environmental impact, respectively, with $w_s + w_c + w_e = 1$. The term V_{Rd} represents the strength contribution from the strengthening method. The term C denotes the total cost of the strengthening material. Where c is the cost per kg, ρ is the material density and V is the volume of the material used.

$$C = c \cdot \rho \cdot V \tag{3.32}$$

The term E represents the environmental impact of the strengthening material. Where e is the environmental impact coefficient (GWP, AP & APDf), ρ is the material density and V is the volume of the material used.

$$E = e \cdot \rho \cdot V \tag{3.33}$$

This objective function balances the trade-offs between maximising strength and minimising cost and environmental impact. The results of optimisation for each strengthening method are illustrated in Figure 3.26. On the axis you can find the design parameters that are subject to optimisation.

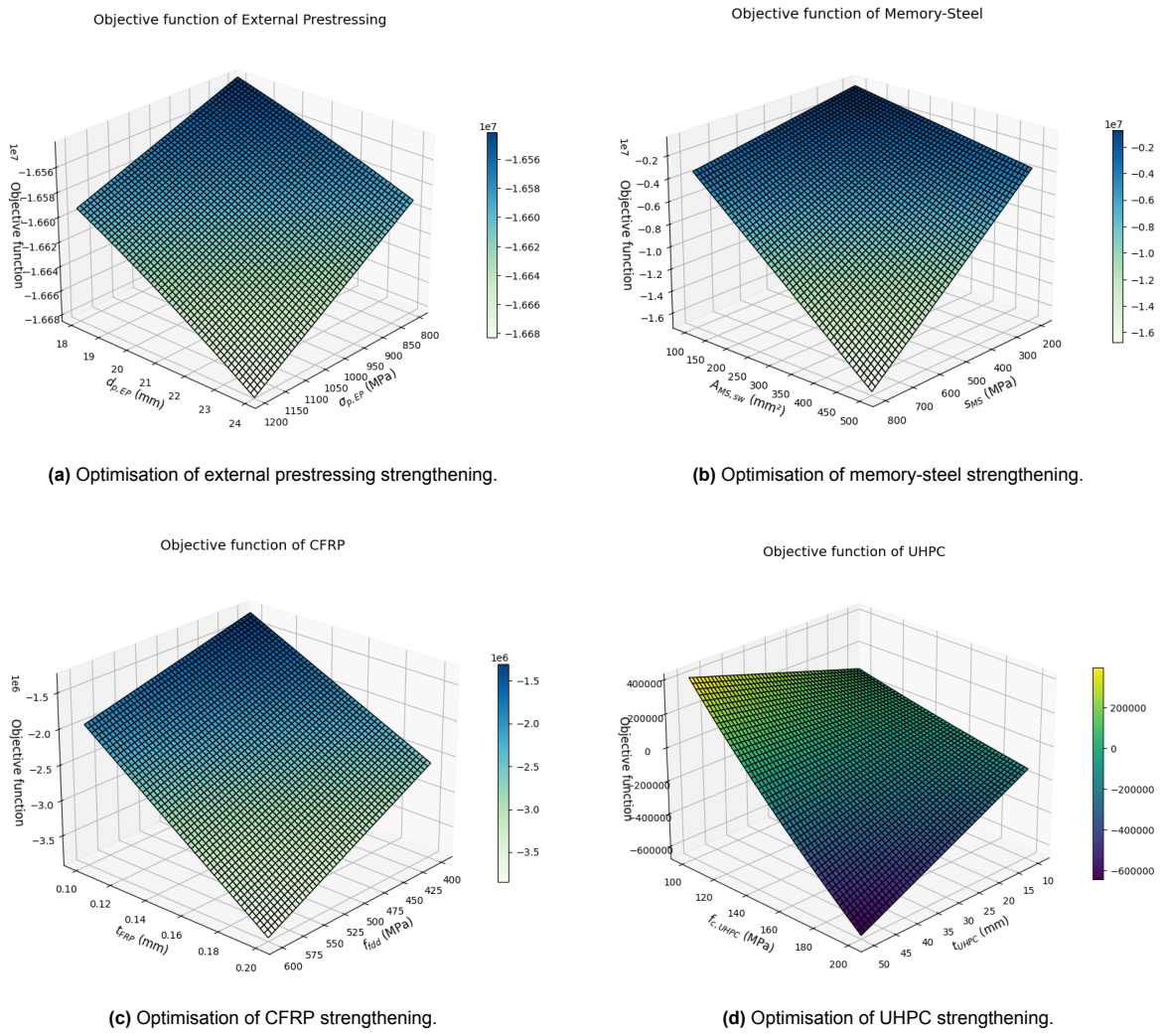

(a) Optimisation of external prestressing strengthening.

(b) Optimisation of memory-steel strengthening.

(c) Optimisation of CFRP strengthening.

(d) Optimisation of UHPC strengthening.

Figure 3.26: Parametric study results, optimisation of different strengthening methods.

Some strengthening methods have a linear relationship (EP, MS) between the amount of material added and the resulting increase in strength, while others do not. In cases of linear behaviour, the approach typically involves adding more material to achieve greater strength. However, this can have undesirable consequences, as increasing material usage may negatively impact decision-making due to higher costs or environmental limits.

In contrast, when the objective function is non-linear (CFRP, UHPC), true optimisation becomes possible. This is because strength improvements are not directly tied to simply adding more material, allowing for a more efficient use of resources to achieve the desired performance outcomes.

3.4. Identification of performance indicators

This chapter provides an overview of the performance indicators used in evaluating various strengthening methods. These indicators reflect the effectiveness and sustainability of the methods, considering factors such as functional height reduction and service-life extension, which depend significantly on the design of the strengthening system. All units are standardised per kilogram of material to ensure consistent and comparable assessment. Dimensionless criteria are expressed in qualitative terms, ranging from very low to very high (1-5). Note that all these performance indicators are subject to debate, as they can vary depending on the reference used.

3.4.1. External prestressing

External prestressing is a highly efficient strengthening method that offers several benefits. In this study, it consists of steel, a material that is not only durable but also recyclable, improving its alignment with principles of circular economy. Recovered steel can be reprocessed and reused, reducing environmental impact. From a circularity perspective, the system must be dismantled prior to transportation, which can complicate on-site operations. Table 3.10 highlights the multi-dimensional benefits and considerations associated with external prestressing, making it a valuable technique for structural strengthening when sustainability and functionality are critical objectives.

Indicator (I)	Value	Unit	Reference
I1. GWP	2.3	$kgCO_2$-eq	[86]
I2. AP	0.0063	$kgSO_2$-eq	[86]
I3. APDf	24.1	MJ/kg	[86]
I4. Material costs	12.30	$Euro/kg$	[87]
I5. Construction speed	High	-	[88]
I6. Construction costs	Low	-	[88]
I7. Maintenance costs	Low	-	[88]
I8. Human toxicity	4.58	$kg1,4DB$-eq	[89]
I9. Traffic hindrance	Very low	-	[88]
I10. Reduction in functional height	-	m	-
I11. Service life extension	-	$years$	-
I12. Durability	Medium	-	[88]
I13. Scarcity	Low	-	[90]
I14. Extensibility	High	-	[88]
I15. Strengthenability	Very high	-	[88]
I16. Disassembility	Very high	-	[88]
I17. Transportability	High	-	[88]

Table 3.10: Assessment criteria for externally prestressing.

3.4.2. Memory-steel

The assessment of memory-steel relies on data extrapolated from titanium and nickel production due to the limited availability of specific information. The alloying elements, such as nickel and titanium, are less abundant and their recycling processes are more complex, which increases the environmental footprint. Additionally, construction with memory-steel can generate significant noise and dust, creating both environmental and logistical challenges. It has a high Global Warming Potential (GWP) and Acidification Potential (AP) due to the resource-intensive production and recycling processes of nickel and titanium. It has low construction speed and high traffic hindrance due to complex installation processes and associated disturbances. On a circularity perspective, it has high durability but low extensibility, strengthenability and disassembility, limiting the adaptability of memory-steel in certain applications. Table 3.11 illustrates the strengths and limitations of memory-steel as a strengthening material, highlighting its high durability and transportability with challenges in construction speed, costs and recyclability.

Indicator (I)	Value	Unit	Reference
I1. GWP	11.4	$kgCO_2$-eq	[91]
I2. AP	0.0345	$kgSO_2$-eq	Estimated
I3. APDf	43	MJ/kg	Estimated
I4. Material costs	22.5	$Euro/kg$	[92]
I5. Construction speed	Very low	-	[92]
I6. Construction costs	High	-	[92]
I7. Maintenance costs	Very low	-	[92]
I8. Human toxicity	2.49	$kg1,4DB$-eq	Estimated
I9. Traffic hindrance	High	-	[42]
I10. Reduction in functional height	-	m	-
I11. Service life extension	-	years	-
I12. Durability	High	-	[92]
I13. Scarcity	Medium	-	[92]
I14. Extensibility	Very low	-	[92]
I15. Strengthenability	Very low	-	[92]
I16. Disassembility	Low	-	[92]
I17. Transportability	Very high	-	[92]

Table 3.11: Assessment criteria for Memory-steel (per kg).

3.4.3. Carbon Fibre Reinforced Polymer

CFRPs are composed of petroleum-based polymers and reinforcing Fibres such as carbon and glass, which present significant challenges in terms of recyclability. The disassembly process is highly complex due to the difficulty in peeling off the wrapping. Additionally, health risks are elevated during the manufacturing stage, as materials like carbon Fibres and resins can cause irritation to the skin, eyes and lungs. Table 3.12 gives an overview of assessment criteria for CFRP. CFRP has a high Global Warming Potential (GWP) and Acidification Potential (AP) due to the petroleum-based production process and energy-intensive fibre manufacturing. While material costs are significant, construction and maintenance costs are comparatively low and the construction speed is very high. The human toxicity indicators reflect the risks associated with exposure to carbon fibres and resin materials during manufacturing, which are relatively low. The strengthened structure, after applying memory-steel, has a low recyclability and disassembly rating, in contrast with the very high durability, which improves service life.

Indicator (I)	Value	Unit	Reference
I1. GWP	18.4	$kgCO_2$-eq	[50]
I2. AP	0.19	$kgSO_2$-eq	[50]
I3. APDf	281	MJ/kg	[50]
I4. Material costs	25	$Euro/kg$	[58]
I5. Construction speed	Very high	-	[93]
I6. Construction costs	Low	-	[93]
I7. Maintenance costs	Low	-	[93]
I8. Human toxicity	5.28	$kg1,4DB$-eq	Estimated
I9. Traffic hindrance	Very low	-	[93]
I10. Reduction in functional height	0	m	[93]
I11. Service life extension	-	$years$	-
I12. Durability	Very high	-	[50]
I13. Scarcity	High	-	[50]
I14. Extensibility	Low	-	[50]
I15. Strengthenability	Very low	-	[50]
I16. Disassembility	Very low	-	[50]
I17. Transportability	Very high	-	[50]

Table 3.12: Assessment criteria for CFRP (per kg).

3.4.4. Ultra-High Performance Concrete

UHPC is a material that heavily relies on resource-intensive components such as cement and additives like silica fume, which are both energy-demanding to produce and less conducive to circularity. The reliance on these materials contributes to its high environmental footprint during production. However, UHPC's exceptional durability and low maintenance requirements offset its initial material and construction costs, making it an attractive option for applications where longevity is a priority. The high costs associated with UHPC materials are detailed in Table 3.13. Cement, although relatively inexpensive, forms the bulk of UHPC mixtures, while additives like silica fume and superplasticisers significantly increase the cost per kilogram. Despite this, UHPC's ability to extend the service life of structures with minimal maintenance highlights its potential for cost-effectiveness over time.

Table 3.13: Cost per kilogram of selected materials in Euro [94].

Material	Cost per kg (€)
Cement	0.080
Silica fume	0.776
Fly ash	0.039
GGBFS	0.097
Limestone powder	0.116
Water	0.001
Superplasticiser	3.298

The performance indicators in Table 3.14 underline the material's strengths and limitations. UHPC has a relatively low Global Warming Potential (GWP) and Acidification Potential (AP) compared to many other advanced materials, showcasing its moderate environmental impact during production. Its durability is rated very high, ensuring long-term reliability and reduced maintenance, while its low traffic hindrance makes it suitable for construction in urban areas or high-traffic environments. However, UHPC exhibits some drawbacks. Its extensibility and disassembility are very low, reflecting challenges in adaptability and reuse. Additionally, the scarcity of certain components like silica fume and GGBFS (Ground Granulated Blast Furnace Slag) raises concerns about resource availability, categorised as medium. Nevertheless, its transportability and construction speed are high, making it a practical choice for projects requiring rapid execution.

Indicator (I)	**Value**	**Unit**	**Reference**
I1. GWP	2.62	$kgCO_2\text{-}eq$	[94]
I2. AP	0.00184	$kgSO_2\text{-}eq$	[95]
I3. APDf	2.75	MJ/kg	Estimated
I4. Material costs	4.4	$Euro/kg$	[94]
I5. Construction speed	High	-	[60]
I6. Construction costs	High	-	[60]
I7. Maintenance costs	Low	-	[60]
I8. Human toxicity	0.968	$kg1,4DB\text{-}eq$	[94]
I9. Traffic hindrance	Very low	-	[96]
I10. Reduction in functional height	-	m	-
I11. Service life extension	-	$years$	-
I12. Durability	Very high	-	[96]
I13. Scarcity	Medium	-	[96]
I14. Extensibility	Very low	-	[96]
I15. Strengthenability	Medium	-	[96]
I16. Disassembility	Very low	-	[96]
I17. Transportability	Very high	-	[96]

Table 3.14: Assessment criteria for UHPC (per kg).

3.4.5. Replacement

The replacement strategy involves producing a new T-beam with improved strength properties while maintaining the same dimensions as the original. This approach offers significant advantages in terms of strengthenability and transportability. However, it is also associated with considerable drawbacks, including high construction costs, substantial traffic disruption and significant environmental impacts due to the production of large quantities of concrete and steel. Replacement is excluded from analyses that compare material performance on a per-kilogram basis. This is because replacement requires substantial amounts of new material, which would bias the outcomes and lead to divergent results. Additionally, accurately assessing the composition and cost of the materials used in replacement is challenging, as these are designed to meet the specific boundary conditions of each project. Another complication arises from the composition of the concrete mix itself, which heavily influences the resulting strength properties. This variability makes direct comparisons involving replacement more complex and less straightforward.

Indicator (I)	Value	Unit	Reference
I1.a. GWP (concrete)	0.514	$kgCO_2$-eq	[97]
I1.b. GWP (steel)	2.3	$kgCO_2$-eq	[86]
I2.a. AP (concrete)	4.328	$kgSO_2$-eq	[98]
I2.b. AP (steel)	0.0063	$kgSO_2$-eq	[86]
I3.a. APDf (concrete)	0.833	MJ/kg	[99]
I3.b. APDf (steel)	24.1	MJ/kg	[86]
I4.a. Material costs (concrete)	0.38	$Euro/kg$	Estimated
I4.b. Material costs (steel)	12.30	$Euro/kg$	[87]
I5. Construction speed	Very long	-	-
I6. Construction costs	Very high	-	-
I7. Maintenance costs	Very low	-	-
I8.a. Human toxicity (concrete)	0.048	$kg1,4DB$-eq	Estimated
I8.b. Human toxicity (steel)	0.0625	$kg1,4DB$-eq	[89]
I9. Traffic hindrance	Very high	-	-
I10. Reduction in functional height	0	m	-
I11. Service life extension	-	years	-
I12. Durability	Medium	-	-
I13. Scarcity	Medium	-	-
I14. Extensibility	High	-	-
I15. Strengthenability	Very high	-	-
I16. Disassembility	Low	-	-
I17. Transportability	Very high	-	-

Table 3.15: Assessment criteria for replacement (per kg).

3.4.6. Overview

Steel tendons applied in external prestressing (EP) have a relatively low environmental impact and are one of the most cost-effective strengthening methods. EP requires anchoring and tensioning, making this method labour intensive. While effective, external tendons are exposed to environmental conditions, limiting their long-term performance. EP can be re-tensioned or supplemented with additional tendons, providing substantial strengthenability and extensibility. Furthermore, EP tendons can be detached, allowing for disassembly and transport.

Memory-steel (MS) has the greatest reduction in functional height due to the applied sprayed mortar. It requires special alloys (shape memory steel), leading to higher costs and environmental impacts. Applying MS is very labour intensive as it requires a lot of preparation. Also, it gives traffic hindrance, since the road surface has to be removed in order to attach the memory-steel to the current structure.

For Carbon Fibre Reinforced Polymer (CFRP), carbon fibre and resin are used which are expensive due to complex manufacturing but require a low material volume. Construction speed is highest for CFRP, as the application is relatively straightforward and requires minimal preparation. Surface preparation and adhesive bonding are necessary. CFRP offers excellent durability and corrosion resistance, significantly extending service life. Once bonded, CFRP is difficult to re-strengthen. No heavy equipment or hazardous materials are involved.

Ultra-High Performance Concrete (UHPC) is applied only at the sides of the web, with replacement resulting in no reduction in height. It is the most expensive strengthening material due to its high cement content, silica fume, and steel fibres. Careful placement, formwork, and curing are required, increasing costs. UHPC offers durability but is susceptible to cracking under high stress concentrations. It is scarce due to complex production and limited availability. UHPC is a permanent solution, reducing disassembly but increasing transport challenges. The process involves silica dust exposure and hazards associated with high-strength concrete placement.

Full replacement involves demolition, disposal, new concrete casting, reinforcement, and curing. Due to demolition, material costs, and labour-intensive reconstruction, it is the slowest and most disruptive method. Replacement carries risks such as high dust levels, heavy machinery use, and demolition hazards.

The three spider charts compare strengthening methods based on the performance per kg material across sustainability, circularity and integrity domains. Although integrity and circularity are elements of sustainability, they are addressed separately for the sake of clarity. To enhance comparability, the values are normalised. The lowest value in each category is set to 0.2, while the highest is set to 1.0, with all other values plotted linearly in between. The sustainability chart, Figure 3.27, evaluates environmental and economic impacts, including GWP, AP, abiotic depletion, material costs, construction speed, construction costs, maintenance costs, traffic hindrance and health risk.

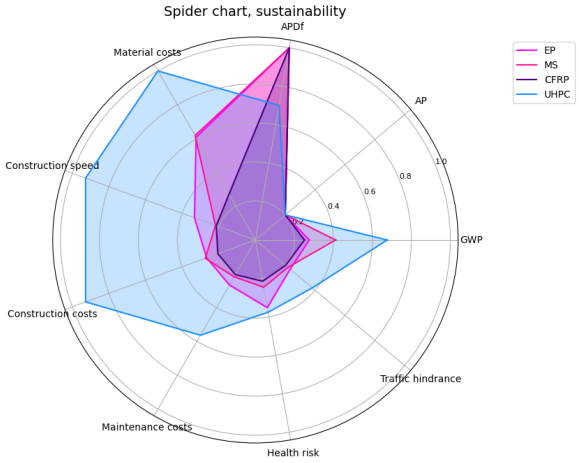

Figure 3.27: Sustainability assessment spider chart.

External prestressing shows balanced cost metrics with moderate sustainability, CFRP has high GWP and AP but low maintenance and construction costs, UHPC is efficient in material and construction costs but environmentally impactful and memory-steel has moderate environmental impacts but high material and construction costs.

The integrity chart, Figure 3.28, analyses reduction in functional height, service life extension and durability. External prestressing minimises traffic hindrance with balanced performance parameters, CFRP offers strong durability but may pose health risks, memory-steel incurs high traffic hindrance with limited functional benefits and UHPC extends service life but offers limited functional benefits and UHPC extends service life but offers limited functional height reduction.

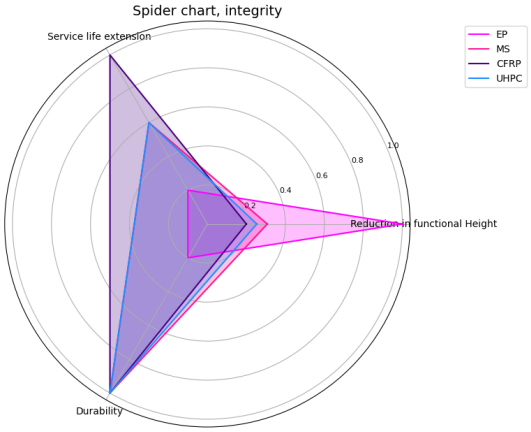

Figure 3.28: Integrity assessment spider chart.

The circularity chart, Figure 3.29, assesses Extensibility, Strengthenability, Scarcity, Transportability and Disassembility. External Prestressing scores well in Disassembility and Transportability, CFRP and UHPC face challenges in Strengthenability and Extensibility due to material properties and Memory Steel has moderate adaptability but lower Disassembility scores.

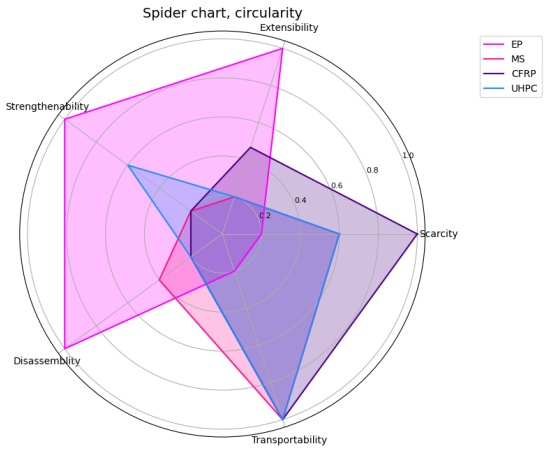

Figure 3.29: Circularity assessment spider chart.

3.5. Multi-criteria decision-making

Since decision making can be very complex with the amount of criteria used, the Analytical Hierarchy Process (AHP) is used and provides a solution for decision-making in complex environments where multiple variables or criteria need to be considered and prioritised.

3.5.1. Analytical Hierarchy Process

The AHP method is developed by Saaty between 1971 and 1975 [100]. The process involves pairwise comparisons to assign weights to each criterion based on their relative importance. These comparisons form a matrix and the consistency of judgements is validated using a Consistency Ratio (CR). If the CR is less than 0.10, the results are considered reliable. The final decision is reached by calculating a weighted sum of scores for each alternative. The hierarchy used is presented in Figure 3.30 and illustrates a decision-making framework for selecting the optimal strengthening method. The input for this process is partly static, derived from existing literature and the model (Alternatives vs. Indicators) and partly flexible (Indicators vs. Goal), determined by stakeholder preferences. This is further on, explained in detail.

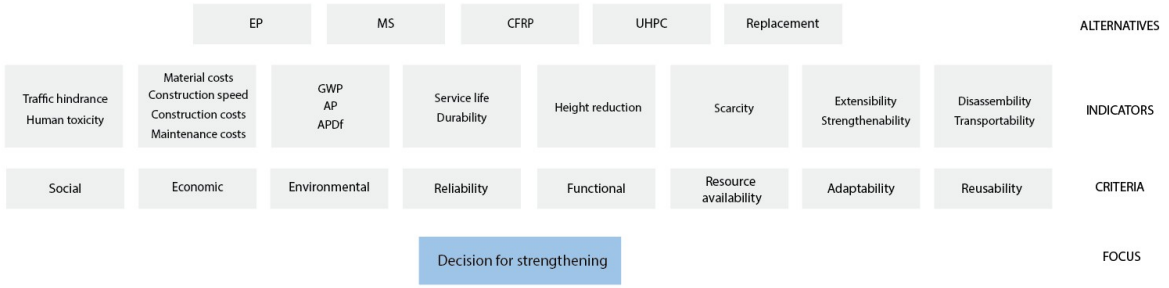

Figure 3.30: Decision hierarchy as used in the synthesis.

The relative importance is assessed by making pairwise comparisons between criteria, where each criterion is evaluated against every other criterion using a scale ranging from 1 to 9. This scale captures the intensity of preference and helps translate subjective judgements into quantifiable values for analysis. Table 3.16 provides a detailed breakdown of this scale.

The fundamental scale for pairwise comparisons		
Intensity of importance	**Definition**	**Description**
1	Equal importance	Both elements contribute equally towards the objective
3	Moderate importance	One element is slightly preferred over the other based on experience and judgement
5	Strong importance	One element is significantly preferred over the other based on experience and judgement
7	Very strong importance	One element is strongly favoured, with clear dominance observed in practical applications
9	Extreme importance	One element is overwhelmingly preferred, with the highest level of evidence supporting its dominance
Intermediate values of 2, 4, 6 and 8 can be used to represent ratings between the defined intensities, while finer adjustments such as 1.1, 1.2, or 1.3 can be applied when the elements have nearly equal importance.		

Table 3.16: The fundamental scale for pairwise comparisons.

First, each alternative is compared against the specified indicator. This step adopts a static approach, as the scores are derived from calculations performed within the predefined framework. For every pair of alternatives (A, B), the comparison value is determined. The comparison value can be determined by dividing A by B or B by A. In the case of GWP, Equation 3.34 and Equation 3.35 can be used.

$$\text{Comparison}(A, B) = \frac{\text{GWP of B}}{\text{GWP of A}} \tag{3.34}$$

$$\text{Comparison}(B, A) = \frac{\text{GWP of A}}{\text{GWP of B}} \tag{3.35}$$

3.5.2. Application

As input for this comparison we derive the GWP values for each method, which are represented visually in the spider chart (Figure 3.27), where the assessment criteria are evaluated on a per-unit kilogram basis. The calculated values for each alternative, expressed in terms of GWP are listed in Table 3.17. In the case for GWP, CFRP scores highest, followed by CFRP and UHPC, EP and Replacement all have around the same values.

Alternative	**GWP [$kg\,CO_2$-eq]**
EP	2.30
MS	11.40
CFRP	18.40
UHPC	2.62
Replacement	2.81

Table 3.17: Global warming potential (GWP) values for the alternatives.

To process the GWP values from Table 3.17, the values are first normalised to a scale between 1 and 9. In this case, EP receives a score of 1, representing the lowest GWP value, whilst CFRP scores 9, representing the highest. Once normalised, these values are used to compare each alternative against the others. This process produces Table 3.18, which illustrates an example of pairwise comparisons based on GWP scores.

Criteria	**EP**	**MS**	**CFRP**	**UHPC**	**R**
EP	1.00	1.34	2.09	0.39	0.16
MS	0.15	1.00	0.51	0.16	0.12
CFRP	0.14	0.26	1.00	0.14	0.11
UHPC	0.32	1.19	1.85	1.00	0.15
Replacement	1.22	5.62	9.00	1.37	1.00

Table 3.18: Pairwise comparison matrix for strengthening methods, normalised between $\frac{1}{9}$ and 9.

Given there are 17 categories (e.g., GWP, AP, APDf, etc.) and 6 unique comparisons for each category (e.g., CFRP vs. EP, CFRP vs. MS, CFRP vs. UHPC, etc.), this results in a total of $17 \times 6 = 102$ comparisons. The implementation is structured as shown in the code snippet below, where `assessment_data` represents the dataframe that collects all assessment criteria after executing the strengthening framework.

```
# Create pairwise comparisons for each criterion
for i, category in enumerate(categories):
    comparisons = {}
    for j, alt1 in enumerate(alternatives):
        for k, alt2 in enumerate(alternatives):
            if j < k:  # Compare each pair only once
                weight1 = assessment_data[alt1][i]
                weight2 = assessment_data[alt2][i]
                comparisons[(alt1, alt2)] = weight1 / weight2

    # Add the comparisons for the current category to the dictionary
    alternative_comparisons[category] = comparisons
```

Then for the variable approach, key stakeholders such as Rijkswaterstaat (RWS) and Arup actively participate in the decision process by assigning relative importance to each criterion through comparative judgments. This method gives decision-makers the possibility to evaluate trade-offs between competing criteria, such as deciding whether reducing global warming potential (GWP) should take precedence over minimising material costs.

The synthesis of the AHP involves a straightforward process of multiplication and summation throughout the entire hierarchy. A code snippet is shown below. The synthesis of these priorities is implemented in the model using a Python package called AHPy, developed by Philip Griffith [101]. The alternative that achieves the highest score is considered the optimal choice. The use of AHP makes it straightforward to trace the decision-making process and justify each step taken. Additionally, the decision-makers have the option to share the details of the process with consultants, candidates, shareholders, or any other stakeholders involved, providing full transparency. Note that the random index 'bb' is used instead of the default 'saaty'. This adjustment is necessary due to the creation of a large dataset, for which 'saaty' is not suitable.

Listing 3.1: Synthesis of the AHP.

```
# Combine all criteria into the overall model
criteria = ahpy.Compare('Criteria', criteria_comparisons, precision=3,
    random_index='bb')
criteria.add_children([gwp, ap, apdf, material_costs, construction_speed,
    construction_costs, maintenance_costs, health_risk,
                       traffic_hindrance, reduction_height, service_life,
                           durability, scarcity, extensibility, strengthenability,
                       disassembility, transportability])

# Get the report and identify the best strengthening method
report = criteria.report(show=True)

best_method = max(report["target_weights"], key=report["target_weights"].get)

print(f'The optimal strengthening method is: {best_method}')
```

3.5.3. Results

The `report()` method on a Compare object provides a detailed summary of its properties and weights. It outputs a Python dictionary with key information, such as global and local weights, target weights and detailed weights for individual elements. Using the `show=True` argument displays this information in JSON format for easier interpretation. Below is an example of calling the `report()` method.

Listing 3.2: Example output of the reporting method.

```
{
    "name": "Criteria",
    "global_weight": 1.0,
    "local_weight": 1.0,
    "target_weights": {
        "UHPC": 0.345,
        "EP": 0.249,
        "CFRP": 0.229,
        "MS": 0.168
    },
    "elements": {
        "global_weights": {
            "GWP": 0.103,
            "APDf": 0.103,
            "Health Risk": 0.103,
            "Scarcity": 0.103,
            "Transportability": 0.103,
            "Traffic Hindrance": 0.08,
            "...",
            "Construction Costs": 0.034,
            "Strengthenability": 0.034,
            "AP": 0.011,
            "Maintenance Costs": 0.011,
            "Service Life Extension": 0.011,
            "Extensibility": 0.011
        },
        "local_weights": {
            "GWP": 0.103,
            "APDf": 0.103,
            "Health Risk": 0.103,
            "Scarcity": 0.103,
            "Transportability": 0.103,
            "Traffic Hindrance": 0.08,
            "...",
            "Construction Costs": 0.034,
            "Strengthenability": 0.034,
            "AP": 0.011,
            "Maintenance Costs": 0.011,
            "Service Life Extension": 0.011,
            "Extensibility": 0.011
        },
        "consistency_ratio": 0.0
    }
}
```

Both global and local weights are set to 1.0, indicating the full weighting of the criteria and their subcategories. For the target Weights, the relative importance of alternatives such as UHPC, EP, CFRP and MS. For example, UHPC holds the highest weight at 34.5%. Within the element weights, global weights represent the overall importance of criteria such as ”GWP” (10.3%) and ”Traffic Hindrance” (8%). Local weights is similar to global weights here, as the criteria are uniformly weighted. The consistency ratio has a value of 0.0 indicates perfect consistency in the pairwise comparisons used to derive the weights.

3.5.4. Validation

To review the reliability and accuracy of the AHP, the process is validated. By validating the framework with a wide range of input data, potential errors, biases or limitations in its design can be identified and corrected. In order to validate, random input data is generated for each criterion, with values ranging between 1 and 9. The Python function for generating random input data is given below. In this case, it gives assessment data for three strengthening methods, using three assessment criteria.

Listing 3.3: Function to generate random input data for AHP validation.

```
# Function to generate random input data for AHP validation
def generate_random_data():
    return {
        "Category": ["GWP", "AP", "APDf"],
        "EP": np.random.randint(1, 9, size=3),
        "MS": np.random.randint(1, 9, size=3),
        "R": np.random.randint(1, 9, size=3),
    }
```

This function outputs randomised values for different criteria across multiple categories, simulating diverse scoring scenarios. These generated scores are then evaluated and validated using pairwise comparisons. For example, when GWP is more important than AP and APDf, the relative weights are drawn from lower values in the AHP scale. This can be switched to considering AP or APDf as the most important assessment criteria, using the same approach.

Listing 3.4: GWP more important than AP and APDf.

```
criteria_set = {
    ("GWP", "AP"): random.choice([1/9, 1/7, 1/5, 1/3]),
    ("GWP", "APDf"): random.choice([1/9, 1/7, 1/5, 1/3]),
    ("AP", "APDf"): random.choice([1/9, 1/7, 1/5, 1/3, 1, 3, 5, 7, 9])
}
```

These configurations are evaluated over a thousand iterations to ensure a robust distribution of inputs and outcomes. The validation process generates an even distribution of choices, reflecting diverse decision-making scenarios. The consistency of the generated pairwise comparisons is measured using the consistency ratio (CR). Across all iterations, the validation consistently produces CR values below this threshold, confirming the framework's reliability. Figure 3.31 visualises the validation outcomes, showing the results of the randomised input data and the distribution of priority weights.

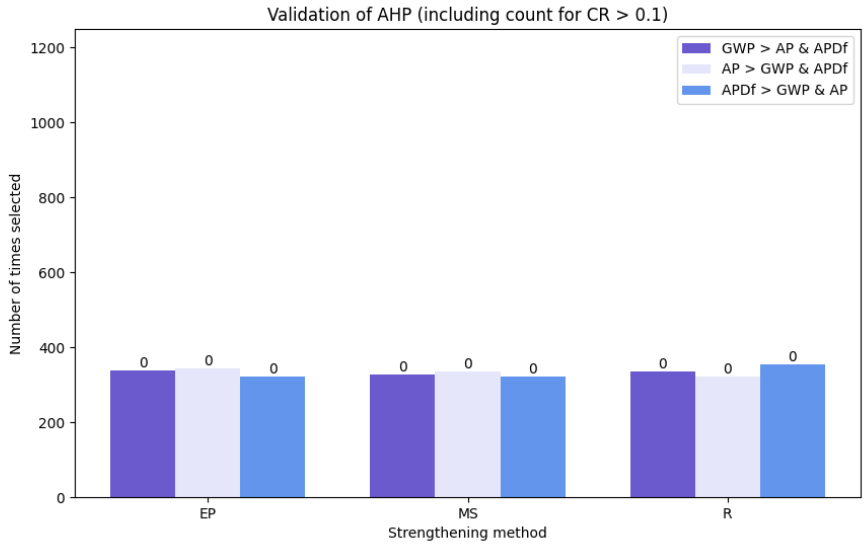

Figure 3.31: Validation outcomes for consistent prioritisation and reliable consistency ratios.

Another validation method involves assigning each strengthening method a high score in a specific assessment criterion. This targeted approach evaluates how the framework responds when a particular criterion is prioritised. For instance, one method might excel in GWP, another in AP and yet another in APDf. By alternating the prioritisation of GWP, AP, or APDf over the others and running the analysis thousands of times, we can observe the framework's behaviour under these scenarios.

Listing 3.5: Function to generate random input data for AHP validation.

```
# Function to generate random input data for AHP validation
def generate_random_data():
    return {
        "Category": ["GWP", "AP", "APDf"],
        "EP": [9, 1, 1],
        "MS": [1, 9, 1]),
        "R": [1, 1, 9],
    }
```

This method evaluates how the framework performs when specific criteria dominate the decision-making process, reflecting targeted priorities where certain methods excel in particular areas while others do not. Figure 3.32 illustrates the results of assigning high scores to methods based on their strengths. This approach highlights how rankings shift when specific methods are prioritised and demonstrates the framework's ability to adapt to diverse priority settings.

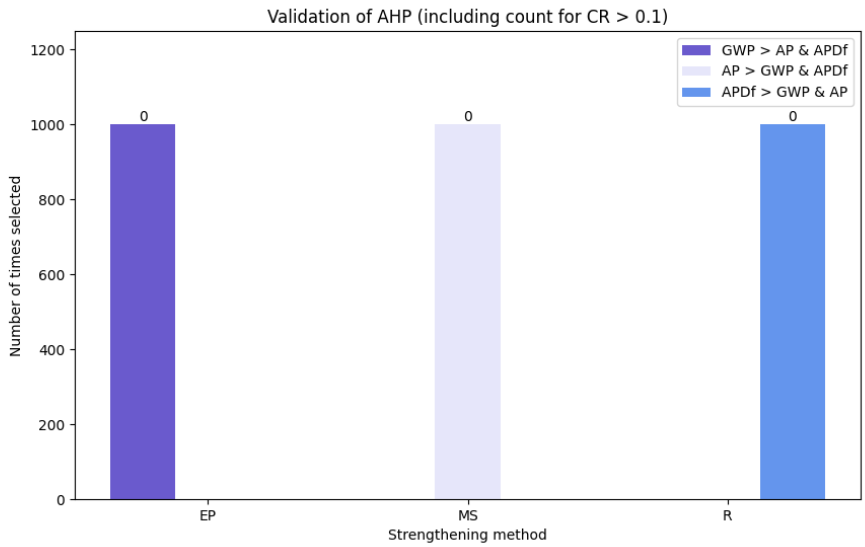

Figure 3.32: Validation outcomes with prioritised scores.

Also what becomes clear, is that in the Analytic Hierarchy Process (AHP), higher scores for criteria indicate better performance in relation to those criteria. However, certain criteria require normalisation adjustments when lower values represent better outcomes. For instance, minimising global warming potential (GWP) or costs is desirable and normalisation must account for this by inverting these values to ensure consistency in scoring.

To address this, the following criteria are set as minimisation criteria within the framework: GWP, AP, APDf, Material Costs, Construction Costs, Maintenance Costs, Health Risk, Traffic Hindrance, Reduction in Functional Height and Scarcity. For these criteria, normalisation is applied such that lower values correspond to higher performance, aligning with the decision-making objectives. This ensures that the framework fairly compares different strengthening methods.

After validation, we can expand the AHP including all 17 criteria and evaluate the strengthening methods purely based on their performance indicators per kilogram of material, excluding replacement. A random selection approach is used for assigning weights to criteria, simulating diverse decision-making scenarios and reflecting variability in stakeholder priorities. The outcomes of this expanded AHP process are illustrated in Figure 3.33.

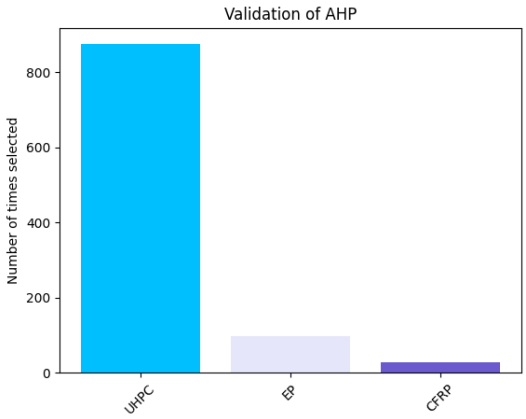

Figure 3.33: Validation outcomes.

The analysis of the average target weights for the strengthening methods over 1000 iterations highlights the performance of each method. The average target weights are presented in Table 3.19. As illustrated in both Figure 3.33 and Table 3.19, the scores for UHPC are the highest among the evaluated methods, indicating its superior performance in the context of this analysis. Meanwhile, the scores for CFRP and MS are closely aligned, showing minimal difference between their performances. EP also demonstrates a competitive score but does not outperform UHPC.

Method	Average	Std.
EP	0.296	0.05
MS	0.162	0.06
CFRP	0.168	0.04
UHPC	0.375	0.03

Table 3.19: Average target weights and standard deviation for strengthening methods.

Regardless of span length and cross-section, UHPC emerges as the optimal strengthening method. On a per-kilogram basis, UHPC, External Prestressing and CFRP achieve high scores, whereas Memory-Steel consistently underperforms and is not selected in any scenario. The AHP framework effectively adapts to diverse input criteria and scenarios, making it a robust tool for structural strengthening decisions. The set-up is validated for all criteria and can now be applied within the decision-making framework.

4

Parametric framework

The parametric framework provides flexibility in adjusting geometrical properties, load demands, assessment methods and strengthening parameters. This adaptability allows for countless combinations of inputs and outputs, which can be analysed statistically to identify similarities, sensitivities and correlations. This chapter outlines the framework and details its parametric study.

4.1. Construction type

The Python-based parametric model evaluates a prestressed concrete T-beam with a cross-section determined by the span length, parabolic tendon profile, shear reinforcement and longitudinal reinforcement. The geometrical properties of the T-beam are based on rules of thumb derived from its span length. Where the span length changed from 10 to 25 meters.

- Flange width: Randomly sampled within $\frac{L}{35}$ to $\frac{L}{25}$
- Flange thickness: Fixed at $\frac{L}{125}$
- Web height: Randomly sampled within $\frac{L}{35}$ to $\frac{L}{25}$
- Web thickness: Fixed at $\frac{L}{100}$

The tendon follows a parabolic profile, aligning with the centroidal axis at the ends (no eccentricity) and reaching maximum eccentricity (e) at midspan, defined by a radius of curvature (R). Shear cracks are assumed to be evenly spaced, inclined at an angle (θ) and extending to a depth of $z = 0.9d$. At the ultimate limit state (ULS), the concrete is cracked and the steel reinforcement is yielding. To maintain consistency, not all parameters are varied. Static parameters are the tendon profile, material properties of concrete and steel and strengthening materials. Variable parameters are load demand, span length, T-beam cross-section, shear and bending resistance and the amount of reinforcement.

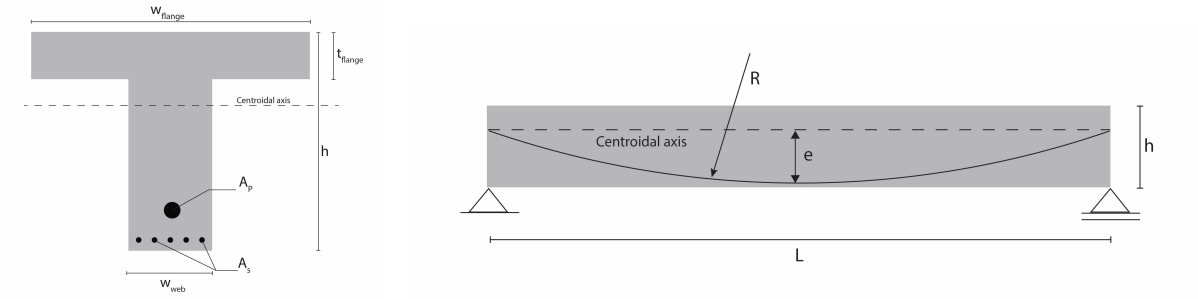

(a) Cross-section. **(b)** Side view.

Figure 4.1: Modelling input for the parametric model.

4.2. Loads

The current loads are based on Load Model 1, with an increase in loads accounting for traffic growth on an average road section in the Netherlands. Two point loads are applied at mid-span, spaced 1.2 metres apart between tandem axles, resulting in the most unfavourable effect. Additionally, a uniformly distributed load (UDL) is applied, corresponding to the structural system. The framework can adapt to variations in carriageway width and tandem axle spacing. The governing loads are a combination of the highest tandem axle load and the highest UDL, represented as a line load. The self-weight is calculated using the density of concrete, the cross-sectional area and the span length. Load factors are specified by Eurocode and combined as outlined in 2.6.2. Reduction factors are specified by RBK and depend on the span length and the desired extension of the structure's lifetime. Figure 4.2a shows the shear force along the length of the beam and Figure 4.2b shows the bending load along the length of the beam.

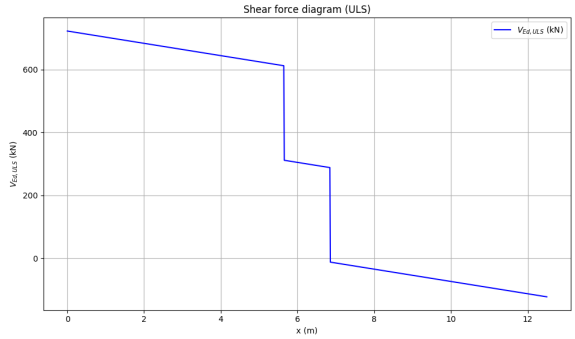

(a) Applied shear load in framework.

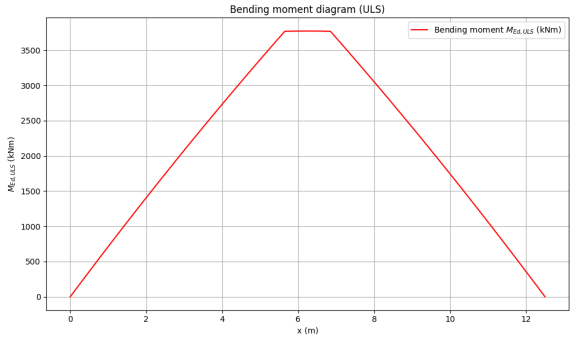

(b) Applied bending load in framework.

Figure 4.2: Applied loads in framework.

It is assumed that a Quick Scan report is available, providing information on the current condition, geometric properties, corrosion rate and prestress loss. This implies that the prestress loss and corrosion rates are accelerated due to the current age of the bridge. Figure 4.3a shows the shear strength along the length of the beam and Figure 4.3b shows the bending strength along the length of the beam.

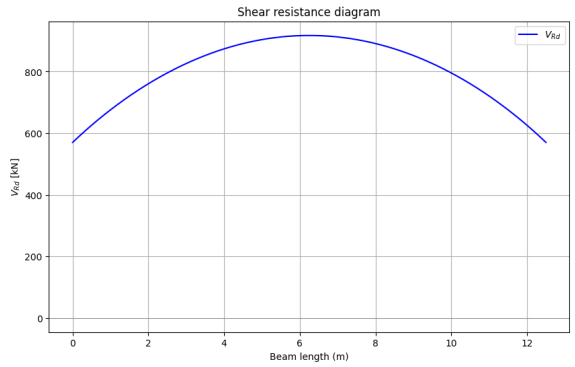

(a) Shear strength.

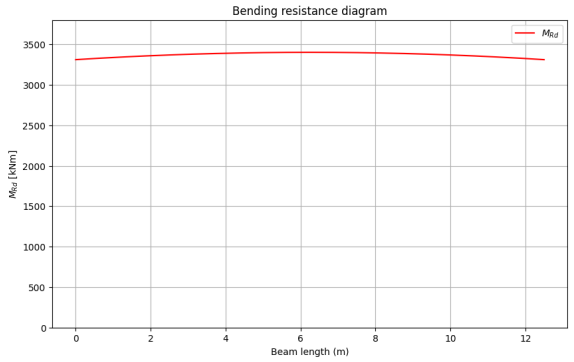

(b) Bending strength.

Figure 4.3: Current strength assessment in framework.

4.3. Assessment

From the starting point of evaluating the load and resistance along the length of the T-beam, it is possible to assess its current strength and reliability. This provides the basis for the design process, where the objective is to identify the most critical point along the beam. At different locations, the governing failure mechanism may vary, shear is often critical at the outer ends of the span, whereas bending is more significant at mid-span. By focusing strengthening design on the critical point, material usage, cost and environmental impact can be minimised. The Unity Check is illustrated in Figure 4.4, where Figure 4.4a (left) presents the UC for shear and Figure 4.4b (right) illustrates the UC for bending.

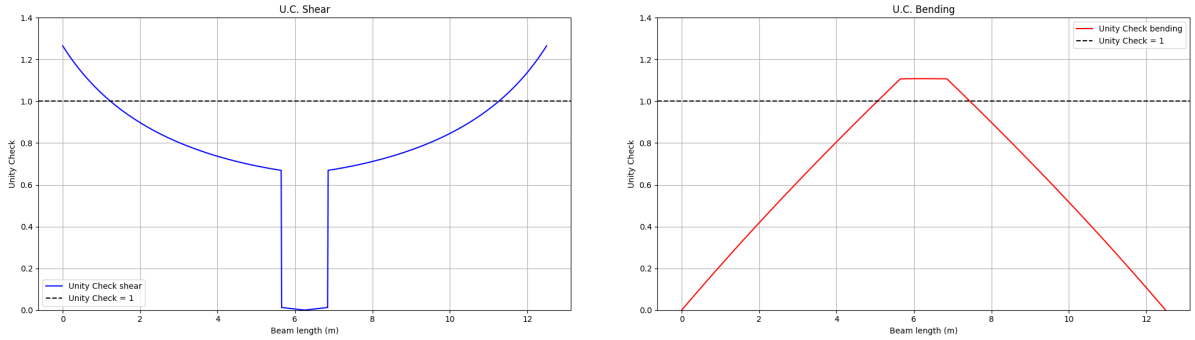

(a) Unity Check for shear.

(b) Unity Check for bending.

Figure 4.4: Unity Checks assessment in framework.

For shear, Unity Check values exceed 1.0 at the outer ends, while for bending, values exceed 1.0 at mid-span, indicating insufficient bending resistance. Strengthening is required for both shear and bending, aligning with the reliability curves in Figure 4.5a and Figure 4.5b. These figures show that shear reliability is currently sufficient but will degrade within seven years, also bending reliability is sufficient but will degrade within 18 years.

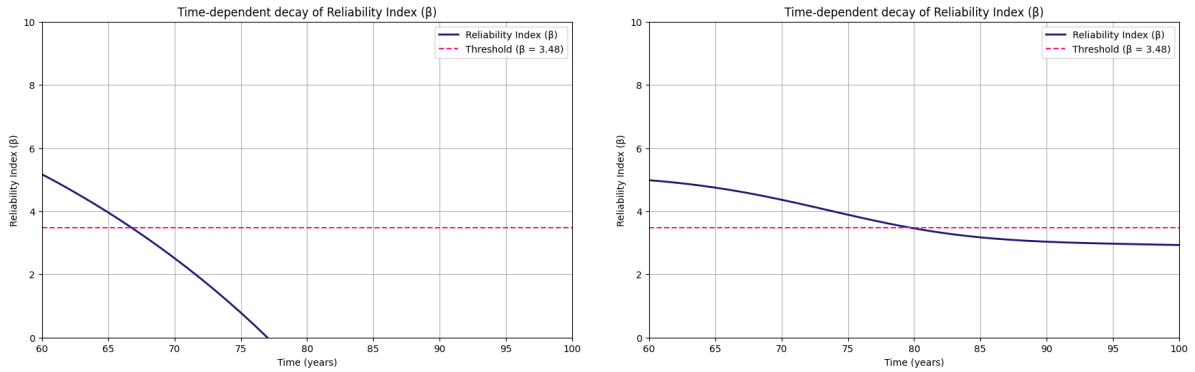

(a) Reliability for shear.

(b) Reliability for bending.

Figure 4.5: Reliability analysis for shear and bending in the framework.

A key distinction between the Unity Check and reliability analysis is that the Unity Check does not account for uncertainties and their distribution. This difference highlights the added insight provided by reliability analysis in assessing the structure's remaining service life.

The framework automatically identifies the most critical location, where demand is highest and capacity lowest. Given that the structure is around 60 years old, corrosion and prestress losses are already affecting its performance. The reliability curve for bending is less developed, which influences the focus of the bending assessment. This limitation is discussed further in Chapter 6. The FORM reliability analysis code is included in Appendix C.12.

4.3.1. Strengthening

As previously discussed in Chapter 2.8, the increase in strengthening is not uniform along the length of the beam. For example, external prestressing enhances shear strength at the outer ends while increasing bending strength at the mid-span. The effectiveness of strengthening can be assessed either by checking the unity check values, which should now be below the critical value of 1.0, or by evaluating the improvement in reliability, taking into account the degradation of the strengthened structure.

The chosen method depends on the available information about the structure. Since a reliability calculation requires numerous current geometric parameters related to the structure's condition, setting it up can be highly complex. Additionally, uncertainties for each parameter must be specified, which can be very time-consuming. However, if the unity check values along the span are available, along with the current capacity and applied load demand, the effect of strengthening can be easily visualised. This method is applied for the case study, described in Chapter 5, since there is less information available about current material states.

4.3.2. Stakeholder input

An interactive approach is designed, allowing stakeholders to adjust sliders and observe how this influences the optimal strengthening decision-making process. Stakeholders engage with the framework through a slider interface, as illustrated in Figure 4.6.

Figure 4.6: Indicators with slider input.

The sliders allow stakeholders to adjust the relative importance of the criteria dynamically. The scale for the sliders ranges from 1 to 9, with a step size of 1, reflecting the fundamental scale of pairwise comparisons used in the AHP. This dynamic adjustment provides a flexible and intuitive mechanism for users to define their criteria weights.

At this stage of the study, stakeholders should engage in discussions to determine the weight assigned to each criterion, as the framework provides the optimal strengthening method based on these inputs. An area for potential expansion is allowing each stakeholder to input their individual criterion weights, with the framework then aggregating these into a final combined weight. However, a challenge arises in that some stakeholders have greater influence over the decision, making it difficult to implement a purely relative weighting system.

4.3.3. Synthesis

As stakeholders modify the slider values, the relative importance of the criteria changes accordingly. These adjustments are visually represented through Sankey flow diagrams, which provide a clear and engaging way to observe the impact of priority shifts. Another advantage, is that users can experiment with different priority settings to test various scenarios, gaining insights into the robustness of the rankings under different conditions.

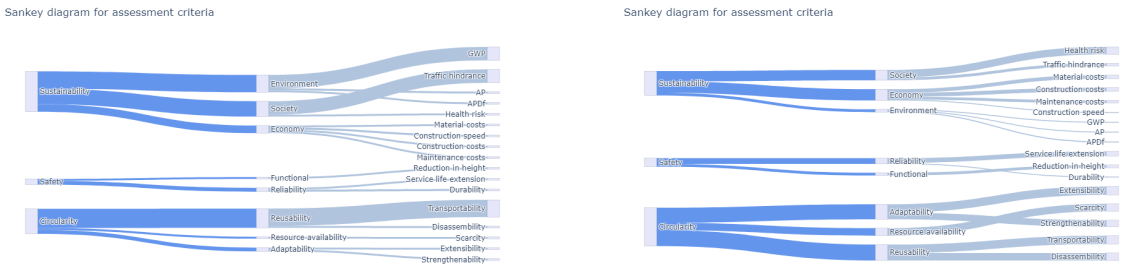

(a) Sustainability is the most important assessment.

(b) Circularity is the most important assessment.

Figure 4.7: Comparison of Sankey diagrams.

These visualisations improve the decision-making process by giving stakeholders the option to see how their preferences influence the overall prioritisation. This iterative and interactive approach ensures that the assessment remains aligned with the goals and values of the project, promoting transparency and consensus among the decision-makers.

4.3.4. Overview of decision-making framework

To provide an overview of the capabilities of the parametric framework, a step-by-step explanation is presented in Figure 4.8.

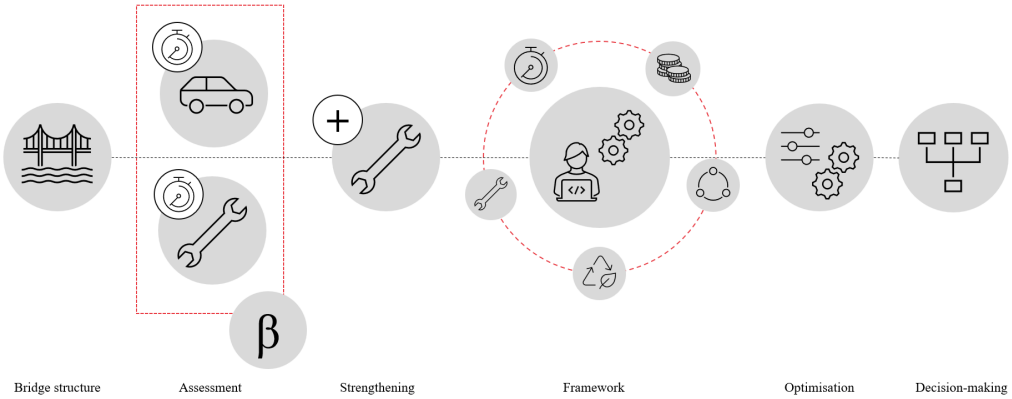

Figure 4.8: Overview of the decision-making framework.

The decision-making framework follows a structured process to determine the optimal strengthening approach. First, the construction type is defined, ensuring that the framework accounts for the specific structural characteristics. This provides the structural strength. Next, the applied loads are identified, which influence the structural assessment. A reliability analysis determines its current performance and identifies any deficiencies. If strengthening is required, appropriate measures are applied to enhance structural capacity. Performance criteria are established, followed by multi-objective optimisation that balances the desired service life, cost and environmental impact reduction, and maximising reliability improvement. Finally, based on the analysis and criteria, the optimal decision is made, ensuring a well-informed and effective strengthening strategy.

The optimal strengthening method is extracted from the report and presented as the final outcome. Since this parametric framework is designed to accommodate variations in geometry, loads, reinforcement prestressing, it enables the analysis of patterns and trends through multiple simulations. This analysis is detailed in Chapter 4.4.

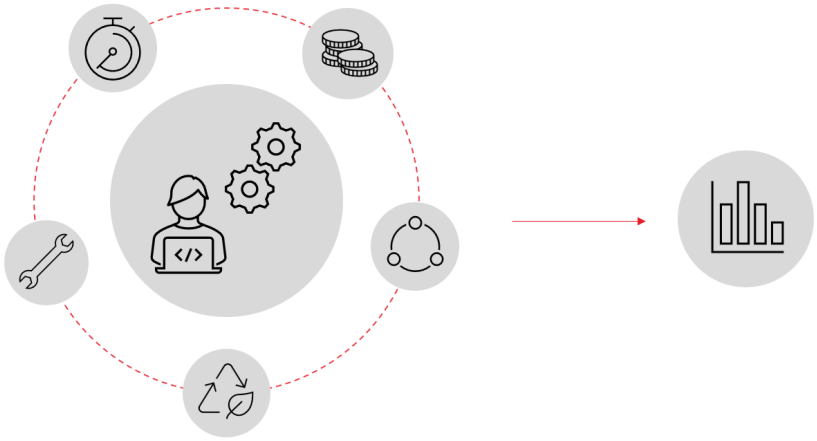

Figure 4.9: Design and analysis of the framework.

If the framework were tailored to a different type of bridge structure, several modifications would be necessary. The geometry would need to be adjusted, as the current code calculates the cross-sectional area specifically for a T-beam. Additionally, the strength prediction model would require recalibration and validation against experimental results, which would be a time-consuming process. Furthermore, reliability assessments and shear calculations would need to be adapted accordingly. While changing the structural type is possible, it would require significant modifications within the code.

However, the framework is also applicable to T-beams in buildings, as adjusting the applied load is relatively straightforward. Performance criteria can be incorporated with relative ease once the underlying mechanics of the code are well understood. This flexibility allows stakeholders to modify the framework if they wish to assess the structure using different evaluation methods.

4.4. Sensitivity analysis

This section examines how design and assessment factors influence strengthening decisions for prestressed concrete T-beams. The sensitivity analysis explores whether the optimal strengthening technique changes based on the desired extension of service life and whether there is a distinction between the most effective methods for bending and shear strengthening. It also considers how factors such as cross-sectional area, reinforcement ratio, load demand and span length influence the choice of strengthening. Furthermore, it investigates whether the preferred strengthening method shifts when considering service life extension in relation to reduction values. Another key aspect is determining which strengthening method is most frequently selected and at what span lengths each technique becomes dominant. Additionally, the study examines whether high reliability index (β) values favour a specific strengthening approach and how material consumption and cost impact the selection process. To identify patterns and trends, the analysis is performed 1000 times per scenario, ensuring a robust indication of variations in strengthening decisions.

Reduction values analysis

As outlined in Chapter 2.6.4, the reliability threshold of a structure depends on its current age, the desired extension of its service life and its span length. Figure 4.10 illustrates the reduction factors for various span lengths and target service life extensions.

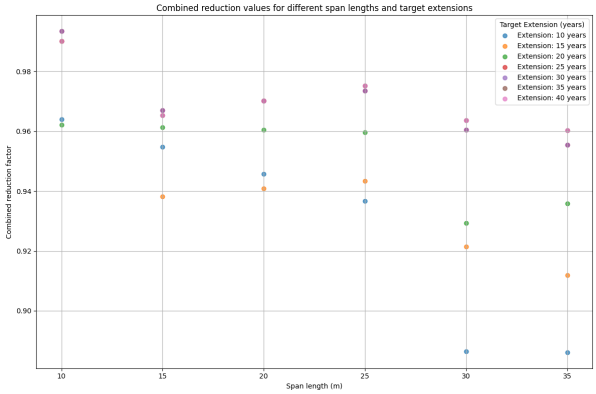

Figure 4.10: Scatter plot of reduction factors.

In most cases, a longer desired extension of service life results in lower reduction values. This is logical, as ensuring the bridge remains safe for an extended period requires a more conservative approach to capacity estimation. Additionally, larger span lengths generally lead to higher reduction factors, as increased spans introduce greater uncertainty in the structural capacity.

Reduction values do not directly influence the selection of a strengthening method, as they only adjust the expected capacity of the structure without favouring a particular strengthening approach. Consequently, when comparing different strengthening methods, the reduction factors introduce no inherent preference for one method over another.

Capacity and costs analysis

The shear capacity increases with span length for all strengthening methods, with EP showing the highest capacity increase, followed by MS, CFRP and UHPC. This indicates that the performance levels of these methods indeed vary with span length, as described earlier. An overview of shear increase related to span-length is given in Figure 4.11. Of course this is dependent on the design parameters that are used, although the linearity is not changing.

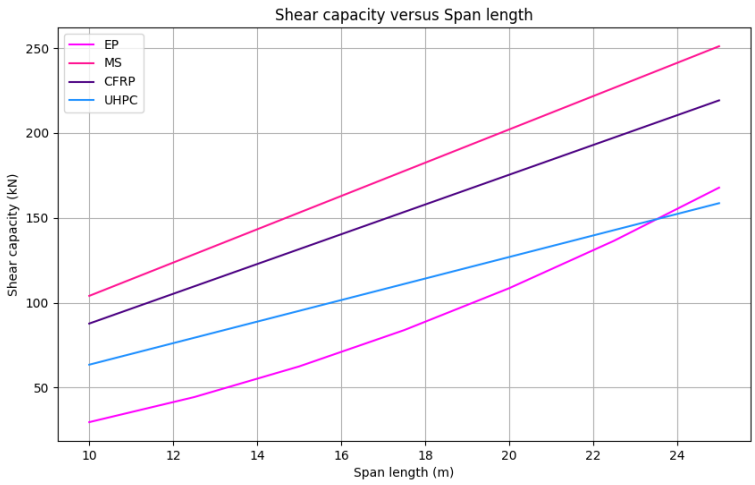

Figure 4.11: Shear strengthening capacity versus span length.

Material costs also increase with span length for all methods, but the rate of cost increase varies, as can be seen in Figure 4.12. EP shows the slowest cost increase, making it the most cost-effective option. CFRP and UHPC have significantly higher material costs, supporting the observation that these methods are on the higher-cost side.

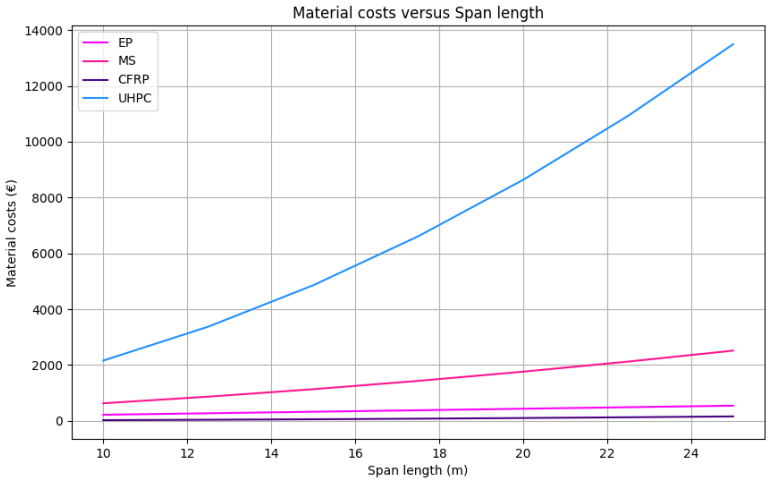

Figure 4.12: Material costs versus span length for shear strengthening.

While the cost for bending increases at the same rate as for shear, it is crucial to assess the growth of bending resistance relative to span length, using consistent strengthening parameters and geometric properties based on span length. The results are illustrated in Figure 4.13.

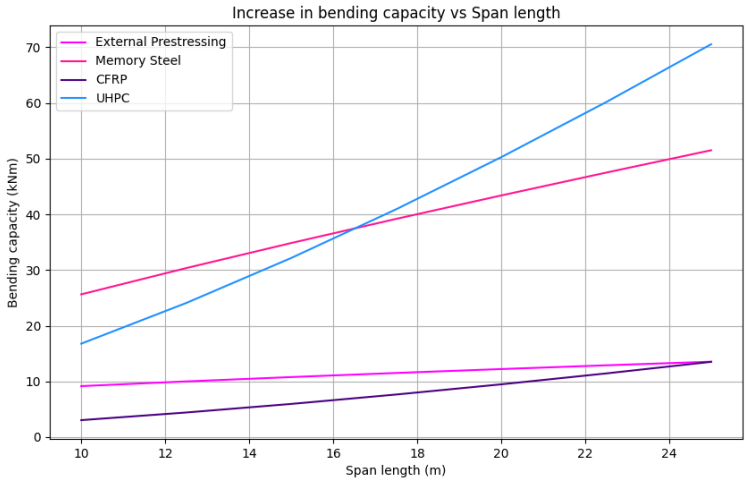

Figure 4.13: Bending strengthening capacity versus span-length.

Comparing bending and shear capacity highlights that bending resistance increases provided by the strengthening method is more significantly with span length, particularly for UHPC and CFRP, which demonstrate great flexural performance in longer spans. Shear capacities increase more moderately, with Memory Steel and CFRP proving most effective due to their efficiency in vertical reinforcement.

Material based analysis

The assessment criteria are based on scoring per kilogram material used, focusing on three criteria groups: sustainability, integrity and circularity. Although integrity and circularity are elements of sustainability, they are addressed separately for the sake of clarity. A random weighting is applied to determine the relative importance of each criterion. In the assessment, which is purely based on performance per kilogram of material, it is crucial to exclude the replacement method since this would give biased results, replacement cost a lot of material which is not accounted for in the per kg analysis.

Figure 4.14 show UHPC scores always as the optimal method in case sustainability is considered. While if the focus is either on integrity or circularity, the optimal strengthening method either choses UHPC or CFRP, dependend on span-length and cross-section. This matches the results of Chapter 3.4.6.

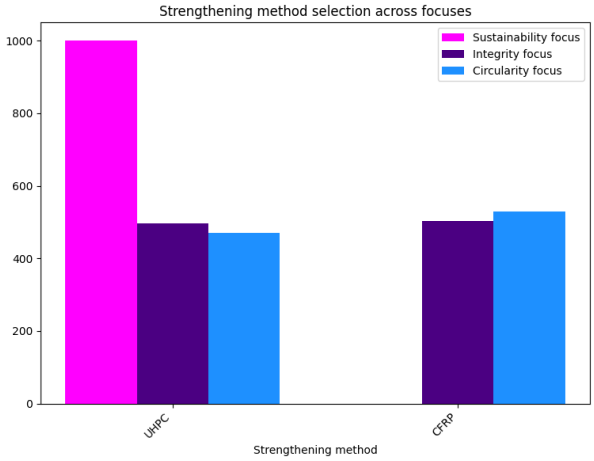

Figure 4.14: Sensitivity analysis, grouped criteria.

Unconditional analysis

The unconditional analysis disregards the current reliability, shear, or bending resistance of the existing structure and instead evaluates strengthening decisions solely based on assessment criteria related to span length and cross-section. This approach focuses on scenarios where decisions are not guided by optimisation processes that aim to balance reliability improvements with the desired extension of the structure's lifespan.

Instead, the cross-sectional properties of the beams are adjusted according to the span lengths, accounting for variations in design and application. When assessment criteria are not grouped and all 17 criteria are assigned random importances, a shift in the optimal strengthening method is observed compared to an analysis purely based on material mass in kilograms and its related performance criteria. This highlights the impact of assessment criteria weighting on the selection of strengthening techniques. Figure 4.15a presents the results including replacement, which, as previously mentioned, may be considered unrealistic. Meanwhile, Figure 4.15b excludes replacement from the analysis, offering a more practical perspective.

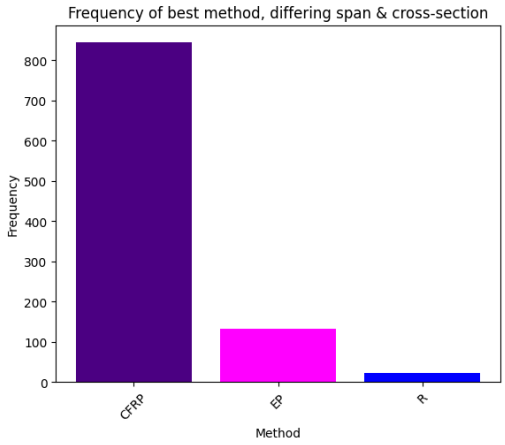

(a) Sensitivity analysis for differing span and cross-section.

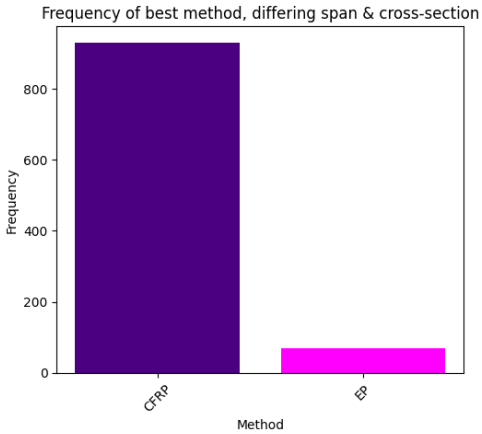

(b) Sensitivity analysis for differing span and cross-section, excluding replacement.

Figure 4.15: Comparison of AHP sensitivity analysis for cross-section and span.

Next, the influence of stakeholder input on the final decision-making is examined. This is done using assessment criteria per kilogram of material and considering different span lengths and cross-sections. Figure 4.16a illustrates the sensitivity analysis using random importance weightings between 1 and 9. These high random values reflect scenarios where stakeholders assign significant variability to the relative importance of criteria. In contrast, Figure 4.16b employs random importance weightings between 1 and 3, resulting in more moderate comparisons. This scenario represents cases where stakeholders are largely indifferent to the assessment criteria.

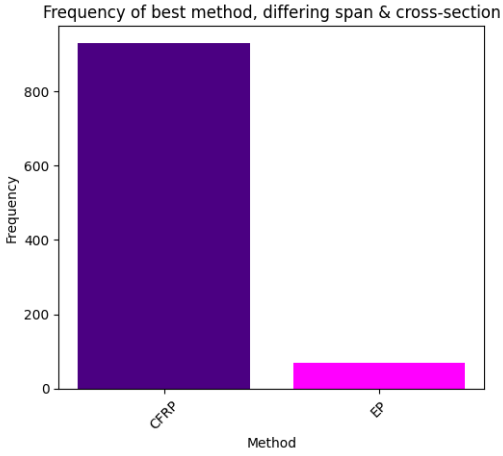

(a) Sensitivity of AHP, high random values.

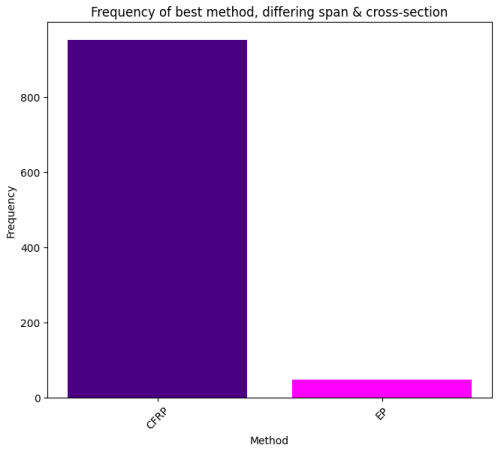

(b) Sensitivity of AHP, low random values.

Figure 4.16: Comparison of AHP sensitivity analysis for cross-section and span, excluding replacement.

Assigning relatively high importance to specific criteria, leads to the selection of strengthening methods that demonstrate exceptional performance in those areas. Reflecting on the differing outcomes, having a balanced opinion results in significantly varied selections, with external prestressing being chosen most frequently, even when the focus shifts between sustainability, integrity and circularity. The outcomes align with the assessment criteria, as external prestressing scores consistently average across multiple criteria, as illustrated in Chapter 3.4.6.

Conditional analysis

The conditional analysis incorporates condition-based optimisation, focusing on the required shear strengthening to achieve a target reliability value. Unlike the unconditional approach, this method excludes the effects of deterioration after strengthening and is guided by the structure's current reliability.

When selecting realistic design parameters, it is important to acknowledge that strengthening is constrained by design limitations and fabrication or production restrictions. Consequently, not every theoretical case within the optimisation process is practically feasible. To ensure realistic strengthening solutions, specific parameter bounds were established for each strengthening method.

For external prestressing, the number of strands is limited between 2 and 8, with strand diameters ranging from 12.7 mm to 17.8 mm. The prestress applied to the strands varies between 100 MPa and 1100 MPa. Additionally, the eccentricity at the start and end of the beam is constrained between 0 mm to 500 mm and 300 mm to 800 mm, respectively. For memory-steel, the prestress applied to the memory-steel reinforcement is restricted between 0 MPa and 450 MPa, while the diameter of the steel wires ranges from 8 mm to 18 mm. The spacing of the metallic strengthening elements is set between 100 mm and 1000 mm. For Carbon Fibre Reinforced Polymer the thickness of the CFRP ranges between 0.111 mm and 0.3 mm, with the number of applied CFRP layers varying from 1 to 3. The elasticity modulus of the CFRP is limited between 120,000 MPa and 300,000 MPa. For Ultra-High-Performance Concrete the compressive strength of the UHPC is defined within a range of 120 MPa to 300 MPa, while its thickness varies from 50 mm to 150 mm.

For this analysis, 1000 simulations were performed, but only reliability values between 2 and 7.5 were considered. Reliability values below 2 were excluded, as they indicate an unacceptably low structural capacity relative to demand, making strengthening infeasible. Conversely, values above 7.5 were disregarded, as strengthening would not be required. This constraint resulted in an analysis covering approximately 280 values, ensuring that the study focuses on practical and relevant scenarios, illustrated in Figure 4.17b.

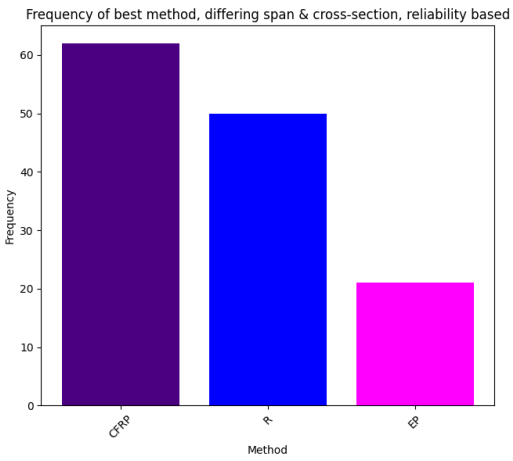

(a) Optimal strengthening, conditional analysis.

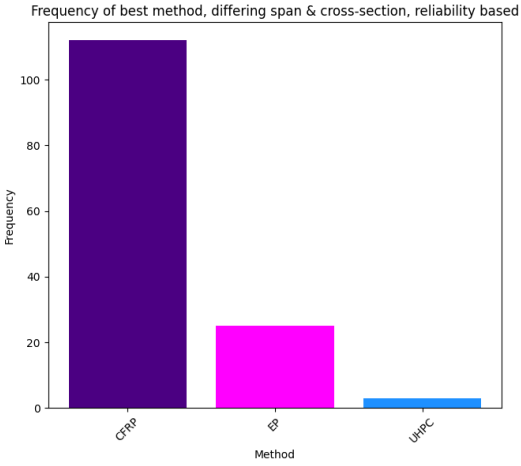

(b) Optimal strengthening, conditional analysis.

Figure 4.17: Comparison of optimal strengthening under different conditions.

The conditional analysis indicates that CFRP is the optimal strengthening method in most cases. When replacement is included as an option, CFRP remains highly recommended. However, the decision to consider replacement should be approached with caution. As previously mentioned, accurately assessing its impact is challenging since the design of replacement can be optimised based on the specific circumstances. At present, the impact is only evaluated for steel and concrete, which limits the scope of the analysis. If replacement is excluded from consideration, the optimal solution also includes UHPC as a viable strengthening method.

Due to applying the Analytical Hierarchy Process (AHP), it is possible to systematically analyse and extract decision reports, providing insight into why specific strengthening methods are selected. In this case, UHPC was chosen primarily for span lengths around 15 metres, where durability and material costs were key assessment criteria. Since UHPC scores highly in both aspects, it became the preferred option under these conditions.

Then, another analysis can be conducted using the assumption that each criterion holds equal importance. This approach implies that the stakeholder does not favour any specific performance criterion over another, ensuring an impartial evaluation of the strengthening methods. By adopting this perspective, the influence of individual criteria on the final decision is balanced, leading to a more neutral assessment of the available options. The results of this analysis are presented in Figure 4.18.

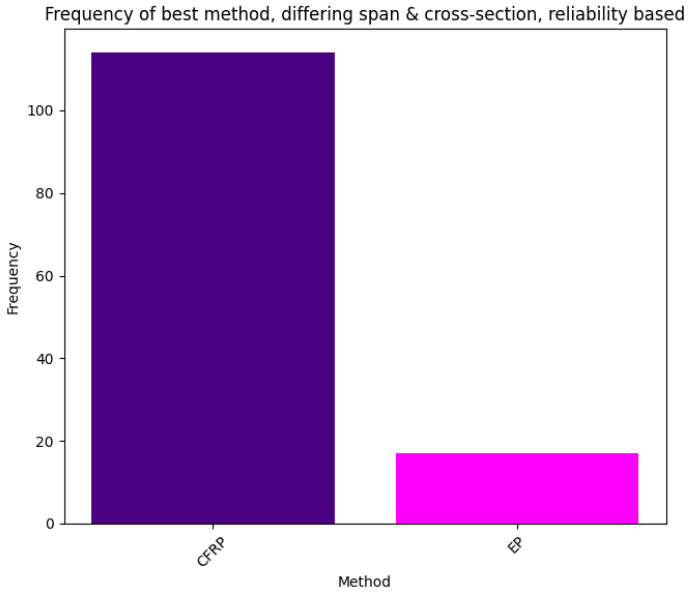

Figure 4.18: Optimal strengthening, conditional analysis, equal importance.

The results illustrate the strong performance of CFRP and EP under these conditions. These methods demonstrate superior strengthening improvement, while considering environment, cost, circularity and service-life. Given their consistently high-quality outcomes, CFRP and EP emerge as the preferred strengthening solutions in this analysis. Furthermore, changing the reinforcement ratio had no impact on the most likely optimal strengthening outcome, which remained CFRP.

By plotting the span length against the web area, we can observe how the structural geometry influences the choice between CFRP and external prestressing (EP). Since the web area is determined randomly within a range of L/25 to L/35, variations in cross-sectional properties naturally affect the selection process.

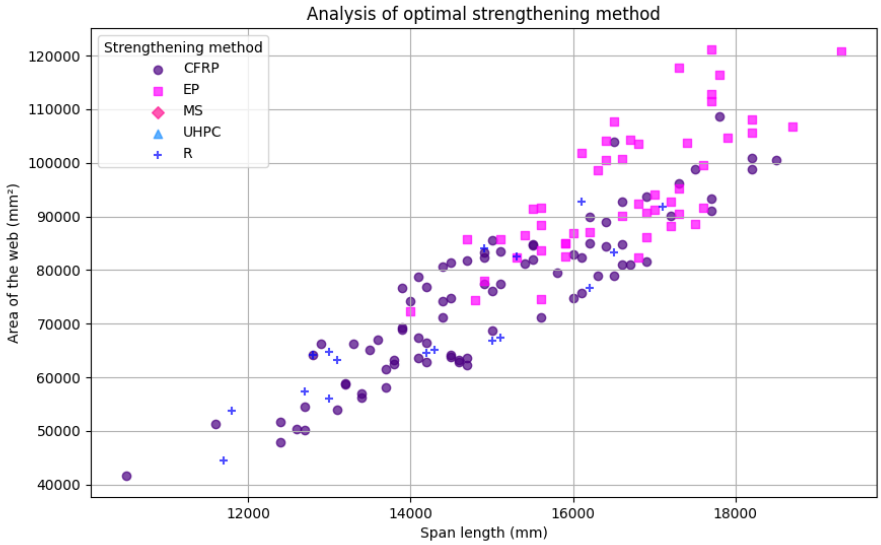

Figure 4.19: Optimal strengthening analysis, area of the web.

The results reveal a clear trend. For large spans with relatively small cross-sections, CFRP is preferred. For larger cross-sections, EP becomes the dominant choice. This selection pattern is logical. In larger cross-sections, the impact of CFRP increases due to the greater available bonding area and load distribution potential. Meanwhile, EP is less dependent on cross-section geometry since it primarily enhances strength by applying external forces, making it a more consistent strengthening option across different web sizes. These findings further confirm how cross-sectional variations influence the optimal strengthening approach.

To further explore these decisions, plotting span length against reliability provides a clearer visual representation of selection patterns. A bar plot confirms that CFRP is the most frequently chosen strengthening method, aligning with previous findings.

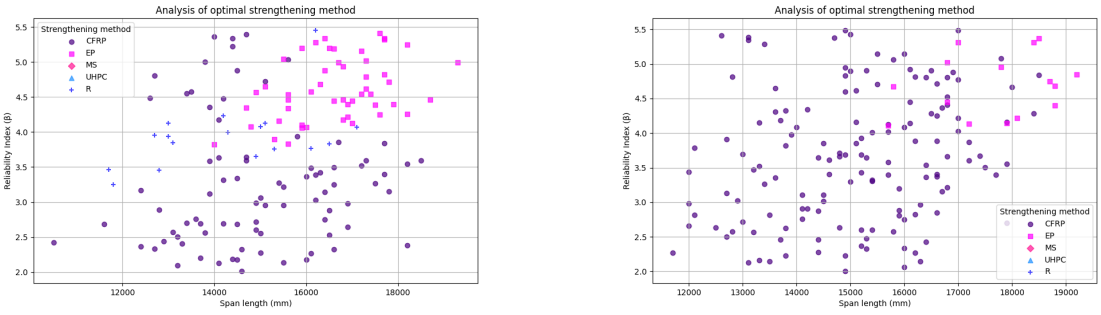

(a) Optimal strengthening analysis, reliability, including replacement.

(b) Optimal strengthening analysis, reliability, excluding replacement.

Figure 4.20: Comparison of optimal strengthening analysis with and without replacement.

The analysis reveals distinct selection trends based on structural conditions and optimisation criteria. Replacement is chosen at specific reliability levels, suggesting that its feasibility depends on the structural state and required performance improvements. When the span length is large and the current reliability is relatively high, external prestressing emerges as the preferred method, indicating its effectiveness in enhancing longer structures without compromising reliability. In all other cases, CFRP remains the dominant strengthening choice, further reinforcing its suitability due to its strong performance and adaptability. These trends highlight how different strengthening methods are selected depending on the interplay between structural demands, span length and reliability, offering valuable insights into the most appropriate interventions for various conditions.

When introducing random importance weighting to the assessment criteria, the selection of the optimal strengthening method shifts. In this case, CFRP emerges as the most frequently chosen method, reinforcing its efficiency in strengthening relative to material use.

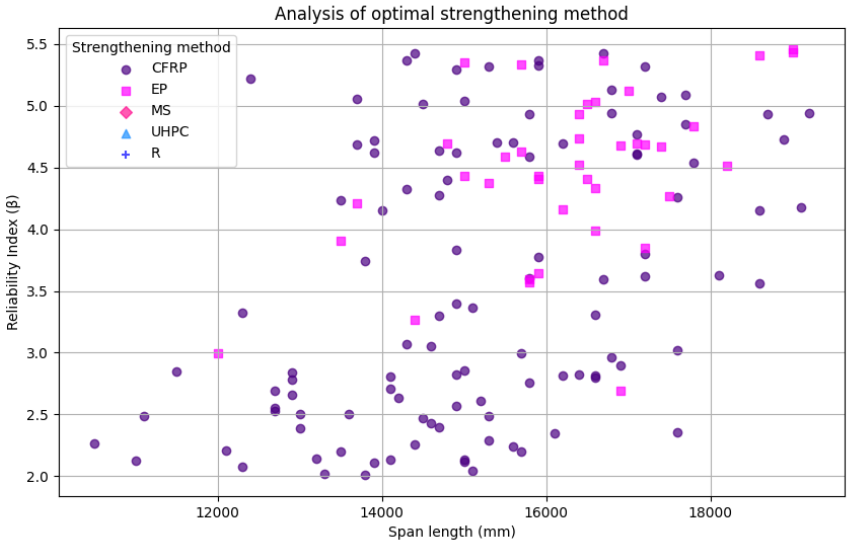

Figure 4.21: Optimal strengthening analysis, random importance.

Additionally, replacement is no longer selected as the optimal strengthening method under these conditions. This suggests that when criteria are weighted randomly rather than being predefined, the balance of factors such as material efficiency, durability and cost shifts in favour of CFRP. This further highlights the method's adaptability and high performance across varying structural conditions.

Correlation of assessment criteria

The correlation matrix, illustrated in Figure 4.22, provides a detailed view of how various assessment criteria influence the selection of strengthening methods. Each row represents a strengthening method while the columns give the relative importance of different performance indicators, such as material costs, durability, construction speed and sustainability.

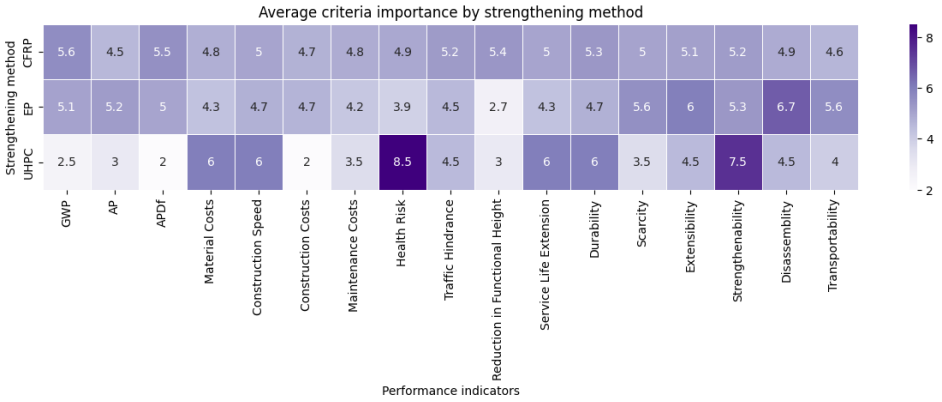

Figure 4.22: Correlation between decision-making and criteria importance.

The correlation matrix illustrates the average weighting of assessment criteria for each specific strengthening method. In this case, UHPC is selected when factors such as health risk, construction speed, material costs and strengthenability are prioritised. CFRP, being chosen in a wide range of scenarios, demonstrates average scores across most criteria, reflecting its consistent and balanced performance. This correlation matrix emphasises the influence of performance indicators on the selection of specific strengthening methods, providing valuable insights into the decision-making process.

To conclude on the sensitivity analysis, it provides valuable insights into the selection of strengthening methods for prestressed concrete T-beams, highlighting how different approaches perform under various structural and assessment conditions.

UHPC is primarily selected when evaluating strengthening based on a per-kilogram material approach, particularly excelling in sustainability aspects. CFRP, on the other hand, consistently emerges as the optimal strengthening method across different conditions. Regardless of how assessment criteria are weighted, CFRP maintains relatively average scores across all factors, ensuring its frequent selection. This suggests that CFRP is a robust and adaptable solution, offering a balanced performance across multiple structural and economic considerations. External prestressing also ranks highly, demonstrating a strong strength-to-impact ratio and proving particularly effective for larger spans. Memory-steel is never selected as the preferred method, likely due to its lower efficiency in providing the necessary strength enhancement compared to other options. Additionally, its high material cost makes it less competitive in this analysis. Furthermore, the change in reinforcement ratio did not alter the optimal strengthening outcome.

However still, predicting precisely when a certain strengthening method will be chosen is challenging, as its selection depends not only on its own performance but also on the relative importance assigned to other assessment criteria. Since these weightings vary in each randomised run, the correlation patterns fluctuate accordingly.

When replacement is included as a strengthening option, it is frequently selected, ranking just behind CFRP in terms of selection frequency. However, its inclusion should be carefully scrutinised, as the feasibility of replacement depends on various structural and economic factors. Furthermore, the impact of replacement is difficult to quantify precisely, as its effectiveness can be optimised depending on the specific structural scenario. Therefore, while replacement may appear as an optimal solution in some cases, its practical implementation should be considered with caution.

5

Case study

The case study selected is the ‘Hamersbrug’ over the ‘Wilhelminakanaal’, part of the A59 motorway connection. The longest span of this bridge is 26.80 metres and it was constructed in 1966. It is located in Noord-Brabant. The bridge is listed by Rijkswaterstaat for potential replacement or strengthening. This particular bridge was chosen, because it offers a wealth of detailed information, as provided by Rijkswaterstaat, including a Quick Scan report from Movares.

5.1. Construction type

The bridge is constructed using T-beams with cast-in-place sections between them. It features a statically determinate configuration. The deck structure is divided longitudinally into two separate road lanes, which are not connected and each lane is supported by six T-beams acting as the primary load-bearing components. The total span of the bridge measures 26.80 metres. The structure is divided longitudinally, ensuring separation between the two road lanes. Built in 1966, the bridge was designed according to the VOSB 1963 standard, reflecting the engineering practices and norms of its time. Figures 5.1a, 5.1b, E.1, E.2 provide an overview of the structure, including its general layout, cross-section and reinforcement details. The geometry and reinforcement of the T-beams include a top flange thickness of 180 mm, a bottom flange thickness of 250 mm and a web thickness of 180 mm. More detailed drawings can be found in Appendix E.

(a) View on the Hamersbrug.

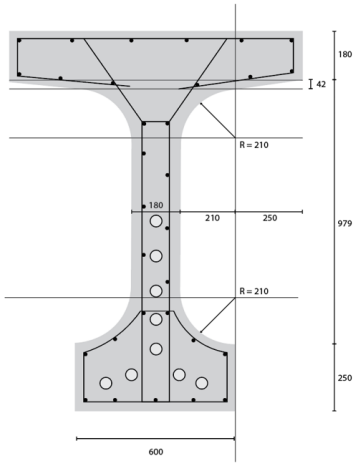

(b) Cross-section of the Hamersbrug T-beam.

Figure 5.1: Overview of the Hamersbrug, including a general view and the T-beam cross-section.

The concrete grade used for the main girders is C50/60, while the cast-in-place sections and cross-beams are made with C40/50 concrete. Prestressing steel consists of longitudinal tendons specified as 12 Ø 7 mm, with the standard being QP150 and an alternative of QP170. The transverse tendons follow the same specifications. Each T-beam is supported individually by elastomeric bearings. The reinforcement consists of 2 vertical stirrups, having a diameter of 10 mm and a spacing of 400 mm. The flexural reinforcement, consists of 6 reinforcement bars in top flange, 10 in the web and 9 in the bottom flange. The centroidal axis of the cross-section is assumed to be 460 mm from the top fibre.

The T-beams feature a curved section at the edges with a radius of 210 mm. Each T-beam contains twelve prestressing cables, contributing to the structural complexity and detailing. While the interaction between the T-beams and the cross-beams exhibits complex behaviour, this interaction is not accounted for in the assessment and strengthening analysis.

The transverse prestressing system integrates the deck slab with the top flanges of the T-beams, ensuring a cohesive structural system. The prestressing design accounts for a friction coefficient of 0.26, a wobble of 0.01 rad/m, relaxation losses of 10 percent and additional losses of 10 percent due to shrinkage and creep. Figure E.1 illustrates the layout of reinforcement and Figure E.2 the prestressing cables.

5.2. Loads

Specific load factors are provided in Appendix E. Reduction values are already incorporated in the quick scan report, eliminating the need for further application within the assessment. As the loads are derived from the quick scan, reduction values and Load Model 1 are excluded from the analysis. Chapter 5.2.1 describes the traffic intensity over time, which can be considered in the reliability assessment. The reduction values applied are detailed in Chapter 5.2.2.

5.2.1. Traffic intensity

The data, sourced from INWEVA and covering the period 2012 to 2023, includes information for two lanes: 5021 and 5070. Lane 5070 corresponds to the northbound road, while lane 5021 represents the southbound road. In comparison to the average road in the Netherlands, this bridge forms part of a highway and experiences high traffic loads. These substantial traffic volumes should be factored into the analysis when assessing the reliability of the structure over time. The average linear increase is derived, illustrated in Figure 5.2.

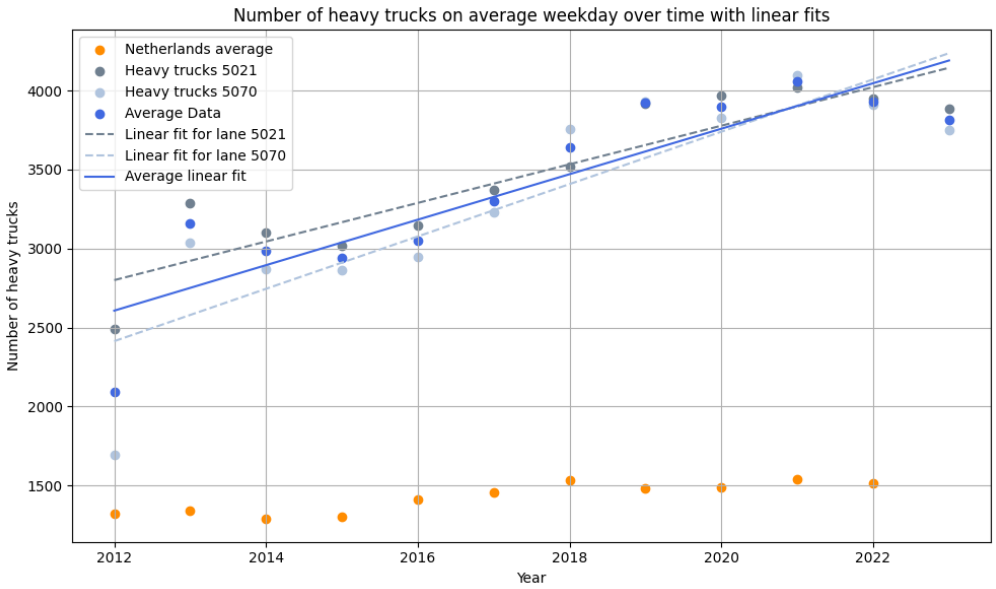

Figure 5.2: Traffic analysis for case study

5.2.2. Load factors

The dead weight of the structure does not include any specific details. The static loads consist of edge elements, such as the edge girder and kerbs, which cover the area on the carriageway starting from the edge of the flange of the edge girder, with the remainder classified as edge elements. The asphalt layer is 140 mm thick and the filling or pressure layer, a non-structural component, measures 50 mm. For mobile loads, LM1 is applied to the main girders. Alpha-factors are set to 1.0 for the critical lane, other lanes and the residual lane. The structure also includes an entrance and exit ramp. Given that the motorway consists of a 2 x 2 lane configuration, an alpha value of 1.00 is applied instead of 1.40/1.15. Usage factors are defined based on the duration and conditions of use. For standard usage, which allows unlimited use over 100 years, the factor is 1.00. For current or planned usage over a 30-year reference period, including a trend factor, the factor is 0.95. For emergency scenarios, the usage factor is reduced to 0.89. Rejection factors are applied for more constrained conditions. For current or planned usage over a 15-year reference period, including a trend factor, the rejection factor is 0.87. In emergencies, this factor decreases to 0.81. The reference year for the trend factor is 2043, derived from the introduction of RBK 1.1 in 2013, with an added 30-year projection.

5.3. Assessment

The assessment is based on the following codes: RBK version 1.1 (May 2013), NEN8700, NEN8701, NEN-EN 1990 + NB, NEN-EN 1991-1 + NB, NEN-EN 1991-2 + NB, NEN-EN 1992-1-1 + NB and NEN-EN 1992-2 + NB. In this study, the analysis focuses on the normative inner beam (beam 2), as it is the governing element in the structure, having the highest Unity Check values.

5.3.1. Load effects

Figure 5.3 illustrates all loads acting along the length of the normative inner beam, as derived from the Quick Scan by Movares. In the figure, ”EG + RB” represents the combination of the beam’s own weight (Eigen Belasting) and the traffic loads (Rijtuigen Belasting). The prestressing forces (”Voorspanning”) are considered as a negative load, counteracting the effects of EG + RB. Figure 5.3a specifically shows the shear forces along the beam, while Figure 5.3b presents the bending moments.

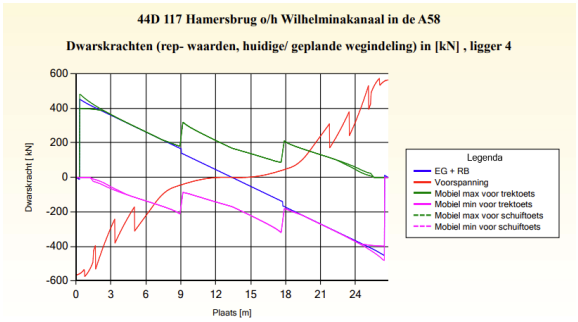

(a) Shear governed by the applied load.

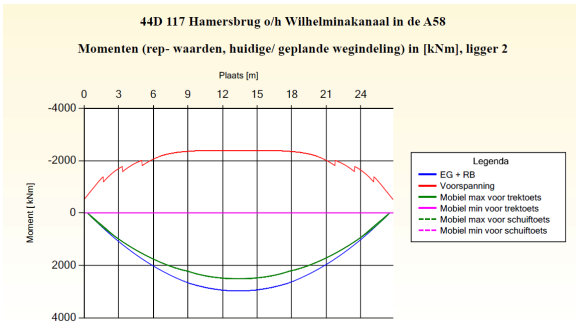

(b) Bending governed by the applied load.

Figure 5.3: Load effects for normative inner beam (2) of Hamersbrug [102].

The blue line representing ”EG + RB,” which combines the self-weight (Eigen Belasting) and traffic loads (Rijtuigen Belasting), has been extracted and analysed for both the shear and bending loads. This line is critical for understanding the structural behaviour under these combined loads.

Figure 5.4a shows the shear load distribution along the normative inner beam (2) of the Hamersbrug, while Figure 5.4b illustrates the bending moment distribution.

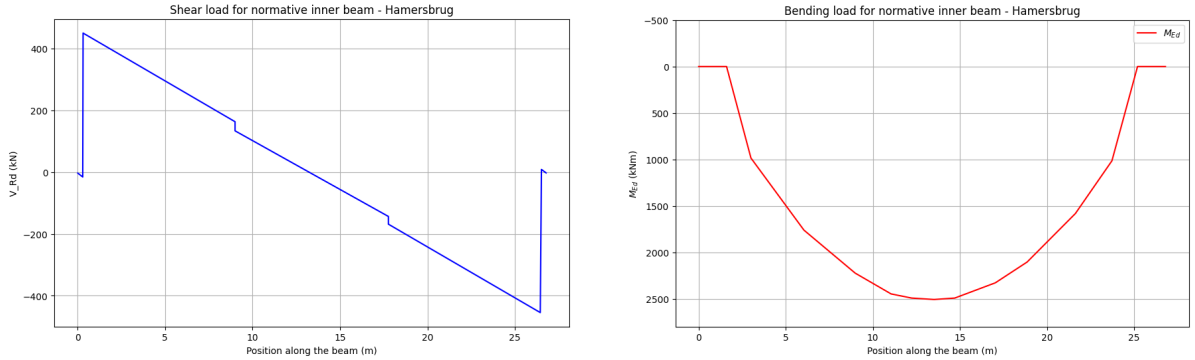

(a) Shear load.

(b) Bending load.

Figure 5.4: Bending load for normative inner beam (2) - Hamersbrug.

5.3.2. Unity Check

A similar approach is applied to the unity checks for shear and bending loads, as illustrated in Figures 5.5a and 5.5b. These unity checks feature three distinct lines representing different scenarios: Norm, current use (”Huidig gebruik”) and calamity (”Calamiteit”). This includes the prestressing force, resulting in a negative load effect.

The norm line corresponds to the Eurocode safety standards, incorporating safety factors to ensure the structure’s reliability under standard conditions. The current use line reflects the current traffic loads and intensities, providing a realistic assessment of the structure under normal operating conditions. The calamity line accounts for specific situations with traffic loads differing from those considered in LM1, such as emergency or exceptional scenarios.

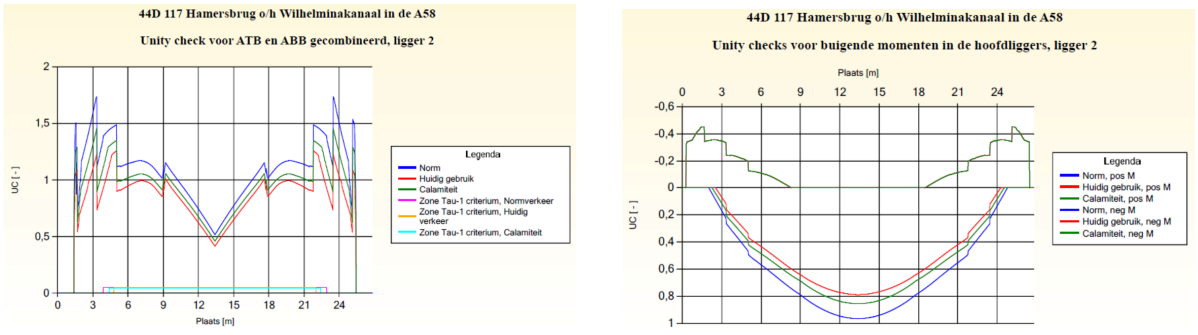

(a) Unity Check for shear.

(b) Unity Check for bending.

Figure 5.5: Unity checks for normative inner beam (2) of Hamersbrug.

The data extracted from the analysis is used to derive the unity check for the calamity scenario, as this represents the governing situation. This condition reflects the structural response under exceptional or emergency traffic loads, which differ from the standard assumptions in LM1. The results for the unity checks in the calamity scenario are presented in the Figure 5.6, detailing the shear and bending effects on the normative inner beam of the Hamersbrug.

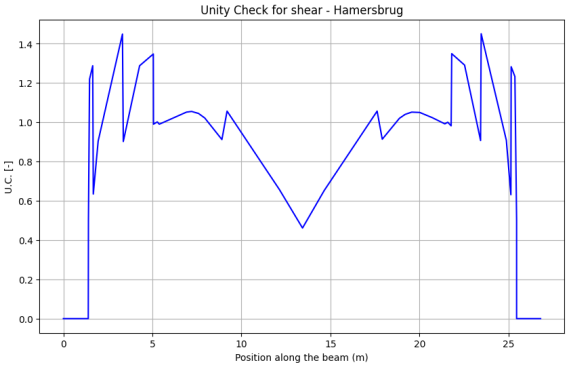

(a) Unity check for shear.

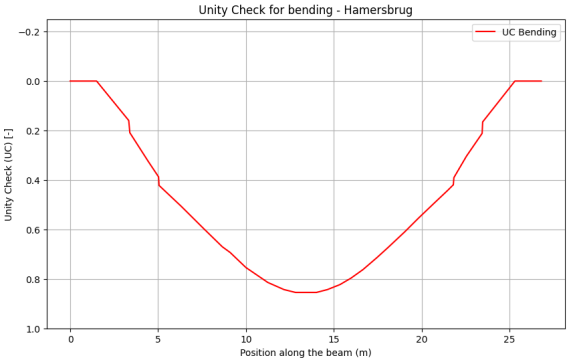

(b) Unity check for bending.

Figure 5.6: Unity checks for normative inner beam (2) - Hamersbrug.

Under the governing scenario with QP150 steel, the Unity Checks (UC) for shear forces exceed 1.0, particularly under calamity conditions. This indicates that the normative inner beam is shear critical, as the unity check values exceed the permissible threshold of 1.0. In contrast, the Unity Checks for bending moments remain within acceptable limits (below 1.0) for both the edge and inner beams across all traffic scenarios. An overview of critical Unity Check values is given in Table 5.1. A difference is made between shear, bending, traffic situation and location of the T-beam relative to the structure. Considering emergency traffic situations, the inner beam is governing, for shear and bending.

Table 5.1: Unity checks for shear and bending - Hamersbrug [102].

Criterion	Traffic situation	Outer beam	Inner beam
UC, shear in main girders	Free road layout	1.764	1.735
	Current road layout	1.203	1.259
	Emergency	1.367	1.456
UC, bending in main girders	Free road layout	0.936	0.966
	Current road layout	0.745	0.789
	Calamity	0.817	0.856

5.3.3. Load resistance

By using the loads and Unity Check values, the resistances of the beam can be derived along its length. This provides a simplified yet effective method of assessing the bridge without requiring a full structural model. Figure 5.7a and 5.7b provide the resistances along the length of the beam.

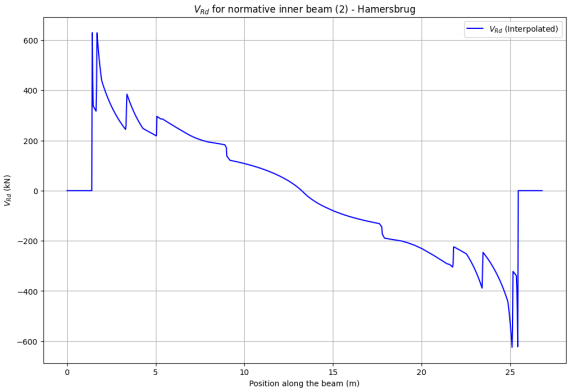

(a) Shear resistance.

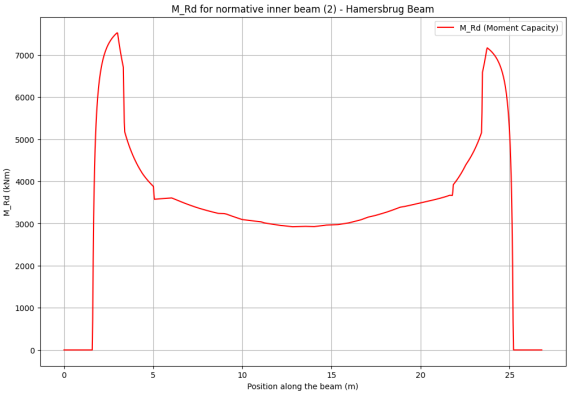

(b) Bending resistance.

Figure 5.7: Shear and bending resistance for normative inner beam (2) of Hamersbrug.

By comparing the load, resistance and Unity Check values, the weak points of the T-beam can be identified. This analysis provides valuable insights for designing an appropriate strengthening method, focusing on the most critical areas to enhance the structural performance. The highest Unity Check value for shear is reached at around 3.5 meters from the left and right support. Furthermore, the T-beam needs shear strengthening from 0 meters upon 9 meters from the support.

5.3.4. Reliability

The unity checks do not directly correspond to a measure of reliability, as they do not account for the uncertainty or variability of parameters. Additionally, unity checks include safety factors, whereas reliability does not. Determining the current level of reliability would be essential for assessing the structure's current state. From this, a deterioration curve could be derived, providing an estimate of the remaining lifetime of the structure. This assessment should ideally focus on the most critical shear point along the beam, identified as the location where the unity check scores highest, approximately 3.5 metres from the left and right of the support. It is expected that the reliability at this point is very low, as the unity check indicates insufficient performance.

Determining the reliability level in this case study is more complex, as it requires assessing the shear strength along the length of the beam. Ensink [8] presents a relevant case study focused on the Vecht bridge, involving seven tendons. Their prestressing forces are modelled using third-degree polynomials, which could be adapted to the Hamersbrug case study, having 12 tendons, to evaluate its resistance due to prestressing. Additionally, Ensink provides methods for calculating shear resistance, shear tension and the ultimate bending moment for such complex geometries.

Once this calculation framework is established, reliability methods such as FORM or Monte Carlo simulations could be applied to assess the current structural reliability. For simplicity, let us assume a rectangular T-beam in this analysis. The prestressing force and applied shear load can be derived from 5.3a and are approximately 370 and 350 kN, respectively. Key input parameters include steel properties (QR40), concrete cover (450 mm) and the annual traffic increase (5.4%) derived from Figure 5.2. Additional factors include, a friction coefficient (0.26), the wobble coefficient (0.01 [rad/m]), a relaxation loss (10%) and losses due to shrinkage and creep (10%). The current reliability is just above the threshold value, illustrated in Figure 5.8.

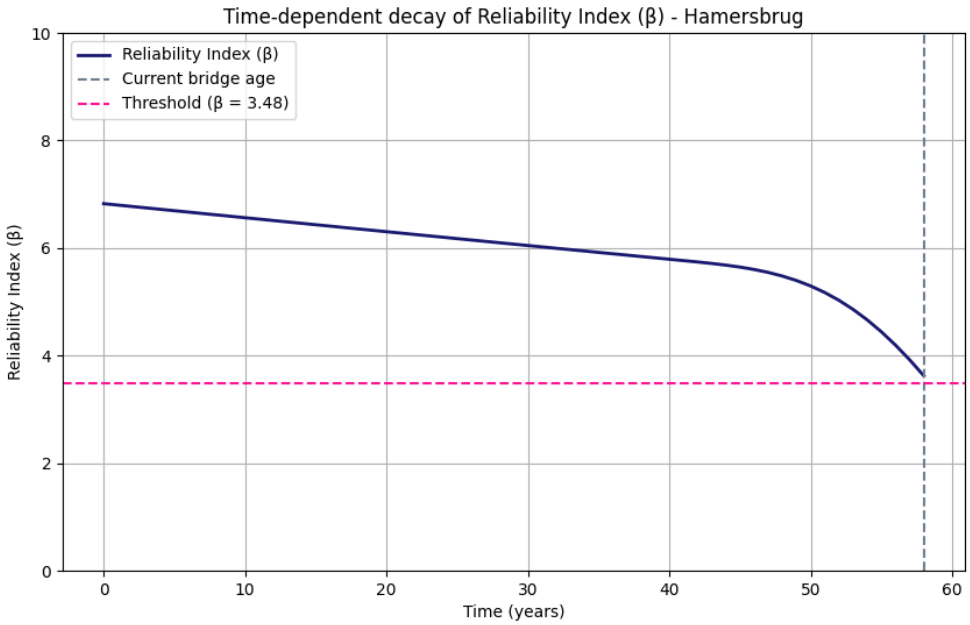

Figure 5.8: Reliability curve - Hamersbrug.

5.4. Strengthening

The strengthening designs are informed by the results presented in Chapter 3.1 and optimised for a desirable life extension of approximately 30 years, as determined by the reliability curve for shear. The critical cross-section is identified at approximately 3.5 metres from left and right of the support, where the Unity Check scores are the highest. As a result, the strengthening measures are primarily focused on this location to address the beam's most vulnerable point. The complex interaction between the T-beam and the cross-beams is not considered in the analysis and no strengthening is applied to these parts of the structure. This simplification ensures the focus remains on the critical section where the greatest need for intervention has been identified.

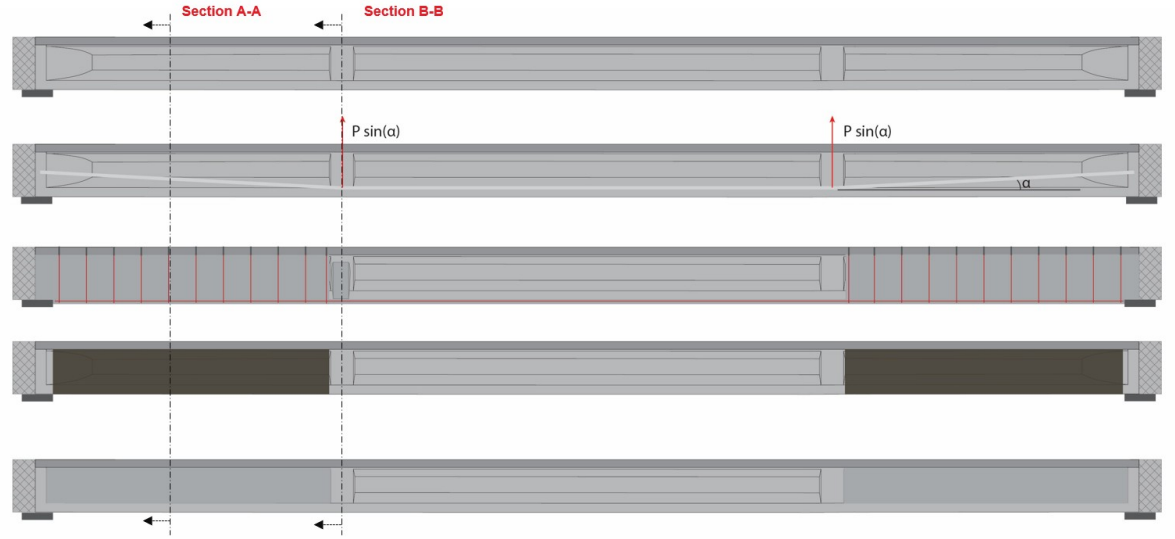

Figure 5.9: Case study strengthening applications over the length.

For external prestressing, the tendons are inclined, reaching optimal strengthening performance for shear and bending. The memory-steel, CFRP and UHPC are applied jut upon the cross-beam. Since we strengthen for shear between the support and cross-beam, that is where the unity check exceeds 1.0. For replacement, it is assumed, it is possible to design for a beam having the exact same dimensions, but now with stronger shear and bending properties. Due to new techniques compared to the building year, 1966, this should be possible.

The strengthening methods for section A-A are illustrated in Figure 5.10, showing external prestressing, memory-steel, CFRP and UHPC, arranged from left to right. The inclined external prestressing tendons reach half the height of the web at section A-A. Memory steel is applied around the bottom flange of the beam, enhancing tensile strength. An alternative approach involves drilling holes through the bottom flange to position the memory steel closer to the web, which would reduce the need for sprayed mortar. However, this method carries a significant risk of damaging existing reinforcement or prestressing steel, as drawings may not fully guarantee the precise placement of these elements within the cross-section. To reduce the risk of delamination, the rounded corners of the cross-section are filled. CFRP is wrapped completely around the web and bottom flange. Anchoring is carried out in the curved sections to minimise the risk of delamination and ensure improved bonding, resulting in a higher strengthening increase. UHPC is used to fill the existing beam profile, transforming it into an alomst rectangular web. The UHPC is reinforced, connecting the existing structure and the UHPC. The reinforcement within the UHPC is not considered when calculating the amount of steel used, as it was not included in the framework. This aspect could be refined in future analyses.

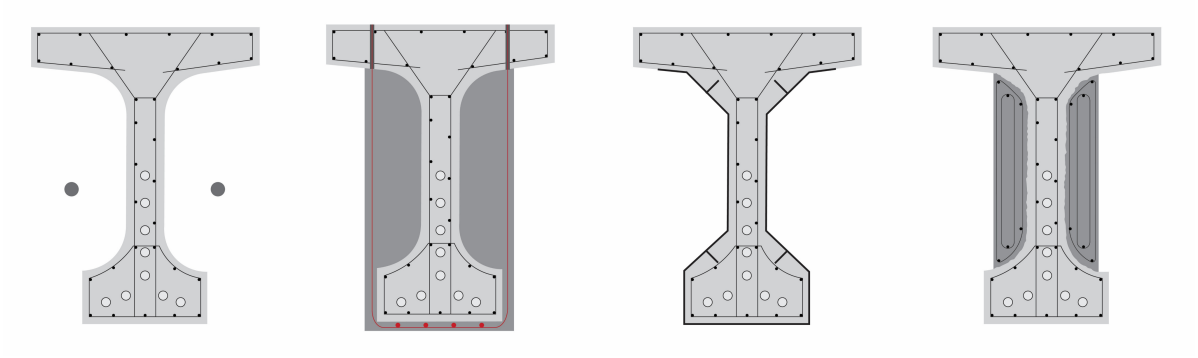

Figure 5.10: Strengthening design cross-sections A-A.

Where for section B-B shows the cross-section at the cross-beams The external prestressing is anchored, at the cross-beams, since high shear force is applied, a steady cross-section is needed, which is provided by the cross-beam. Then the memory-steel is applied over the full length of bottom flange. UHPC and CFRP are not applied at the cross-beam section.

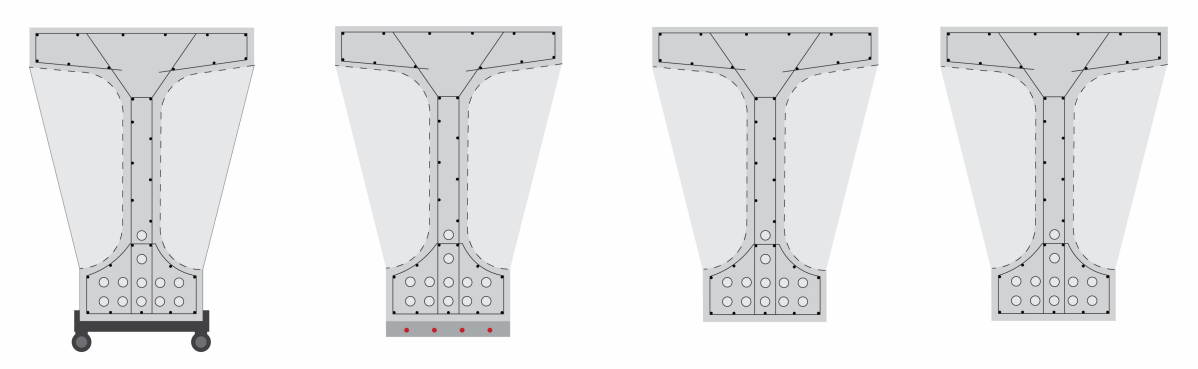

Figure 5.11: Strengthening design cross-sections B-B.

In this specific case, memory-steel can already be excluded due to the significant weight increase caused by the sprayed mortar. Over a length of approximately 9.5 metres on both sides, with a density of $2200\,\mathrm{kg/m^3}$ and a cross-sectional area of $508{,}000\,\mathrm{mm^2}$, the additional weight would reach values of $21{,}250\,\mathrm{kg}$ ($2165.0\,\mathrm{kN}$) in total or an extra load of $115\,\mathrm{kN/m}$.

After strengthening, the Unity Check can be considered again If the unity check is very low, optimisation is possible, since the strengthening method is over performing. It is possible to reduce the amount of strengthening material, reducing the strength increase, environmental impact and material costs. As explained before, some methods cannot be optimised since they have certain design boundaries. As is illustrated in Figure 5.13 Where some unity checks remain way below 1.0. The adjustment of design parameters is an iterative process and done by hand for this case study.

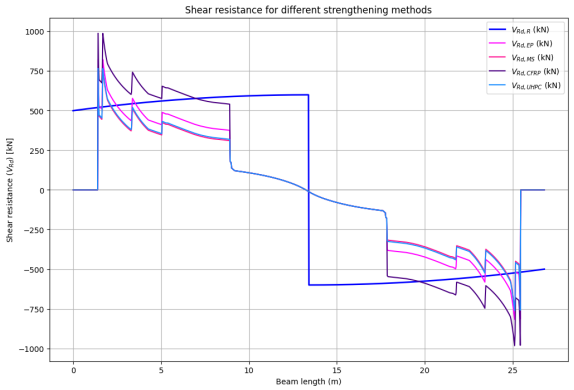

Figure 5.12: Shear increase after strengthening.

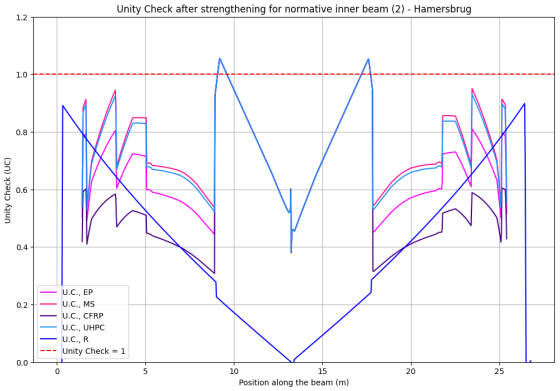

Figure 5.13: Unity checks after strengthening.

The external prestressing system includes an angle of 4.5 degrees and uses prestressing steel with a diameter of 12 mm. Two tendons are placed, each experiencing a prestressing stress of 100 MPa. The tensile strength of the steel (f_{pk}) is 1860 MPa. Four anchors are used in total, with two located at the supports and two at the cross-beams. The anchors are positioned at the web for the supports and at the bottom flange for the cross-beams. The memory-steel stirrups have a diameter of 8 mm, while the longitudinal reinforcement bars have a diameter of 10 mm. The memory-steel stirrups are spaced 850 mm apart and the sprayed mortar used has a thickness of 50 mm. The CFRP system consists of a single sheet with a thickness of 0.13 mm. The fibres are oriented at an angle of 90 degrees. The ultra-high performance concrete layer has a thickness of 20 mm. Figure 5.14 shows the reliability curve after strengthening.

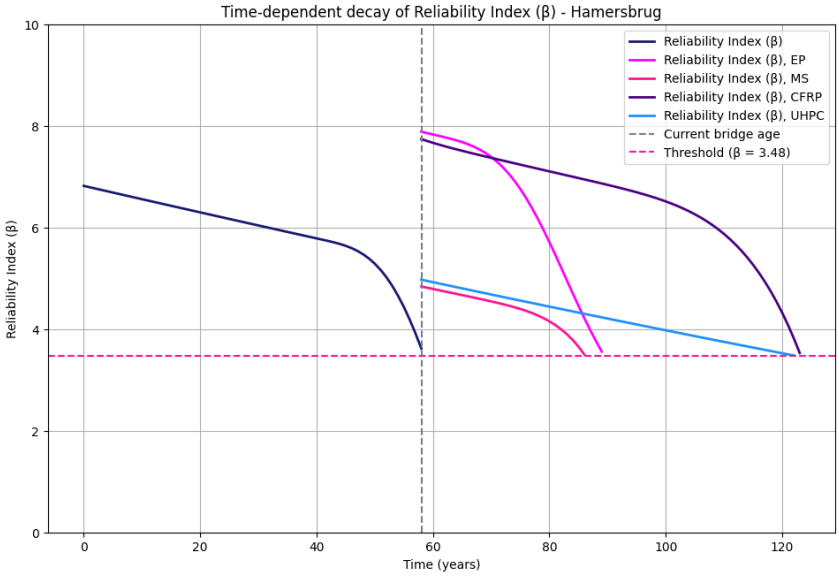

Figure 5.14: Reliability curves for shear after strengthening - Hamersbrug.

As illustrated in Figure 5.5a, the unity check still exceeds 1.0 at the location of the cross-beams. Although this indicates insufficient performance, it is impractical to rely on the framework to address this issue. The service life extensions for external prestressing, memory-steel, CFRP, UHPC and replacement are estimated at 24, 30, 63, 64 and 80 years, respectively. These values are set within the decision-making process, with the extension of lifetime considered as a key criterion. Once the strengthening parameters have been optimised, the Analytical Hierarchy Process (AHP) and further analysis of the results can be performed.

5.5. Sensitivity analysis

The sensitivity analysis focuses on identifying trends and patterns in the decision-making process, specifically in the context of the case study. The previously described optimisation for strengthening is applied, whereupon the amount of material calculated and combined with qualitative performance criteria; GWP, AP, APDf, material costs and health risk. Quantitative considerations are based on insights from Chapter 2.8 and 3.4. The results are presented in Table 5.2.

Category	EP	MS	CFRP	UHPC	R
GWP	102.48	901.34	133.74	7038.44	18690.60
AP	0.28	2.73	1.38	4.94	142895.26
APDf	1073.77	3399.81	2042.40	7387.67	45531.73
Material Costs	548.03	1778.97	2907.33	11820.28	21747.84
Construction Speed	4.00	1.00	5.00	4.00	1.00
Construction Costs	2.00	4.00	2.00	2.00	5.00
Maintenance Costs	2.00	1.00	2.00	4.00	1.00
Health Risk	204.06	196.87	38.38	2600.46	1631.50
Traffic Hindrance	1.00	1.00	1.00	1.00	5.00
Reduction in Functional Height	0.00	50.00	0.13	0.00	0.00
Service Life Extension	24.00	30.00	63.00	64.00	80.00
Durability	3.00	5.00	5.00	5.00	3.00
Scarcity	2.00	3.00	4.00	3.00	3.00
Extensibility	4.00	1.00	2.00	1.00	4.00
Strengthenability	5.00	1.00	1.00	3.00	5.00
Disassembility	5.00	2.00	1.00	1.00	2.00
Transportability	4.00	5.00	5.00	5.00	5.00

Table 5.2: Performance criteria, Hamersbrug.

The values from Table 5.2 are plotted in spider charts to visually illustrate the impact of each strengthening method and provide deeper insights into the results. Below, the performance of different criteria is categorised into the aspects of sustainability, integrity and circularity. While integrity and circularity are components of sustainability, they are considered separately for clarity. To enhance comparability, the values are normalised. The lowest value in each category is set to 0.2, while the highest is set to 1.0, with all other values plotted linearly in between. The sustainability aspects of the performance criteria are illustrated in Figure 5.15.

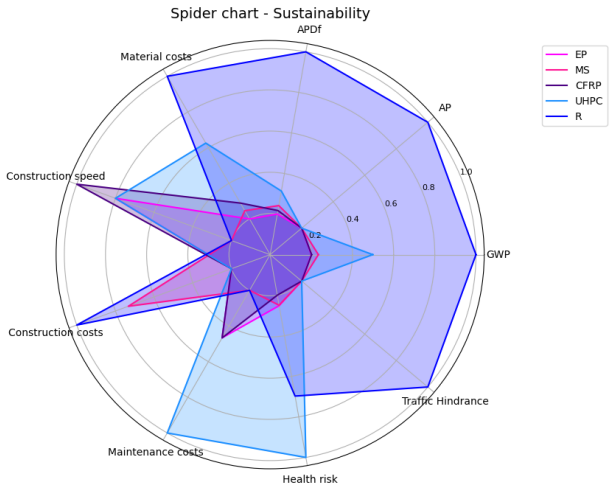

Figure 5.15: Spider chart sustainability - Hamersbrug.

Replacement has a very high environmental impact and therefore dominates the chart. UHPC, while effective, presents significant health risks and high maintenance costs. Since this chart focuses on minimising environmental impact, traffic hindrance and material costs, replacement emerges as the least favourable scenario. Conversely, CFRP performs well in terms of construction speed and scores low on criteria that should be minimised. Integrity aspects, related to safety considerations, are illustrated in Figure 5.16.

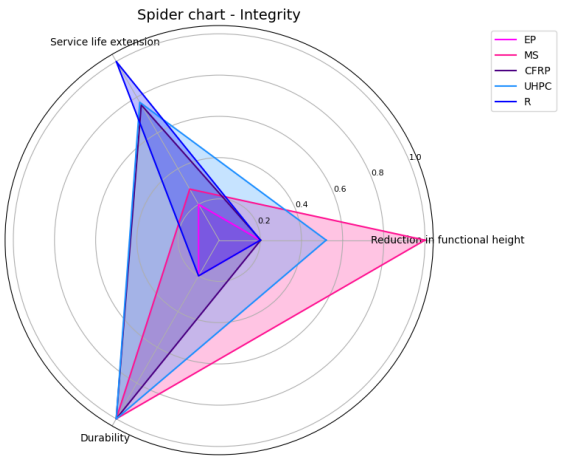

Figure 5.16: Spider chart integrity - Hamersbrug.

Minimising the reduction in functional height is a key objective, making memory steel the least favourable option in this regard. Extending the service life is also crucial, with replacement scoring highest. However, external prestressing and replacement are susceptible to corrosion, resulting in lower durability.

From a circularity perspective, minimising material scarcity is a priority. CFRP scores high in this regard, which is undesirable. In contrast, replacement and external prestressing are considered favourable methods when assessed based on circularity principles.

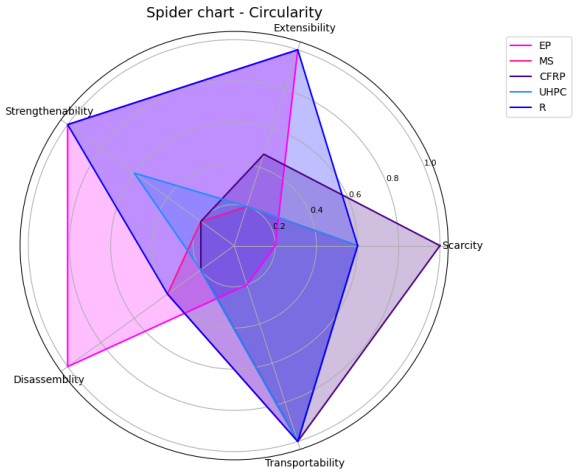

Figure 5.17: Spider chart circularity - Hamersbrug.

After considering the performance criteria, which remain fixed in the sensitivity analysis, the framework's sensitivity to these criteria can be assessed. Assigning random weights to the criteria and repeating the analysis 1,000 times results in EP being selected in the majority of iterations, with only two or three exceptions. This is illustrated in Figure 5.18.

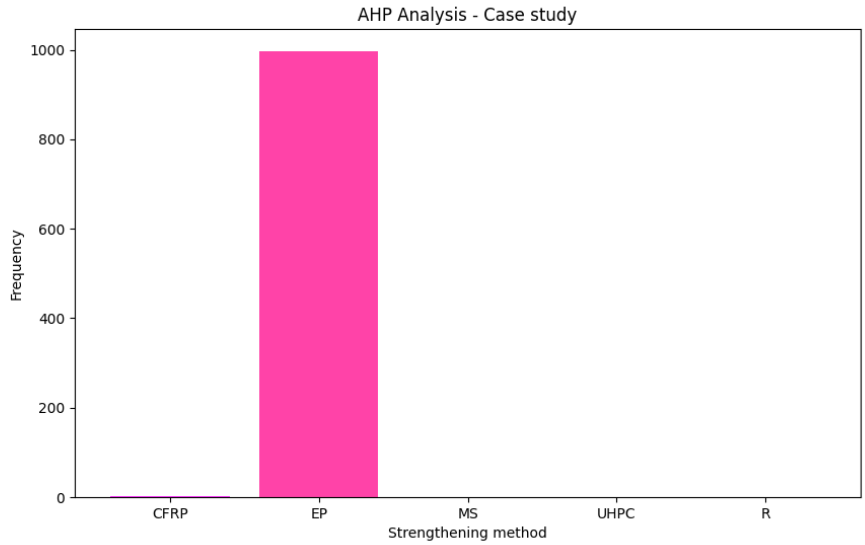

Figure 5.18: Random decision-making for strengthening of Hamersbrug.

This aligns with the results illustrated in Figure 4.19, where a larger span length leads to external prestressing being selected as the optimal strengthening method, underlining external prestressing becomes more effective while having less impact on the environment and costs increase is reduced. This relates to Figure 4.11 and 4.12. CFRP is preferred when durability, health risk, service life extension and global warming potential (GWP) are prioritised, whereas material costs, disassemblability, acidification potential (AP) and reduction in functional height are considered less critical. External prestressing achieves a nearly equivalent ranking, with a difference of no more than 0.010. On average, EP attains a target weight of 0.334, distinguishing itself significantly from other methods, with CFRP ranking second, as shown in Table 5.3.

Method	Average	Std.
EP	0.334	0.02
MS	0.157	0.03
CFRP	0.227	0.01
UHPC	0.140	0.01
R	0.140	0.02

Table 5.3: Average target weights and standard deviation for strengthening methods - Hamersbrug.

The results highlight the potential of the framework to support decision-making in the case study. However, these findings should not be considered as appropriate results. Applying the same framework used for a rectangular T-beam, with identical strengthening outcomes, to this specific case may lead to unrealistic conclusions. For instance, always selecting external prestressing as the preferred option seems unrealistic, as there are scenarios where other methods might be more appropriate. Rather than delivering definitive conclusions, the framework should be viewed as a tool to assist and guide the decision-making process. It provides a structured approach but does not replace the need for critical evaluation and contextual strengthening design in each unique case.

6

Discussion

6.1. Summary

Since a lot of concrete bridges and viaducts have a designed service-life of 80 years and were built around 1970, these structures will reach the end of their service-life between 2040-2060 [3]. When structures no longer meet current safety or reliability requirements, either strengthening or replacement is needed. Strengthening can significantly reduce the amount of material used, lower costs and environmental impact when compared to replacement [5]. However, replacement highly increases the extended service-life. If it is decided to apply strengthening, many different strengthening methods and designs can be applied. Comparing these methods is complex, since many criteria can influence the decision-making and the importance weighting of criteria can differ per stakeholder. Therefore, decision-making frameworks are designed, supporting the decision-maker in understanding and comparing different strengthening and replacement scenarios. While most existing frameworks focus on technical and cost aspects [12, 13, 14], they lack sustainability criteria and performance prediction.

Therefore, the key objective of this study was to develop a framework for evaluating different strengthening methods based on sustainability and service-life considerations focused on prestressed concrete T-beams in bridges. The framework considers (environmental) costs, service-life, circularity and reliability. The study compares strengthening methods external prestressing (EP), memory-steel (MS), carbon fibre reinforced polymer (CFRP) and ultra-high performance concrete (UHPC) against total replacement.

Since shear deficiencies are very common in T-beams [8], the emphasis is more on shear strengthening then on bending strengthening. Validation is performed by comparing theoretical and experimental results. The design of strengthening methods is based on multi-objective optimisation, maximising strength increase while minimising environmental impact and costs. This is integrated into a multi-criteria decision-making process, specifically using the Analytical Hierarchy Process [100], ensuring transparency and covering the complexity of comparison. It combines all performance indicators and their relative importance as defined by stakeholders. Ultimately, the framework results in an interactive tool for calculating the optimal strengthening method. The parametric framework is applied to a case study, the Hamersbrug, to validate its applicability to real-world cases.

The parametric framework provides the opportunity for repeated assessments, identifying trends across different spans, cross-sections, current structure states and deterioration phenomena. CFRP consistently emerges as the optimal method for most cases considered, due to its lightweight nature, high strength, corrosion resistance and ease of application, as mentioned by Hosseini et al. [46] and Wang et al. [47]. External prestressing scores high as well, particularly for larger spans, due to its strong strength-to-impact ratio and low amount of material usage [38], which relates directly to the environmental impact. Whereas memory-steel is never selected, likely due to its high material costs, construction costs and low circularity score. In rare cases, where criteria such as durability and reducing the health risk are very important and specific span lengths, UHPC can be the optimal method. This reflects and confirms why EP and CFRP are widely used, as mentioned in [34, 35, 36, 37].

6.2. Interpretations

This paragraph elaborates on how to interpreter the framework and its results. AHP has been validated as a reliable tool for strengthening decision applications, enhancing the clarity of comparisons between strengthening methods and final decisions made by the framework. Through a parametric study, the framework provides valuable insights into different strengthening approaches, particularly for prestressed concrete T-beams. Although, it introduces a highly analytical perspective on decision-making, which may not always be preferred in practice.

It should be noted that the considerations in performance criteria, described in Chapter 3.4, are incomplete since the full LCA was not included due to time constraints. Also, the quantitative values are hard to define and can differ per reference. Since the framework is coded in Python and the code is provided, it should be relatively easy to add or adapt assessment criteria if needed. In the case study, external prestressing was frequently selected, raising concerns about the general applicability of the framework to real-world cases and complex geometries. This suggests that the framework may become less reliable for other geometries than standard T-beams.

The framework is highly adaptable, being coded in Python, with key components outlined in Appendix C. An overview of the framework components is shown in Figure 4.8. Each component—geometry, capacity, material properties, loads over time, structural assessment, reliability calculation, strengthening prediction, and the multi-criteria decision-making process—is clearly defined, modelled and designed to be adaptable or improved. Different strengthening methods can easily be attached to the current methods, if enough literature and experiments are available. Also different kind of analysis can easily be set-up, this could give the user specific insights needed to validate the conclusion or compare on certain aspects. While modifications to geometry, loads, or other parameters are possible, adjustments to strengthening predictions require careful recalibration and validation, which can be time-consuming.

Any user of the framework should carefully consider the outcome. Because the framework provides structured decision-making support and should be regarded as a guiding tool rather than a definitive decision-maker. The framework represents an initial step towards improving decision-making on strengthening versus replacement, though it remains a work in progress and is far from complete.

6.3. Implications

The study provides a new perspective on decision-making by gathering all sorts of considerations impacting decision-making and aiming to simplify the complexities in decision-making for bridge renovation versus replacement. It makes a first attempt in considering circularity as part of sustainability, the service-life of structures, linking safety and reliability to long-term performance. By including the application of the AHP, the creation of detailed reports that provide clear insights into the decision-making process is available. This method is both flexible and intuitive, offering stakeholders a sense of transparency and satisfaction in their decision-making process.

In doing so, the framework advances and upgrades existing decision-making models found in the literature, bridging gaps discussed in Chapter 2.1. The sensitivity analysis provides valuable insights into strengthening decisions, leading to several conclusions and interpretations. However, these should not be viewed as definitive recommendations for the optimal strengthening method in general, as many factors influence decision-making. Nonetheless, the findings are significant and could serve as a basis for further investigation. Overall, the proposed framework equips decision-makers with a powerful tool to balance environment, society, cost and circularity considerations when evaluating strengthening versus replacement strategies.

6.4. Limitations

Despite its adaptability, the framework has several limitations that should be acknowledged. First of all, the load model applied in the framework includes simplifications, which may reduce its accuracy in capturing the complexities of real-world conditions. Similarly, the deterioration mechanisms considered for both existing structures and post-strengthening conditions are restricted in scope and may not fully represent all possible modes of degradation. These modes are very simplified and based on a limited amount of deterioration phenomena, described in Chapter 3.3.4.

Furthermore, strengthening methods offer numerous design options, but to maintain focus, certain choices were made to limit the research scope. Additionally, the analysis does not account for the interaction between shear and bending forces, which may influence the overall structural performance. Due to time constraints, the study primarily focused on shear deficiencies and shear strengthening, as these were the main concerns in the case study. Consequently, the reliability curve for bending strength is less developed than for shear, making comparisons between bending and shear challenging. Since there is no FORM (First-Order Reliability Method) model for bending strength, no direct comparison can be made regarding the increase in bending strength, making it difficult to validate differences in outcomes.

The shear strengthening predictions for CFRP [78] remain under evaluation and are not entirely reliable. Although these are based on Eurocode, further research is needed to improve the accuracy of CFRP performance assessments, a limitation that applies to all strengthening methods.

The comparison with replacement also presents challenges. Accurately assessing the composition and cost of materials used in replacement is difficult, as these are project-specific and vary based on boundary conditions. Additionally, the composition of the concrete mix significantly influences strength properties [60, 59], making direct comparisons with replacement more complex. Since the framework does not optimise a replacement design by calculating the required strength, evaluating replacement strategies remains case-dependent, with no universal solution.

The combination of different strengthening methods is theoretically possible but not explicitly accounted for in the framework. If applied to distinct locations—such as bending strengthening in the middle and shear strengthening at the ends—such an approach could be feasible. However, the interaction effects between different strengthening methods are not considered in the framework and would require further investigation.

6.5. Recommendations

Future research could improve the framework by addressing several critical areas, improving its scope, accuracy and applicability. The framework could be expanded by incorporating additional LCA stages and refining the performance indicators outlined in Chapter 2.9 (Appendix B). Additionally, improving the AHP weighting process by allowing criteria to be grouped and weighted against each other, as described in Chapter 3.5.1, would provide more flexibility and refinement in decision-making.

Including more complex geometries in the analysis and applying the framework to a broader range of case studies would improve its robustness and real-world applicability. Using Ensink's methodology [8] to assess the strength, reliability and remaining lifetime of T-beams could lead to more precise conclusions for the specific case study considered. This would require new strengthening predictions and a reassessment of the Python-based framework, redefining its scope and validation process.

Currently, the framework optimises strengthening primarily for shear deficiencies. A more integrated approach, considering the interaction between bending and shear, would improve accuracy and efficiency. By optimising for shear or bending and checking whether both shear bending meets required performance levels, strengthening designs could be further refined. This would enable material, cost and environmental impact reductions, leading to more efficient solutions (Chapter 3.3.5).

A deeper analysis of deterioration mechanisms for both existing and strengthened structures is essential for predicting long-term performance more accurately. This could be achieved by examining degradation patterns for various strengthening materials using literature reviews and experimental data. Existing research on structural degradation could be incorporated into the framework, such as Arup's service-life predictions and machine learning-based estimations (AI and Uncertainty Quantification for assessing the remaining useful life of concrete structures) (see Figure 3.19).

A different perspective on structural reliability could further refine decision-making. Literature by De Vries, which bases reliability calculations on the continued existence of a structure—implying an increase in reliability over time—presents an interesting approach. Incorporating this concept could lead to a more efficient service-life extension strategy, potentially reducing the necessary reliability increases for the same lifetime extension.

By addressing these areas, the framework could evolve into a more complete and accurate decision-making tool for prestressed concrete strengthening, balancing technical, economic and environmental considerations more effectively.

7

Conclusion

The study presents a framework for comparing the sustainability, cost, societal impact, service-life performance and circularity of strengthening strategies for prestressed concrete T-beams. Current decision-making frameworks primarily focus on performance and cost without addressing sustainability, reliability and service-life performance (Chapter 4.3.4). The objective of this research, as defined in Chapter 1.3, was to develop a decision-making framework capable of balancing many criteria to optimise the selection of strengthening strategies versus replacement for prestressed concrete T-beams.

The study compares strengthening methods external prestressing (EP), memory-steel (MS), carbon fibre reinforced polymer (CFRP) and ultra-high performance concrete (UHPC) against total replacement. The development of the framework involved multiple steps. Chapter 3 details the methodological approach, which included deterministic and probabilistic analyses to evaluate structural deterioration, traffic loads and strengthening impacts. The study considered common deterioration mechanisms such as corrosion and prestress loss (Chapter 2.7) and incorporated these factors into a parametric model. In this manner, the time-dependent factor was incorporated.

The framework integrates the Analytic Hierarchy Process (AHP) to evaluate multi-criteria decision-making. AHP was chosen due to its proven reliability in prioritising complex variables, as explained in Chapter 3.5. This integration allowed for a systematic assessment of strengthening methods based on performance indicators such as environmental costs, societal implications and service-life extension. Integration of all performance criteria, allowing for adaptation, is feasible due to the flexibility of the AHP. As outlined in Chapter 2.9, this also includes circularity, based on the framework of Coenen et al. [70].

The parametric study, described in Chapter 4, provided useful insights into the relative performance of different strengthening methods. External prestressing, memory-steel, CFRP and UHPC were evaluated for their impact on shear and bending performance. The analysis revealed that UHPC is primarily selected when assessing strengthening on a per-kilogram material basis, excelling in sustainability aspects. CFRP consistently emerges as the optimal strengthening method, maintaining relatively balanced scores across all assessment criteria, making it a robust and adaptable solution. External prestressing ranks highly, particularly for larger spans, due to its strong strength-to-impact ratio. Memory-steel is never selected as the preferred method, likely due to its lower efficiency in strength enhancement and high material cost. While predicting the exact selection of a strengthening method is challenging, as it depends on the relative importance of assessment criteria, general trends remain observable. The randomised weightings influence selection patterns, causing fluctuations in outcomes. When replacement is included as an option, it is frequently selected. Although replacement may appear optimal in some cases, its practical implementation requires careful consideration. In scenarios with varying cross-Chapters and span lengths, CFRP demonstrated superior performance and was the most frequently chosen method. This finding, detailed in Chapter 4.4, underscores CFRP's adaptability and efficiency in diverse structural contexts. Conversely, memory-steel consistently underperformed in all evaluated scenarios, indicating limited applicability within the scope of this framework.

To validate the framework, a case study was conducted on the Hamersbrug, as described in Chapter 5. This real-world application tested the framework's ability to predict optimal strengthening methods based on more complex geometries. However, the results significantly differed from the theoretical outcomes predicted by the framework. While the framework finds CFRP as optimal strengthening method in many cases, EP arises as the optimal method for the case study, which is a trend for large spans, although always selecting EP as the preferred option seems unrealistic, as there are scenarios where other methods might be more appropriate. These differences, discussed in Chapter 5.5, suggest that the framework's current scope may be insufficient for complex, system-wide applications.

The framework has several limitations that should be acknowledged. The load model in the framework includes simplifications that may reduce its accuracy in capturing real-world complexities and the deterioration mechanisms considered for both existing and post-strengthening conditions are limited in scope. Strengthening methods offer various design options, but certain choices were made to narrow the research focus, excluding shear-bending interaction effects. Due to time constraints, the study primarily focused on shear deficiencies. Since the First Order Reliability Method separates shear and bending, only shear reliability was considered, resulting in a less developed reliability curve for bending strength and preventing direct comparisons between their impacts. While bending strengthening was predicted, validated and incorporated into the framework, no optimisation or further analysis was conducted. However, in some cases, the optimal strengthening method may vary if bending deficiencies are present, as certain methods are better suited for addressing bending issues. Finally, comparing strengthening with replacement is also challenging, as material composition and costs vary by project and boundary conditions. Additionally, the framework does not optimise replacement design based on required strength, making evaluations case-dependent.

Despite its limitations, the framework represents a significant step forward in integrating sustainability, reliability and service-life considerations into decision-making for strengthening of prestressed concrete. The use of AHP enables the generation of detailed reports that improve transparency and stakeholder satisfaction, offering a structured yet adaptable tool for evaluating strengthening strategies. Therefore, the use of AHP in decision-making is highly recommended.

The findings also have broader implications for research and practice. By prioritising UHPC and CFRP as optimal strengthening materials under different scenarios, the framework provides insights into the material selection process. These materials' superior performance, as demonstrated in Chapter 3.1, supports their wider adoption in infrastructure projects aiming to balance performance, cost and environmental impact. Building on the findings and limitations of this study, several recommendations for future research are outlined in Chapter 6:

1. The framework could be expanded by incorporating additional LCA stages and refining the performance indicators outlined in Chapter 2.9 and Appendix B.
2. Improving the AHP weighting process by allowing criteria to be grouped and weighted against each other (Chapter 3.5.1), would provide more flexibility and refinement in decision-making.
3. Currently, the framework optimises strengthening primarily for shear deficiencies. A more integrated approach, considering the interaction between bending and shear, would improve the strengthening designs and could be further refined. Considering bending and shear together, assessing their impact, and then optimising for either one may lead to a different choice of the optimal strengthening method.
4. A further analysis of deterioration mechanisms for both existing and strengthened structures is essential for predicting long-term performance more accurately. This could be achieved by examining degradation patterns for various strengthening materials using literature reviews and experimental data. Existing research on structural degradation could be incorporated into the framework, such as Arup's service-life predictions and machine learning-based estimations.
5. A different perspective on structural reliability could further refine decision-making. Literature by De Vries [23], which bases reliability calculations on the continued existence of a structure—implying an increase in reliability over time—presents an interesting approach. Incorporating this concept could lead to a more efficient service-life extension strategy, potentially reducing the necessary reliability increases for the same lifetime extension. The varying reliability threshold proposed by Kotes et al. [20] is also excluded, as its application remains under discussion.

In conclusion, this study demonstrates that a systematic framework integrating multi-criteria decision-making tools like AHP can effectively compare strengthening methods. Although it is very hard to include the comparison with replacement, since replacement can be designed on minimising cost, environmental impact or any other criteria. The framework allows for evaluating methods based on performance indicators, environmental impact, societal costs and service-life predictions. Although the proposed framework offers a structured and transparent approach to decision-making, it should be viewed as a decision-support tool rather than a replacement for engineering judgment. Future research aimed at extending its applicability to more complex systems will further enhance its value for managing the ageing infrastructure challenges facing the Netherlands.

Final recommendations for stakeholders, of a R&R decision-making processes, reading this report can be considered. First of all, use the framework to compare strengthening options systematically but consider practical constraints when making final decisions. Secondly, treat the results as a guidance tool rather than an absolute selection mechanism, incorporating engineering expertise and real-world constraints. Thirdly, consider further refinement of the AHP weighting process to reflect specific project requirements. And finally, future research is encouraged and data could be integrated to enhance the framework's ability to model complex deterioration mechanisms and long-term performance predictions.

References

[1] Harald Arlander. *Grayscale photo of concrete bridge*. Accessed: 2025-02-19. 2017. URL: https://unsplash.com/photos/grayscale-photo-of-concrete-bridge-DW3_QkRIdmo.

[2] R. Imming W. Jonger. *Strategische oplossingen in het kader van de Vervanging en Renovatieopgave van bruggen en viaducten*. 2019.

[3] HKV Consultants. *Lifetime and replacement cost analysis for bridges and overpasses in the Dutch RN*. Tech. rep. Accessed: 2024-06-16. 2020. URL: https://www.hkv.nl/wp-content/uploads/2020/08/Lifetime_and_replacement_cost_analysis_for_bridges_and_overpasses_in_the_Dutch_RN_SvV.pdf.

[4] Ir. A.N. Bleijenberg. *Instandhouding civiele infrastructuur; Proeve van landelijk prognoserapport vervanging en renovatie*. Tech. rep. TNO, 2021.

[5] *R-Strategies for a Circular Economy*. URL: https://www.circularise.com/blogs/r-strategies-for-a-circular-economy (visited on 05/01/2024).

[6] A. Hartmann and J. Bakker. "The End-of-Life of Bridges: Integrating Functional, Technical and Economic Perspective". In: *CRC Press eBooks*. CRC Press, 2023, pp. 981–988. DOI: 10.1201/9781003323020-119. URL: https://doi.org/10.1201/9781003323020-119.

[7] Ali H. Omar, M. Fethi Gullu, and Ghafur H. Ahmed. "Experimental and analytical investigation of T-beams retrofitted through the external post-tensioning using steel and various FRP strands". In: *Structures* 68 (2024), p. 107129. ISSN: 2352-0124. DOI: https://doi.org/10.1016/j.istruc.2024.107129. URL: https://www.sciencedirect.com/science/article/pii/S2352012424012815.

[8] S.W.H. Ensink. "System behaviour in prestressed concrete T-beam bridges". English. Dissertation (TU Delft). Delft University of Technology, 2024. DOI: 10.4233/uuid:15f5628b-9175-4ef3-8f39-41a97cb7749a.

[9] Y. Xie et al. "Quantifying the Performance Age of highway bridges". In: *Life Cycle Analysis and Assessment in Civil Engineering: Towards an Integrated Vision*. 1st. CRC Press, 2018, p. 14.

[10] S.C.A. Mooren. *To Replace or Not to Replace: Developing a Model for Bridges' Future Functional Performance Level*. 2022. URL: http://essay.utwente.nl/93121/.

[11] Neel Renne et al. "Sustainable Assessment of Concrete Repairs through Life Cycle Assessment (LCA) and Life Cycle Cost Analysis (LCCA)". In: *Infrastructures* 7.10 (2022). ISSN: 2412-3811. DOI: 10.3390/infrastructures7100128. URL: https://www.mdpi.com/2412-3811/7/10/128.

[12] B. Briseghella et al. "The greenway for bridge column rehabilitation: a comparison between different techniques based on multi-criteria decision analysis". In: *Revista IBRACON de Estruturas E Materiais* 15.6 (2022). DOI: 10.1590/s1983-41952022000600001. URL: https://doi.org/10.1590/s1983-41952022000600001.

[13] Saad Raza et al. "Strengthening and Repair of Reinforced Concrete Columns by Jacketing: State-of-the-Art Review". In: *Sustainability* 11.11 (2019), p. 3208. DOI: 10.3390/su11113208. URL: https://doi.org/10.3390/su11113208.

[14] Vittoria Borghese et al. "Sustainable retrofits on reinforced concrete infrastructures". In: (2024). DOI: 10.4430/bgo00436.

[15] Christoph Scope, Maria Vogel, and Edeltraud Guenther. "Greener, cheaper, or more sustainable: Reviewing sustainability assessments of maintenance strategies of concrete structures". In: *Sustainable Production and Consumption* 26 (2021), pp. 838–858. ISSN: 2352-5509. DOI: https://doi.org/10.1016/j.spc.2020.12.022. URL: https://www.sciencedirect.com/science/article/pii/S2352550920314214.

[16] T.P. Houten and Linda Zhang. “Managing Assets in The Infrastructure Sector”. In: *International Journal of Engineering Business Management* 2 (2010). DOI: 10.5772/9722.

[17] Jianjun Qin Michael H. Faber Simona Miraglia and Mark G. Stewart. “Bridging resilience and sustainability - decision analysis for design and management of infrastructure systems*”. In: *Sustainable and Resilient Infrastructure* 5.1-2 (2020), pp. 102–124. DOI: 10.1080/23789689.2017.1417348. eprint: https://doi.org/10.1080/23789689.2017.1417348. URL: https://doi.org/10.1080/23789689.2017.1417348.

[18] Masoud Mohammadi et al. “Integration of TLS-derived Bridge Information Modeling (BrIM) with a Decision Support System (DSS) for digital twinning and asset management of bridge infrastructures”. In: *Computers in Industry* 147 (2023), p. 103881. ISSN: 0166-3615. DOI: https://doi.org/10.1016/j.compind.2023.103881. URL: https://www.sciencedirect.com/science/article/pii/S0166361523000313.

[19] Arup. *Ove Arup Key Speech*. 2025. URL: https://www.arup.com/perspectives/publications/speeches-and-lectures/section/ove-arup-key-speech (visited on 04/30/2024).

[20] P. Koteš and J. Vičan. “Reliability Levels for Existing Bridges Evaluation According to Eurocodes”. In: *Procedia Engineering* 40 (2012). STEEL STRUCTURES AND BRIDGES 2012 - 23rd Czech and Slovak International Conference, pp. 211–216. ISSN: 1877-7058. DOI: https://doi.org/10.1016/j.proeng.2012.07.082. URL: https://www.sciencedirect.com/science/article/pii/S187770581202468X.

[21] B. Eisinger et al. “Comparative Life Cycle Analyses of Regular and Irregular Maintenance of Bridges with Different Support Systems and Construction Technologies”. In: *DOAJ (DOAJ: Directory Of Open Access Journals)* (2022). DOI: 10.3303/cet2294095. URL: https://doi.org/10.3303/cet2294095.

[22] T. B. Balogun et al. “Sustainability of bridge maintenance”. In: *Proceedings Of The Institution Of Civil Engineers. Bridge Engineering/Proceedings Of ICE. Bridge Engineering* 172.1 (2019), pp. 54–64. DOI: 10.1680/jbren.15.00027. URL: https://doi.org/10.1680/jbren.15.00027.

[23] R. de Vries, R.D.J.M. Steenbergen, and J. Maljaars. “Annual reliability requirements for bridges and viaducts”. In: *TNO, Department of Structural Reliability* (2024). Also affiliated with Ghent University and Eindhoven University of Technology.

[24] Ishwarya Srikanth and Madasamy Arockiasamy. “Deterioration models for prediction of remaining useful life of timber and concrete bridges: A review”. In: *Journal of Traffic and Transportation Engineering (English Edition)* 7.2 (2020), pp. 152–173. ISSN: 2095-7564. DOI: https://doi.org/10.1016/j.jtte.2019.09.005. URL: https://www.sciencedirect.com/science/article/pii/S2095756419301084.

[25] Ravi Kumar et al. “Remaining Service Life Asset Measure, Phase 1”. In: (2018). Retrieved from the University Digital Conservancy. URL: https://hdl.handle.net/11299/200642.

[26] Michael P. Enright and Dan M. Frangopol. “Condition Prediction of Deteriorating Concrete Bridges Using Bayesian Updating”. In: *Journal of Structural Engineering* 125.10 (1999). Downloaded from ASCE Library, pp. 1118–1125. ISSN: 0733-9445. DOI: 10.1061/(ASCE)0733-9445(1999)125:10(1118).

[27] Xueping Fan, Heng Zhou, and Yuefei Liu. “Time-Dependent Reliability Analysis of RC Bridges Considering Shrinkage, Creep, Resistance Degradation, and Vehicle Load Flows”. In: *Advances in Civil Engineering* 2023 (2023), pp. 1–14. DOI: 10.1155/2023/5111719.

[28] Carlos M. Chang and Abid Hossain. *Life-Cycle Cost Analysis of Ultra High-Performance Concrete (UHPC) in Retrofitting Techniques for ABC Projects*. Final Report ABC-UTC-2016-C4-FIU03. Miami, FL: Florida International University, Department of Civil and Environmental Engineering, 2022, p. 112. URL: https://www.abc-utc.fiu.edu.

[29] Abdoul S. Bah et al. “Assessing the condition state of a concrete bridge combining visual inspection and nonlinear deterioration model”. In: *Journal of Bridge Engineering* 27.5 (2022), pp. 149–164. DOI: 10.1080/15732479.2022.2081987. URL: https://doi.org/10.1080/15732479.2022.2081987.

[30] Bing Tu et al. “Time-variant reliability analysis of widened deteriorating prestressed concrete bridges considering shrinkage and creep”. In: *Engineering Structures* 153 (2017), pp. 1–16. ISSN: 0141-0296. DOI: https://doi.org/10.1016/j.engstruct.2017.09.060. URL: https://www.sciencedirect.com/science/article/pii/S0141029617322253.

[31] K. A. T. Vu and M. G. Stewart. “Structural reliability of concrete bridges including improved chloride-induced corrosion models”. In: *Structural Safety* 22 (2000), pp. 313–333. DOI: 10.1016/S0167-4730(00)00010-3.

[32] Wafa Nor El Houda Cherifi, Youcef Houmadi, and Omar Benali. “Probabilistic analysis for estimation of the initiation time of corrosion”. In: *Mathematical Modelling in Civil Engineering* 15.2 (2019), pp. 1–13. DOI: 10.2478/mmce-2019-0004. URL: https://www.sciendo.com/article/10.2478/mmce-2019-0004.

[33] D.V. Val and R.E. Melchers. “Reliability of Deteriorating RC Slab Bridges”. In: *Journal of Structural Engineering* 123 (1997), pp. 1638–164.

[34] Hadi Abbas et al. “Axial Compression Behavior of Wall-like Reinforced Concrete Columns Retrofitted Using Different FRP Schemes”. In: *Buildings* 13.1 (2022), p. 26. DOI: 10.3390/buildings13010026. URL: https://doi.org/10.3390/buildings13010026.

[35] Constantine Chalioris et al. “Repair of Heavily Damaged RC Beams Failing in Shear Using U-Shaped Mortar Jackets”. In: *Buildings* 9.9 (2019), p. 146. DOI: 10.3390/buildings9070146. URL: https://doi.org/10.3390/buildings9070146.

[36] Giuseppe Santarsiero and Angelo Masi. “Seismic Upgrading of RC Wide Beam–Column Joints Using Steel Jackets”. In: *Buildings* 10.10 (2020), p. 203. DOI: 10.3390/buildings1010203. URL: https://doi.org/10.3390/buildings1010203.

[37] Pengfei Men et al. “Bending behaviour of reinforced concrete T-beams damaged by overheight vehicle impact strengthened with ultra-high performance concrete (UHPC)”. In: *Case Studies in Construction Materials* 21 (2024), e03393. ISSN: 2214-5095. DOI: https://doi.org/10.1016/j.cscm.2024.e03393. URL: https://www.sciencedirect.com/science/article/pii/S2214509524005448.

[38] J. C. Walraven and C. R. Braam. *CIE3150/4160 Prestressed Concrete*. Prof.dr.ir.Dr.-Ing.h.c. J.C. Walraven, dr.ir.drs. C.R. Braam. 2019.

[39] Håkan Nordin. *Strengthening structures with externally prestressed tendons: Literature review*. Tech. rep. 2005:06. Department of Civil and Environmental Engineering, Division of Structural Engineering: Luleå University of Technology, 2005. ISRN: LTU-TR–05/06–SE.

[40] AbdulMuttalib I Said, Ali Hussein Ali Al-Ahmed, and AL-Fendawy Dhafer. “Strengthening Behavior of Reinforced Concrete T-Beams Using External Prestress Tendons”. In: *Applied Research Jornal* 2.11 (2016).

[41] Freyssinet. *Structural Strengthening with UHPFRC*. Accessed: 2024-12-08. 2024. URL: https://www.freyssinet.com/solution/repair/structural-strengthening/uhpfrc-2/.

[42] Christoph Czaderski, Moslem Shahverdi, and Julien Michels. “Iron based shape memory alloys as shear reinforcement for bridge girders”. In: *Construction and Building Materials* 274 (2021), p. 121793. ISSN: 0950-0618. DOI: https://doi.org/10.1016/j.conbuildmat.2020.121793. URL: https://www.sciencedirect.com/science/article/pii/S0950061820337971.

[43] Muhammad Arslan Yaqub, Stijn Matthys, and Christoph Czaderski. “Potential of Memory Steel Reinforcement for Shear Strengthening of Concrete Bridge Girders with I-Sections”. English. In: *IABSE Symposium Prague 2022: Challenges for Existing and Oncoming Structures*. Vol. 118. Prague, Czech Republic: International Association for Bridge and Structural Engineering (IABSE), 2022, pp. 1180–1187. ISBN: 978-3-85748-183-3. URL: http://doi.org/10.2749/prague.2022.1180.

[44] Antoni Cladera et al. “Shear strengthening of slender reinforced concrete T-shaped beams using iron-based shape memory alloy strips”. In: *Engineering Structures* 221 (2020), p. 111018. ISSN: 0141-0296. DOI: https://doi.org/10.1016/j.engstruct.2020.111018. URL: https://www.sciencedirect.com/science/article/pii/S0141029620305587.

[45] J. Michels and B. Schranz. “Iron-Based Shape Memory Alloys in Civil Engineering – From Early Developments to Market Implementation”. In: *Proceedings of the 6th International Conference on Smart Monitoring, Assessment and Rehabilitation of Civil Structures*. Ed. by X. L. Gu et al. Vol. 259. Lecture Notes in Civil Engineering. Singapore: Springer, 2024. DOI: 10.1007/978-981-99-3362-4_3.

[46] Ardalan Hosseini et al. “Development of prestressed unbonded and bonded CFRP strengthening solutions for tensile metallic members”. In: *Engineering Structures* 181 (2019), pp. 550–561. ISSN: 0141-0296. DOI: https://doi.org/10.1016/j.engstruct.2018.12.020. URL: https://www.sciencedirect.com/science/article/pii/S0141029618312926.

[47] Wen-Wei Wang et al. “Prestress Losses and Flexural Behavior of Reinforced Concrete Beams Strengthened with Posttensioned CFRP Sheets”. In: *Journal of Composites for Construction* 16.2 (2012), pp. 207–216. DOI: 10.1061/(ASCE)CC.1943-5614.0000255. eprint: https://ascelibrary.org/doi/pdf/10.1061/%28ASCE%29CC.1943-5614.0000255. URL: https://ascelibrary.org/doi/abs/10.1061/%28ASCE%29CC.1943-5614.0000255.

[48] Luke A. Bisby. “Fire Behaviour of Fibre-Reinforced Polymer (FRP) Reinforced or Confined Concrete”. PhD thesis. Kingston, ON, Canada: Queen’s University, 2003.

[49] TianQiao Liu et al. “Carbon emissions of durable FRP composite structures in civil engineering”. In: *Engineering Structures* 315 (2024), p. 118482. ISSN: 0141-0296. DOI: https://doi.org/10.1016/j.engstruct.2024.118482. URL: https://www.sciencedirect.com/science/article/pii/S0141029624010447.

[50] Nadine Stoiber, Mathias Hammerl, and Benjamin Kromoser. “Cradle-to-gate life cycle assessment of CFRP reinforcement for concrete structures: Calculation basis and exemplary application”. In: *Journal of Cleaner Production* 280 (2021), p. 124300. ISSN: 0959-6526. DOI: https://doi.org/10.1016/j.jclepro.2020.124300. URL: https://www.sciencedirect.com/science/article/pii/S0959652620343456.

[51] S. Chataigner et al. “Design and testing of an adhesively bonded CFRP strengthening system for steel structures”. In: *Engineering Structures* 177 (2018), pp. 556–565. ISSN: 0141-0296. DOI: https://doi.org/10.1016/j.engstruct.2018.10.004. URL: https://www.sciencedirect.com/science/article/pii/S0141029618304905.

[52] Duaa M. S. Hamza and Muhammad Jawad Kadhim. “Flexural strengthening of RC inverted t-beams by using CFRP strips”. In: *AIP Conference Proceedings* 3009.1 (2024), p. 030071. ISSN: 0094-243X. DOI: 10.1063/5.0193248. eprint: https://pubs.aip.org/aip/acp/article-pdf/doi/10.1063/5.0193248/19672311/030071_1_5.0193248.pdf. URL: https://doi.org/10.1063/5.0193248.

[53] Junaedi Utomo et al. “Experimental Investigation on the Failure Behavior of Carbon Fiber Reinforced Polymer (CFRP) Strengthened Reinforced Concrete T-beams”. In: *Civil Engineering Dimension* 23.2 (2021), pp. 115–122. DOI: 10.9744/ced.23.2.115-122. URL: https://ced.petra.ac.id/index.php/civ/article/view/23978.

[54] Mohammad Beramly et al. “Shear Strengthening and Rehabilitating of Reinforced Concrete T-Beams Using Externally Carbon Fiber Reinforced Polymer Sheets”. In: *Journal of Applied Engineering Science* 20.2 (2022), pp. 498–510. DOI: 10.5937/jaes0-34390. URL: https://doi.org/10.5937/jaes0-34390.

[55] Ayssar Al-Khafaji and Hani Salim. “Flexural Strengthening of RC Continuous T-Beams Using CFRP”. In: *Fibers* 8.6 (2020). ISSN: 2079-6439. DOI: 10.3390/fib8060041. URL: https://www.mdpi.com/2079-6439/8/6/41.

[56] K. Soudki and T. Alkhrdaji. “Guide for the Design and Construction of Externally Bonded FRP Systems for Strengthening Concrete Structures (ACI 440.2R-02)”. In: *Structures Congress 2005*. 2012, pp. 1–8. DOI: 10.1061/40753(171)159. eprint: https://ascelibrary.org/doi/pdf/10.1061/40753%28171%29159. URL: https://ascelibrary.org/doi/abs/10.1061/40753%28171%29159.

[57] W. Bae, A. Belarbi, and A. Brancaccio. “Shear Strengthening of Full-Scale RC T-Beams Using Externally Bonded CFRP Sheets”. In: *Proceedings of the First Middle East Conference on Smart Monitoring, Assessment and Rehabilitation of Civil Structures*. 2011.

[58] Mand Kamal Askar, Ali Falyeh Hassan, and Yaman S.S. Al-Kamaki. “Flexural and shear strengthening of reinforced concrete beams using FRP composites: A state of the art”. In: *Case Studies in Construction Materials* 17 (2022), e01189. ISSN: 2214-5095. DOI: https://doi.org/10.1016/j.cscm.2022.e01189. URL: https://www.sciencedirect.com/science/article/pii/S2214509522003217.

[59] Doo-Yeol Yoo and Young-Soo Yoon. “A Review on Structural Behavior, Design, and Application of Ultra-high-performance Fiber-Reinforced Concrete”. In: *International Journal of Concrete Structures and Materials* 10 (2016), pp. 125–142. DOI: 10.1007/s40069-016-0143-x. URL: https://doi.org/10.1007/s40069-016-0143-x.

[60] Eugen Brühwiler. “Structural UHPFRC to Enhance Bridges”. In: *Proceedings of the 2nd International Conference on UHPC Materials and Structures UHPC 2018*. UHPC 2018 - China 129. Fuzhou, China, 2018, pp. 140–158.

[61] Ben DuBose. “New Method for Repairing Damaged Concrete Bridge Girders”. In: *Materials Performance* (2019). URL: https://www.materialsperformance.com/articles/material-selection-design/2019/07/new-method-for-repairing-damaged-concrete-bridge-girders.

[62] Ashraf Hossain and Chih-Min Chang. “Life-Cycle Cost Analysis of Ultra High-Performance Concrete (UHPC) in Retrofitting Applications”. In: *International Interactive Symposium on Ultra-High Performance Concrete* 3.1 (2023), p. 82. DOI: 10.21838/uhpc.16694. URL: https://doi.org/10.21838/uhpc.16694.

[63] Mugahed Amran et al. “Sustainable development of eco-friendly ultra-high performance concrete (UHPC): Cost, carbon emission, and structural ductility”. In: *Construction and Building Materials* 398 (2023), p. 132477. ISSN: 0950-0618. DOI: https://doi.org/10.1016/j.conbuildmat.2023.132477. URL: https://www.sciencedirect.com/science/article/pii/S0950061823021931.

[64] Zachary B. Haber and Benjamin A. Graybeal. “Strengthening of Steel Through-Girder Bridges Using UHPC and Post-Tensioning”. In: *Journal of Bridge Engineering* 29.3 (2024), p. 04024004. DOI: 10.1061/JBENF2.BEENG-6272. eprint: https://ascelibrary.org/doi/pdf/10.1061/JBENF2.BEENG-6272. URL: https://ascelibrary.org/doi/abs/10.1061/JBENF2.BEENG-6272.

[65] Tongxu Liu and Jean-Philippe Charron. “Experimental Study on the Shear Behavior of UHPC-Strengthened Concrete T-Beams”. In: *Journal of Bridge Engineering* 28.9 (2023), p. 04023064. DOI: 10.1061/JBENF2.BEENG-6122. eprint: https://ascelibrary.org/doi/pdf/10.1061/JBENF2.BEENG-6122. URL: https://ascelibrary.org/doi/abs/10.1061/JBENF2.BEENG-6122.

[66] Yitao Huang et al. “Strengthening of concrete structures with ultra high performance fiber reinforced concrete (UHPFRC): A critical review”. In: *Construction and Building Materials* 336 (2022), p. 127398. ISSN: 0950-0618. DOI: https://doi.org/10.1016/j.conbuildmat.2022.127398. URL: https://www.sciencedirect.com/science/article/pii/S0950061822010753.

[67] Aijun Li et al. “Experimental study on flexural fatigue behavior of composite T-beams in ultra-high performance concrete reinforced and normal-strength concrete”. In: *International Journal of Fatigue* 167 (2023), p. 107330. ISSN: 0142-1123. DOI: https://doi.org/10.1016/j.ijfatigue.2022.107330. URL: https://www.sciencedirect.com/science/article/pii/S0142112322005801.

[68] World Commission on Environment and Development. *Our Common Future*. Oxford: Oxford University Press, 1987.

[69] Michael D. Lepech, Mette Geiker, and Henrik Stang. “Probabilistic design and management of environmentally sustainable repair and rehabilitation of reinforced concrete structures”. In: *Cement and Concrete Composites* 47 (2014). Special issue: Durability of concrete, pp. 19–31. ISSN: 0958-9465. DOI: https://doi.org/10.1016/j.cemconcomp.2013.10.009. URL: https://www.sciencedirect.com/science/article/pii/S0958946513001674.

[70] Tom B. J. Coenen et al. “Development of a bridge circularity assessment framework to promote resource efficiency in infrastructure projects”. In: *Journal of Industrial Ecology* 25.2 (2021), pp. 288–304. DOI: https://doi.org/10.1111/jiec.13102. eprint: https://onlinelibrary.wiley.com/doi/pdf/10.1111/jiec.13102. URL: https://onlinelibrary.wiley.com/doi/abs/10.1111/jiec.13102.

[71] Jianan Qi et al. “Shear Behavior of Externally Prestressed Concrete Beams with Draped Tendons”. In: *Aci Structural Journal* 113 (2016), pp. 677–688. DOI: 10.14359/51688746.

[72] Xin Wang et al. “Effectiveness of basalt FRP tendons for strengthening of RC beams through the external prestressing technique”. In: *Engineering Structures* 101 (2015), pp. 34–44. ISSN: 0141-0296. DOI: https://doi.org/10.1016/j.engstruct.2015.06.052. URL: https://www.sciencedirect.com/science/article/pii/S0141029615004289.

[73] Moslem Shahverdi et al. “Strengthening of RC beams by iron-based shape memory alloy bars embedded in a shotcrete layer”. In: *Engineering Structures* 117 (2016), pp. 263–273. ISSN: 0141-0296. DOI: https://doi.org/10.1016/j.engstruct.2016.03.023. URL: https://www.sciencedirect.com/science/article/pii/S0141029616300438.

[74] André Picard, Bruno Massicotte, and Eric Boucher. “Strengthening of reinforced concrete beams with composite materials: theoretical study”. In: *Composite Structures* 33.2 (1995), pp. 63–75. ISSN: 0263-8223. DOI: https://doi.org/10.1016/0263-8223(95)00106-9. URL: https://www.sciencedirect.com/science/article/pii/0263822395001069.

[75] Long Nguyen-Minh et al. “Flexural-strengthening efficiency of cfrp sheets for unbonded post-tensioned concrete T-beams”. In: *Engineering Structures* 166 (2018), pp. 1–15. ISSN: 0141-0296. DOI: https://doi.org/10.1016/j.engstruct.2018.03.065. URL: https://www.sciencedirect.com/science/article/pii/S0141029617336301.

[76] Hayder A. Rasheed and Shariq Pervaiz. “Closed form equations for FRP flexural strengthening design of RC beams”. In: *Composites Part B: Engineering* 34.6 (2003), pp. 539–550. ISSN: 1359-8368. DOI: https://doi.org/10.1016/S1359-8368(03)00047-7. URL: https://www.sciencedirect.com/science/article/pii/S1359836803000477.

[77] Sung-Gul Hong and Woo-Young Lim. “Strengthening of shear-dominant reinforced concrete beams with ultra-high-performance concrete jacketing”. In: *Construction and Building Materials* 365 (2023), p. 130043. ISSN: 0950-0618. DOI: https://doi.org/10.1016/j.conbuildmat.2022.130043. URL: https://www.sciencedirect.com/science/article/pii/S0950061822036996.

[78] Constantin E. Chalioris, Adamantis G. Zapris, and Chris G. Karayannis. “U-Jacketing Applications of Fiber-Reinforced Polymers in Reinforced Concrete T-Beams Against Shear—Tests and Design”. In: *Laboratory of Reinforced Concrete and Seismic Design of Structures, Department of Civil Engineering, Democritus University of Thrace* (2020).

[79] Tongxu Liu and Jean-Philippe Charron. “Shear strengthening of concrete T-beams with lateral layers of UHPC”. In: *MATEC Web of Conferences* 364 (2022). DOI: 10.1051/matecconf/202236404016.

[80] Afshin Firouzi, Amirmasoud Taki, and Saeed Mohammadzadeh. “Time-dependent reliability analysis of RC beams shear and flexural strengthened with CFRP subjected to harsh environmental deteriorations”. In: *Engineering Structures* 196 (2019), p. 109326. ISSN: 0141-0296. DOI: https://doi.org/10.1016/j.engstruct.2019.109326. URL: https://www.sciencedirect.com/science/article/pii/S0141029619301610.

[81] André Orcesi Dr. “Investigating Partial Factors for the Assessment of Existing Reinforced Concrete Bridges”. In: *Structural Engineering International* 34.1 (2024), pp. 55–70. DOI: 10.1080/10168664.2023.2204115. eprint: https://doi.org/10.1080/10168664.2023.2204115. URL: https://doi.org/10.1080/10168664.2023.2204115.

[82] *InfoBridge: Data Dashboard*. URL: https://infobridge.fhwa.dot.gov/Data/Dashboard (visited on 01/08/2025).

[83] Lihe Zhang, Dudley R. Morgan, and Sidney Mindess. *Modelling the Service Life of Structures with Cast-in-Place Concrete vs. Wet-Mix Shotcrete*. https://shotcrete.org/wp-content/uploads/2024/08/Modelling-the-Service-Life-of-Structures-with-Cast-in-Place-Concrete-vs-Wet-Mix-Shotcrete.pdf. Accessed: 2024-12-28. 2024.

[84] Khaled Galal. "FRP Retrofitting of Bridges". In: *The Second International Conference on Infrastructure Management, Assessment and Rehabilitation Techniques (ICIMART'16)* (Mar. 8–10, 2016). Keynote Lecture. Department of Building, Civil and Environmental Engineering, Concordia University. Montréal, Québec, Canada, 2016.

[85] Ji-Hua Zhu et al. "Recycling of carbon fibre reinforced plastics by electrically driven heterogeneous catalytic degradation of epoxy resin". In: *Green Chemistry* 21.7 (2019), pp. 1635–1647. DOI: 10.1039/C8GC03672A. URL: https://pubs.rsc.org/en/content/articlehtml/2019/gc/c8gc03672a.

[86] World Steel Association. *Water Management in the Steel Industry*. Position Paper. Accessed: 2024-12-31. 2015. URL: https://www.seaisi.org/storage/adminUploads/newsroom/NR_5cff0409b0ae6.pdf.

[87] K. M. Fiorotti, G. F. Silva, A. F. G. Calenzani, et al. "Optimization of Steel Beams with External Pretension, Considering the Environmental and Financial Impact". In: *Asian Journal of Civil Engineering* 24 (2023), pp. 3331–3344. DOI: 10.1007/s42107-023-00715-0. URL: https://doi.org/10.1007/s42107-023-00715-0.

[88] Min-Jae Lee and Kangmin Lee. "Performance and Cost Effectiveness Analysis of the Active External Post Tensioning System". In: *Unknown (Please replace with the journal name)* (2024). Associate Professors, Department of Civil and Architectural Engineering. URL: Please%20replace%20with%20the%20correct%20URL%20if%20available.

[89] Sami Sbahieh, Gordon Mckay, and Sami G. Al-Ghamdi. "A comparative life cycle assessment of fiber-reinforced polymers as a sustainable reinforcement option in concrete beams". In: *Frontiers in Built Environment* 9 (2023). ISSN: 2297-3362. DOI: 10.3389/fbuil.2023.1194121. URL: https://www.frontiersin.org/journals/built-environment/articles/10.3389/fbuil.2023.1194121.

[90] C. Davis et al. "Reuse, remanufacturing and recycling in the steel sector". In: *Philosophical Transactions of the Royal Society A* 382 (2024), p. 20230244. DOI: 10.1098/rsta.2023.0244. URL: https://doi.org/10.1098/rsta.2023.0244.

[91] Philip Nuss and Matthew J. Eckelman. "Life Cycle Assessment of Metals: A Scientific Synthesis". In: *PLOS ONE* 9.7 (2014), pp. 1–1. DOI: 10.1371/journal.pone.0101298. URL: https://doi.org/10.1371/journal.pone.0101298.

[92] re-fer AG. *Shape Memory Alloy Solutions for Construction*. Accessed: 2024-12-31. 2024. URL: https://www.re-fer.eu/en/downloads/.

[93] Sika Netherlands. *Sika CarboDur® M - Structurele Versterking en Verlijming*. Accessed: 2024-12-31. 2024. URL: https://nld.sika.com/nl/bouw/afbouw-renovatie/structurele-versterking-enverlijming/sika-carbodur-m.html.

[94] Tadesse G. Wakjira, Adeeb A. Kutty, and M. Shahria Alam. "A novel framework for developing environmentally sustainable and cost-effective ultra-high-performance concrete (UHPC) using advanced machine learning and multi-objective optimization techniques". In: *Construction and Building Materials* 416 (2024), p. 135114. ISSN: 0950-0618. DOI: https://doi.org/10.1016/j.conbuildmat.2024.135114. URL: https://www.sciencedirect.com/science/article/pii/S0950061824002551.

[95] T. Stengel and P. Schießl. "Life cycle assessment (LCA) of ultra high performance concrete (UHPC) structures". In: *Eco-efficient construction and building materials*. Ed. by Francisco Pacheco-Torgal et al. Woodhead Publishing Limited, 2014. Chap. 22, pp. 528–555. DOI: 10.1533/9780857097729.3.528.

[96] Gregor Kravanja, Ahmad Rizwan Mumtaz, and Stojan Kravanja. "A Comprehensive Review of the Advances, Manufacturing, Properties, Innovations, Environmental Impact and Applications of Ultra-High-Performance Concrete (UHPC)". In: *Buildings* 14.2 (2024). ISSN: 2075-5309. DOI: 10.3390/buildings14020382. URL: https://www.mdpi.com/2075-5309/14/2/382.

[97] Jonathan Kerr et al. “Comparative Analysis of the Global Warming Potential (GWP) of Structural Stone, Concrete and Steel Construction Materials”. In: *Sustainability* 14.15 (2022). ISSN: 2071-1050. DOI: 10.3390/su14159019. URL: https://www.mdpi.com/2071-1050/14/15/9019.

[98] Sunita Kumari and Rinku Walia. “A Comparative Study of Life Cycle Assessment for Sustainable Concrete Mixes”. In: *Journal of Materials and Engineering Structures* 9 (2022).

[99] ACC Limited. *Environmental Product Declaration of 1m³ of Average Ready Mix Concrete*. ISO 14025:2006, EN 15804:2012, EPD Registration Number: S-P-01116, Validity Date: 2023-12-19, Geographical Scope: India. 2018. URL: https://www.epd-system.com.

[100] R.W. Saaty. “The analytic hierarchy process—what it is and how it is used”. In: *Mathematical Modelling* 9.3 (1987), pp. 161–176. ISSN: 0270-0255. DOI: https://doi.org/10.1016/0270-0255(87)90473-8. URL: https://www.sciencedirect.com/science/article/pii/0270025587904738.

[101] Philip Griffith. *AHPy: A Python Library for Analytical Hierarchy Process (AHP)*. Version 0.5.3, accessed on [current date]. 2019. URL: https://github.com/PhilipGriffith/AHPy.

[102] Movares Nederland B.V. *Quick Scan T-liggers 2017: 44D 117 Hamersbrug Wilhelminakanaal, Berekening Basisvariant en Alternatief*. Tech. rep. Utrecht, 2017.

A

Appendix | Bi-linear stress-strain diagram

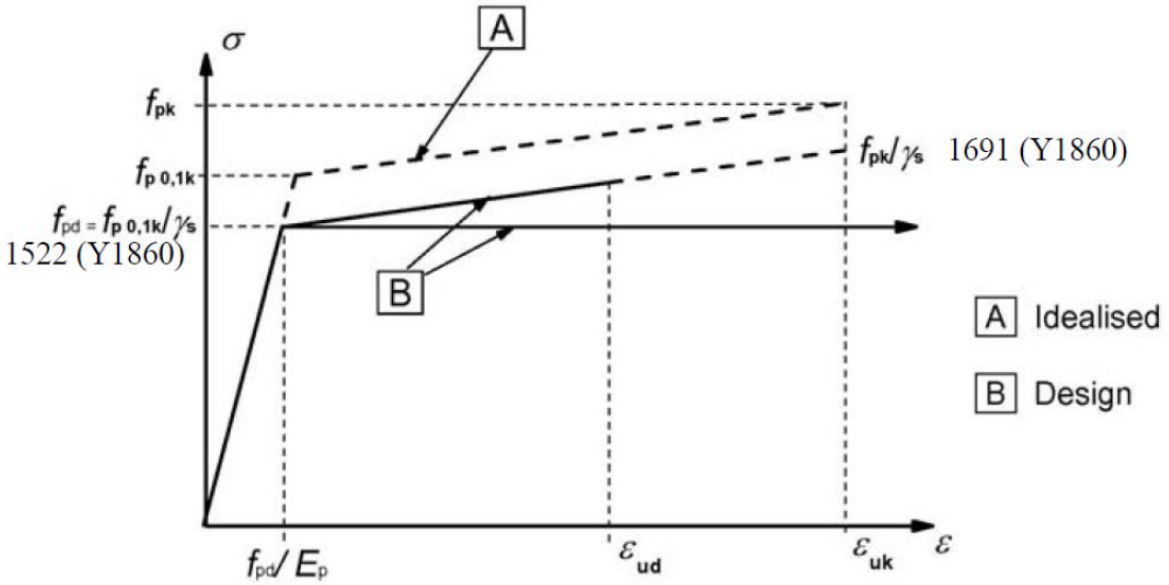

Figure A.1: Bi-linear stress strain diagram [38].

B

Appendix | LCA stages

The analysis considers the following Life Cycle Assessment (LCA) stages.

1. **Production Stage (A1, A3)**
    - **A1**: Raw material extraction
    - **A3**: Manufacturing
2. **Construction Stage (A5)**
    - **A5**: Construction and installation process
3. **Use Stage (B1, B2, B3, B4, B5)**
    - **B1**: Use
    - **B2**: Maintenance
    - **B3**: Repair
    - **B4**: Replacement
    - **B5**: Refurbishment
4. **End-of-Life Stage (C1, C2)**
    - **C1**: Deconstruction/demolition
    - **C2**: Transport
5. **Circular Economy (D)**
    - Reuse
    - Recovery
    - Recycling potential

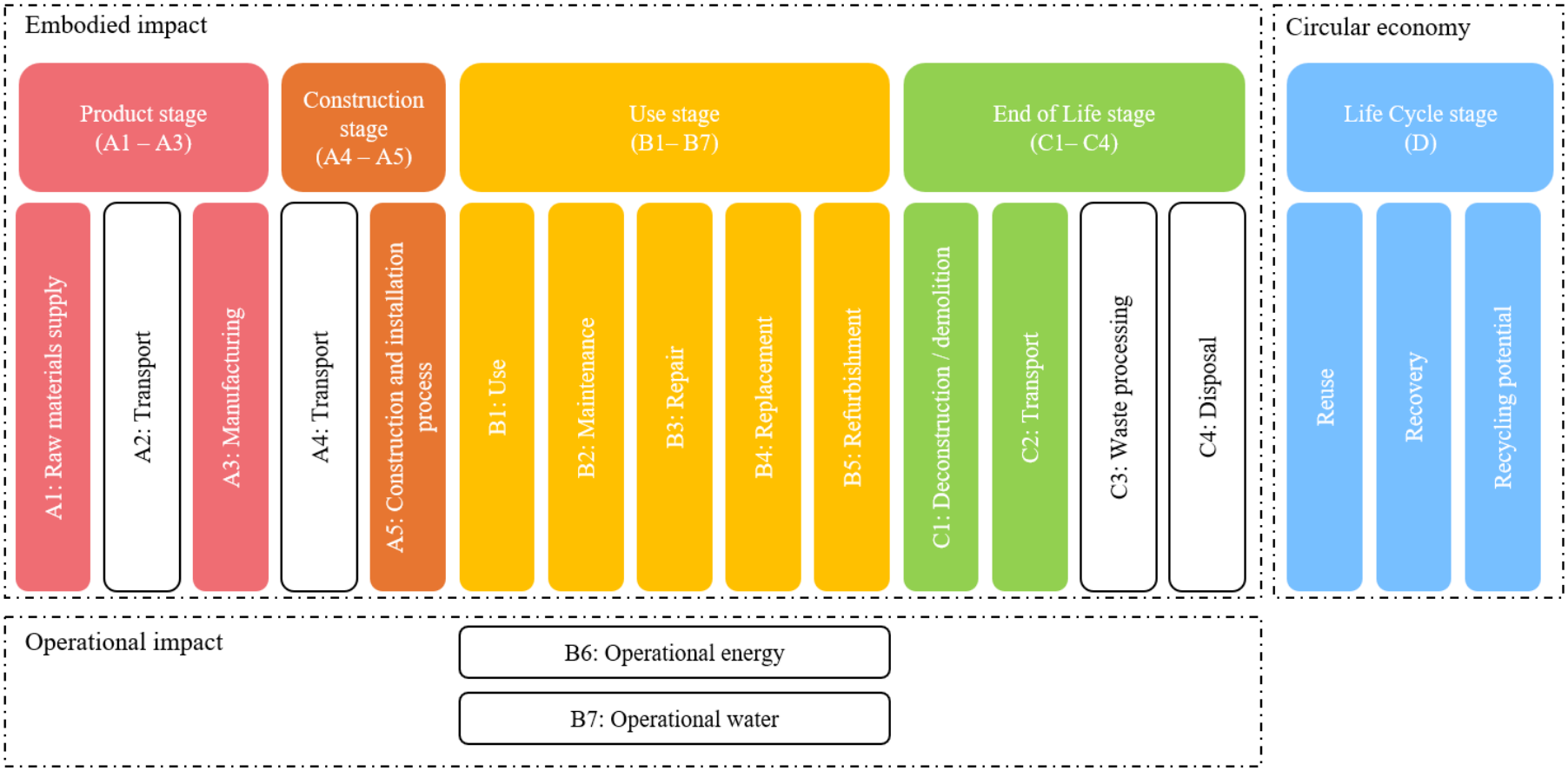

Figure B.1: Considered LCA stages.

C

Appendix | Script fragments

C.1. Input parameters

Listing C.1: Input parameters.

```
gamma_c = 1.5           # Partial safety factor, concrete
gamma_s = 1.15          # Partial safety factor, steel
k_1 = 0.15              # Shear resistance coefficient, concrete
alpha_1 = 1.0           # Shear resistance coefficient, prestressing

# Beam dimensions
w_flange = 800          # Flange width of T-beam in mm
t_flange = 350          # Flange thickness of T-beam in mm
h_web = 800             # Height of web in mm
t_web = 350             # Thickness of web in mm
d = t_flange + h_web    # Total effective depth in mm
L = 12500               # Length of the beam in mm

# Reinforcement steel B500
n_rebars_sl = 5         # Number of rebars, longitudinal direction
n_rebars_sw = 2         # Number of rebars, width direction
rebar_diameter_sl = 12  # Diameter of rebars in mm. longitudinal direction
rebar_diameter_sw = 10  # Diameter of rebars in mm, width direction
d_s = 1100              # Distance from top fiber to reinforcement in mm
t_cov = d - d_s         # Thicknes of concrete cover
s = 200                 # Spacing between vertical stirrups in mm
f_y = 500               # Yield strength of reinforcing steel in MPa
f_yd = f_y / gamma_s    # Design value of yield strength in MPa
E_s = 200 * 1e3         # Modulus of elasticity for steel in MPa

# Area of reinforcement in mm², longitudinal direction
A_sl = n_rebars_sl * 0.25 * np.pi * rebar_diameter_sl**2
# Area of reinforcement in mm², width direction
A_sw = n_rebars_sw * 0.25 * np.pi * (rebar_diameter_sw)**2

# Prestressing steel Y1860S7 properties
duct_diameter = 120         # Diameter of metal duct for tendons in mm
d_p = 1050                  # Distance to prestressing steel centroid in mm
R = L**2 / (8 * (d - d_p))  # Radius of curvature of beam in mm
A_p = 2000                  # Area of prestressing steel in mm²
e_support = 0               # Eccentricity at supports in mm
e_midspan = 700             # Eccentricity at midspan in mm
f_pd = 1522                 # Design stress for prestressing steel in MPa
f_pk = 1860                 # Characteristic strength of prestressing steel in MPa
```

```
f_pk2 = 1691                # Characteristic strength of prestressing steel in MPa
E_p = 195 * 1e3             # Modulus of elasticity for prestressing steel in MPa
sigma_p_inf = 1522          # Long-term prestress in MPa
mu = sigma_p_inf / f_pk     # Relaxation coefficient

# Strain parameters for concrete
epsilon_c3 = 1.75 * 1e-3    # Strain related to maximum compressive stress
epsilon_cu = 3.5 * 1e-3     # Ultimate compressive strain

# Strain parameters for prestressing steel
epsilon_p_inf = sigma_p_inf / E_p  # Long-term strain
epsilon_uk = 35 * 1e-3             # Ultimate strain

# Concrete C50/60 properties
f_ck = 50              # Characteristic compressive strength (cylinder) in MPa
f_cd = f_ck / gamma_c  # Design compressive strength in MPa
f_ctd = 1.90           # Design tensile strength of concrete in MPa
f_ctm = 4.07           # Mean tensile strength of concrete in MPa
f_ctk_005 = 2.9        # 5% fractile tensile strength of concrete in MPa
E_c = 34 * 1e3         # Modulus of elasticity for concrete in MPa

# Stirrup angle
alpha = 90                          # Stirrup angle in degrees
alpha_rad = np.radians(alpha)
cot_alpha = 1/ np.tan(alpha_rad)

# Crack angle
theta = 21.5                        # Crack angle in degrees
theta_rad = np.radians(theta)
tan_theta = np.tan(theta_rad)
cot_theta = 1 / np.tan(theta_rad)

# Densities
rho_c = 2350                        # Unit weight of concrete in kg/m³
rho_steel = 7750                    # Unit weight of steel in kg/m³
rho_1000 = 1.5                      # Reinforcement percentile
```

C.2. Section properties

C.2.1. Tendon profile

```
def tendon_profile(x, e_0, L):
    """
    Calculate the eccentricity of a parabolic tendon profile at a given point x.

    Parameters:
    x: Distance from the left support [m].
    e_0: Maximum eccentricity at the midpoint [m].
    L: Total length of the beam [m].

    Returns:
    float: Eccentricity at point x [m].
    """
    return -4 * e_0 / L**2 * x * (x - L)
```

C.2.2. Concrete area

Listing C.2: Concrete area.

```python
def calculate_area(w_flange, t_flange, h_web, t_web):
    """
    Parameters:
    w_flange: Width of the flange in mm
    t_flange: Thickness of the flange in mm
    h_web: Height of the web in mm
    t_web: Thickness of the web in mm

    Returns:
    A_flange: Area of the flange in mm²
    A_web: Area of the web in mm²
    A_c: Total concrete area in mm²
    """
    # Calculate area of the flange
    A_flange = w_flange * t_flange

    # Calculate area of the web
    A_web = t_web * h_web

    # Total area
    A_c = A_flange + A_web

    return A_flange, A_web, A_c
```

C.2.3. Centroidal axis

```python
def calculate_centroidal_axis(A_web, A_flange, t_flange, h_web):
    """
    Parameters:
    A_web: Area of the web in mm²
    A_flange: Area of the flange in mm²
    t_flange: Thickness of the flange in mm
    h_web: Height of the web in mm

    Returns:
    centroid: Distance from top fiber to centroidal axis in mm
    """
    # Height of the centroid of the web (located at half the height of the web)
    y_flange = t_flange / 2
    y_web = t_flange + h_web / 2

    A_c = A_web + A_flange

    centroid = (A_web * y_web + A_flange * y_flange) / A_c

    return centroid
```

C.2.4. Moment of inertia

Listing C.3: Moment of inertia.

```python
def calculate_moment_of_inertia(w_flange, t_flange, h_web, t_web, centroid_y, A_flange, A_web):
    """
    Parameters:
    w_flange: Width of the flange in mm
    t_flange: Thickness of the flange in mm
    h_web: Height of the web in mm
    t_web: Thickness of the web in mm
    centroid_y: Distance from top fiber to centroidal axis in mm
    A_flange: Area of the flange in mm²
    A_web: Area of the web in mm²

    Returns:
    I_c: Moment of inertia of the beam in  mm
    """
    # Moment of inertia of the flange about its own centroid
    I_flange = (w_flange * t_flange**3) / 12

    # Moment of inertia of the web about its own centroid
    I_web = (t_web * h_web**3) / 12

    # Distances from the section centroids to the total centroid (parallel axis theorem)
    y_flange = t_flange / 2
    d_f = abs(y_flange - centroid_y)  # Distance from flange centroid to total centroid

    y_web = t_flange + h_web / 2
    d_w = abs(y_web - centroid_y)  # Distance from web centroid to total centroid

    # Applying the parallel axis theorem
    I_c = I_flange + A_flange * d_f**2 + I_web + A_web * d_w**2

    return d_w, d_f, I_c
```

C.2.5. Section modulus

Listing C.4: Section modulus.

```python
def calculate_section_properties(t_flange, h_web, centroid_y, d_w, d_f, I_c, A_flange, A_web):
    """
    Parameters:
    t_flange: Thickness of the flange in mm
    h_web: Height of the web in mm
    centroid_y: Distance from top fiber to centroidal axis in mm
    d_w: Distance from web centroid to total centroid in mm
    d_f: Distance from flange centroid to total centroid in mm
    I_c: Moment of inertia of the beam in  mm
    A_flange: Area of the flange in mm²
    A_web: Area of the web in mm²

    Returns:
    S_bottom: Section modulus for the bottom fiber in mm³
    S_top: Section modulus for the top fiber in mm³
    S_c: Section modulus for the cross-section in mm³
    """
    # Distance from neutral axis to top fiber
    d_top = centroid_y

    # Distance from neutral axis to bottom fiber
    d_bottom = (h_web + t_flange) - centroid_y

    # Section modulus for the bottom fiber
    S_bottom = I_c / d_bottom

    # Section modulus for the top fiber
    S_top = I_c / d_top

    # Section modulus for the concrete
    S_c = A_flange * d_f + A_web * d_w

    return S_bottom, S_top, S_c
```

C.3. Load Model 1

Listing C.5: Load Model 1.

```
# Load Model 1
carriageway_width = 13.75   # Example carriageway width in meters
tandem_axle_spacing = 1.2   # Given value
influence_length = L / 1000 # Influence length of bridge element
reference_period = 10       # Required strengthening extension in years

def determine_notional_lanes(carriageway_width):
    if carriageway_width < 5.4:
        # Case 1: One lane of width 3 m
        n1 = 1
        w1 = 3.0
        remaining_area = carriageway_width - 3.0
    elif 5.4 <= carriageway_width < 6.0:
        # Case 2: Two lanes of equal width
        n1 = 2
        w1 = carriageway_width / 2
        remaining_area = 0
    else:
        # Case 3: More than two lanes, use integer division by 3 to find the
            number of lanes
        n1 = math.floor(carriageway_width / 3.0)
        w1 = 3.0  # Width of each notional lane
        remaining_area = carriageway_width - 3 * n1

    return n1, w1, remaining_area

n1 = determine_notional_lanes(carriageway_width)[0]
w1 = determine_notional_lanes(carriageway_width)[1]
remaining_area = determine_notional_lanes(carriageway_width)[2]

class LoadModel1:
    def __init__(self, n1, adjustment_factors=None, tandem_axle_spacing=None,
        lane_width=None):
        """
        Initialises the Load Model 1 with the given adjustment factors.
        If no adjustment factors are provided, defaults are set to 1.

        Parameters:
        n1: Number of lanes.
        adjustment_factors: Adjustment factors for tandem and UDL systems.
        tandem_axle_spacing: Spacing between axles in the tandem system.
        lane_width: Width of each lane.
        """
        self.n1 = n1  # Number of notional lanes

        # Default adjustment factors
        if adjustment_factors is None:
            adjustment_factors = {
                'alphaQ1': 1.0,  # Lane 1 Tandem
                'alphaQ2': 1.0,  # Lane 2 Tandem
                'alphaQ3': 1.0,  # Lane 3 Tandem
                'alphaQr': 1.0,  # Remaining Area Tandem
                'alphaq1': 1.15,  # Lane 1 UDL
                'alphaq2': 1.40,  # Lane 2 UDL
                'alphaq3': 1.40,  # Lane 3 UDL
                'alphaqr': 1.40,  # Remaining Area UDL
            }

```

```
        # Set adjustment factors
        self.alphaQ1 = adjustment_factors['alphaQ1']
        self.alphaQ2 = adjustment_factors['alphaQ2']
        self.alphaQ3 = adjustment_factors['alphaQ3']
        self.alphaQr = adjustment_factors['alphaQr']
        self.alphaq1 = adjustment_factors['alphaq1']
        self.alphaq2 = adjustment_factors['alphaq2']
        self.alphaq3 = adjustment_factors['alphaq3']
        self.alphaqr = adjustment_factors['alphaqr']

        # Characteristic values for each lane
        self.Qk_values = {'Lane 1': 300, 'Lane 2': 200, 'Lane 3': 100}
        self.qk_values = {'Lane 1': 9.0, 'Lane 2': 2.5, 'Lane 3': 2.5, 'Remaining
            area': 2.5}

        # Tandem axle spacing and lane width
        self.tandem_axle_spacing = tandem_axle_spacing
        self.lane_width = lane_width

    def tandem_load(self, lane):
        """Calculates the tandem load for a given lane based on the alphaQ
            adjustment factor and Qk values."""
        if lane == 1:
            return self.alphaQ1 * self.Qk_values['Lane 1']
        elif lane == 2:
            return self.alphaQ2 * self.Qk_values['Lane 2']
        elif lane == 3:
            return self.alphaQ3 * self.Qk_values['Lane 3']
        else:
            return 0  # Other lanes have no tandem load

    def udl_load(self, lane):
        """Calculates the uniformly distributed load for a given lane or remaining
             area based on the alphaq adjustment factor and qk values."""
        if lane == 1:
            return self.alphaq1 * self.qk_values['Lane 1'] * self.lane_width
        elif lane == 2:
            return self.alphaq2 * self.qk_values['Lane 2'] * self.lane_width
        elif lane == 3:
            return self.alphaq3 * self.qk_values['Lane 3'] * self.lane_width
        else:
            return self.qk_values['Remaining area'] * self.lane_width  # Handling
                for remaining area

    def total_tandem_load(self, lane):
        """Calculates the total tandem load for both axles in the tandem system
            for the given lane."""
        return self.tandem_load(lane)  # This already accounts for two axles

    def get_loads(self):
        """Returns a dictionary with tandem and UDL loads for all lanes and the
            remaining area."""
        loads = {}
        for lane in range(1, self.n1 + 1):
            loads[f'Lane {lane}'] = {
                'Tandem Load (Total)': self.total_tandem_load(lane),
                'UDL Load (Total)': self.udl_load(lane)
            }

        # Add remaining area if applicable
        if self.n1 < 3:
```

```
            loads['Remaining Area'] = {
                'Tandem Load (Total)': self.total_tandem_load('Remaining area'),
                'UDL Load (Total)': self.udl_load('Remaining area')
            }

        return loads

# Example usage
adjustment_factors = None  # Or provide specific adjustment factors if needed

load_model = LoadModel1(n1, adjustment_factors, tandem_axle_spacing=1.2,
    lane_width=w1)
loads = load_model.get_loads()

# Extract the highest lane load
def extract_highest_lane_load(loads):
    highest_tandem_load = max(
        ((lane, values['Tandem Load (Total)']) for lane, values in loads.items()),
        key=lambda x: x[1]
    )
    highest_udl_load = max(
        ((lane, values['UDL Load (Total)']) for lane, values in loads.items()),
        key=lambda x: x[1]
    )

    return {
        "Highest Tandem Load": {"Lane": highest_tandem_load[0], "Load":
            highest_tandem_load[1]},
        "Highest UDL Load": {"Lane": highest_udl_load[0], "Load": highest_udl_load
            [1]}
    }

# Call the function
highest_loads = extract_highest_lane_load(loads)

# Print results
TL = highest_loads['Highest Tandem Load']['Load']
UDL = highest_loads['Highest UDL Load']['Load']
```

C.4. Load combinations

Listing C.6: Load combinations.

```
# Input parameters
Gk = [G_k, 1500]                # List of permanent loads (G_k,j)
P_m_inf = sigma_p_inf * A_p     # Prestressing force in N
Pk = P_m_inf / R                # Prestressing force in N given by parabolic curve
Qk = [UDL, 1520, 560]           # Variable actions, wind and snow

# Load factors considering renovation
gamma_Ga = 1.30                 # Load factor for permanent load, characteristic
gamma_Gb = 1.15                 # Load factor for permanent load, frequent
gamma_P = 1.30                  # Load factor for prestressing

gamma_Q = [1.60, 1.50, 1.50]    # Load factors for variable actions
Psi_0 = [0.7, 0.5, 0.5]         # Combination factors for quasi-permanent loads
Psi_1 = [0.5, 0.3, 0.3]         # Combination factors for frequent loads
Psi_2 = [0.3, 0.2, 0.2]         # Combination factors for rare loads

ksi = 0.9                       # Reduction factor for prestressing force loss

# Ultimate Limit State (ULS)
# Function for the characteristic value combination
def characteristic_ULS(Gk, Pk, Qk, gamma_G, gamma_P, gamma_Q, Psi_0):
    """
    Calculate the ultimate limit state based on Equation 6.10a.

    Parameters:
    Gk : list : List of permanent loads (G_k,j)
    Qk : list : List of other variable actions (Q_k,i)
    gamma_G : list : List of load factors for permanent loads (gamma_G,j)
    gamma_Q : list : List of load factors for variable actions (gamma_Q,i)
    Psi_0 : list : Combination factors (Psi_0,i) for equation 6.10a

    Returns:
    float : The calculated ultimate limit state for equation 6.10a
    """

    ultimate_limit_state_6_10a = sum([gamma_Ga * Gk[j] for j in range(len(Gk))]) \
                        - gamma_P * Pk \
                        + gamma_Q[0] * Psi_0[0] * Qk[0] \
                        + sum([gamma_Q[i] * Psi_0[i] * Qk[i] for i in range(1, len
                            (Qk))])

    return ultimate_limit_state_6_10a

# Function for the frequent value combination
def frequent_ULS(Gk, Pk, Qk, gamma_Gb, gamma_P, gamma_Q, Psi_1, Psi_2):
    """
    Calculate the ultimate limit state based on Equation 6.10b.

    Parameters:
    Gk : List of permanent loads (G_k,j)
    Qk : List of other variable actions (Q_k,i)
    gamma_G : List of load factors for permanent loads (gamma_G,j)
    gamma_Q : List of load factors for variable actions (gamma_Q,i)
    Psi_1 : Combination factors (Psi_1,i) for equation 6.10b
    Psi_2 : Combination factors (Psi_2,i) for equation 6.10b
    ksi : Reduction factor for unfavorable permanent actions

    Returns:
```

```
    float : The calculated ultimate limit state for equation 6.10b
    """

    ultimate_limit_state_6_10b = sum([gamma_Gb * Gk[j] for j in range(len(Gk))]) \
                        - gamma_P * Pk \
                        + gamma_Q[0] * Psi_1[0] * Qk[0] \
                        + sum([gamma_Q[i] * Psi_2[i] * Qk[i] for i in range(1, len
                            (Qk))])

    return ultimate_limit_state_6_10b

# Calculate ULS combinations
uls_6_10a = characteristic_ULS(Gk, Pk, Qk, gamma_Ga, gamma_P, gamma_Q, Psi_0)
uls_6_10b = frequent_ULS(Gk, Pk, Qk, gamma_Gb, gamma_P, gamma_Q, Psi_1, Psi_2)
print(uls_6_10a, uls_6_10b)

# Determine the highest combination, gives distributed load
q_Ed_ULS = max(uls_6_10a, uls_6_10b)
```

C.5. Reduction factors for reference period

Listing C.7: Reduction factors for reference period.

```
#Reduction for reference period below 100 years
reference_y_data = {
    "Reference time y": [100, 50, 30, 15, 1, 0.08],
    "20": [1.00, 0.99, 0.99, 0.98, 0.95, 0.91],
    "50": [1.00, 0.99, 0.99, 0.98, 0.94, 0.91],
    "100": [1.00, 0.99, 0.98, 0.96, 0.89, 0.81],
    "200": [1.00, 0.99, 0.97, 0.96, 0.88, 0.81]}

# Creating a DataFrame
df_reference_period = pd.DataFrame(reference_y_data)

# Define the function to find the closest intervals for length and reference time
def find_closest_intervals(length, ref_time, df):
    length_cols = df.columns[1:]  # The span length columns
    ref_times = df['Reference time y'].tolist()  # The reference times

    # Find the two closest lengths
    length_vals = [float(col) for col in length_cols]
    closest_lengths = sorted(length_vals, key=lambda x: abs(x - length))[:2]

    # Find the two closest reference times
    closest_ref_times = sorted(ref_times, key=lambda x: abs(x - ref_time))[:2]

    return closest_lengths, closest_ref_times

# Define the function to extract the four  -factors
def extract_psi_factors(length, ref_time, df):
    closest_lengths, closest_ref_times = find_closest_intervals(length, ref_time,
        df)

    psi_factors = []
    for ref in closest_ref_times:
        row = df[df['Reference time y'] == ref]
        for length in closest_lengths:
            psi_factors.append(row[str(int(length))].values[0])

    return psi_factors

# Define the bilinear interpolation function
def bilinear_interpolation(x, y, x1, x2, y1, y2, Q11, Q12, Q21, Q22):
    return (Q11 * (x2 - x) * (y2 - y) +
            Q21 * (x - x1) * (y2 - y) +
            Q12 * (x2 - x) * (y - y1) +
            Q22 * (x - x1) * (y - y1)) / ((x2 - x1) * (y2 - y1))

# Extract the closest lengths, reference times, and  -factors
closest_lengths, closest_ref_times = find_closest_intervals(length, ref_time,
    df_reference_period)
psi_factors = extract_psi_factors(length, ref_time, df_reference_period)

# Set the known coordinates and perform the bilinear interpolation
x1, x2 = closest_lengths
y1, y2 = closest_ref_times
Q11, Q12, Q21, Q22 = psi_factors

# Perform the bilinear interpolation
interpolated_value = bilinear_interpolation(length, ref_time, x1, x2, y1, y2, Q11,
     Q12, Q21, Q22)
```

C.6. Trend reduction for year 2060

Listing C.8: Trend reduction for year 2060.

```
#Trendreduction for year 2060
trend_reduction_data = {
    'Invloedslengte [m]': ['0', '20', '50', '75', '100', '150', '  200'],
    '2010': [1.00, 0.89, 0.82, 0.78, 0.76, 0.75, 0.75],
    '2020': [1.00, 0.91, 0.86, 0.83, 0.81, 0.80, 0.80],
    '2030': [1.00, 0.93, 0.88, 0.87, 0.85, 0.85, 0.85],
    '2040': [1.00, 0.96, 0.91, 0.90, 0.90, 0.90, 0.90],
    '2050': [1.00, 0.98, 0.95, 0.95, 0.95, 0.95, 0.95],
    '2060': [1.00, 1.00, 1.00, 1.00, 1.00, 1.00, 1.00]}

# Creating a DataFrame
df_trend = pd.DataFrame(trend_reduction_data)

# Convert 'Invloedslengte [m]' to numeric, except for  ' 200' which we will treat as 200
df_trend['Invloedslengte [m]'] = pd.to_numeric(df_trend['Invloedslengte [m]'].replace('  200', 200))

# Define a new function to extract the closest values for length and year
def find_closest_intervals_trend(length, year, df):
    length_vals = df['Invloedslengte [m]'].tolist()
    year_vals = df.columns[1:].astype(int).tolist()

    # Find the two closest lengths
    closest_lengths = sorted(length_vals, key=lambda x: abs(x - length))[:2]

    # Find the two closest years
    closest_years = sorted(year_vals, key=lambda x: abs(x - year))[:2]

    return closest_lengths, closest_years

# Define a function to extract the four trend factors
def extract_trend_factors(length, year, df):
    closest_lengths, closest_years = find_closest_intervals_trend(length, year, df)

    trend_factors = []
    for yr in closest_years:
        row = df[str(yr)]
        for length in closest_lengths:
            trend_factors.append(row[df['Invloedslengte [m]'] == length].values[0])

    return trend_factors

# Define the bilinear interpolation function
def bilinear_interpolation(x, y, x1, x2, y1, y2, Q11, Q12, Q21, Q22):
    return (Q11 * (x2 - x) * (y2 - y) +
            Q21 * (x - x1) * (y2 - y) +
            Q12 * (x2 - x) * (y - y1) +
            Q22 * (x - x1) * (y - y1)) / ((x2 - x1) * (y2 - y1))

# Get the current year
current_year = datetime.now().year

# Calculate the target year
target_year_trend = current_year + ref_time

```

```
# Ensure the target year does not exceed the maximum year in the dataframe
target_year_trend = min(target_year_trend, max([int(col) for col in df_trend.
    columns[1:]]))

# Extract the closest lengths and years
closest_lengths_trend, closest_years_trend = find_closest_intervals_trend(length,
    target_year_trend, df_trend)

# Extract the trend factors for the closest intervals
trend_factors = extract_trend_factors(length, target_year_trend, df_trend)

# Perform bilinear interpolation using the extracted factors
x1, x2 = closest_lengths_trend
y1, y2 = closest_years_trend
Q11, Q12, Q21, Q22 = trend_factors

# Perform the bilinear interpolation
interpolated_trend_value = bilinear_interpolation(length, target_year_trend, x1,
    x2, y1, y2, Q11, Q12, Q21, Q22)

# Combined interpolation value
combined_interpolated_reduction_value = interpolated_value *
    interpolated_trend_value

q_Ed = combined_interpolated_reduction_value * q_Ed_ULS
```

C.7. Shear resistance

C.7.1. Shear resistance without reinforcement

Listing C.9: Shear resistance without reinforcement.

```python
def calculate_V_Rd_c_I(t_web, duct_diameter, f_ctk_005, gamma_c, P_m_inf, A_c, alpha_1, I_c, S_c):
    """
    Parameters:
    b_w: Width of the cross-section at the centroidal axis in mm
    duct_diameter: Diameter of the duct in mm
    f_ctk_005: 5% Fractile strength of the conrete in MPa
    P_m_inf: Long-term prestressing force in N
    alpha_1: Factor for prestressing and concrete interaction
    I_c: Moment of inertia of the beam in  mm
    S_c: Section modulus of the beam in mm³

    Returns: Shear resistance in Region I, uncracked in bending.
    """
    b_w = t_web
    if duct_diameter > t_web / 8:
        b_w = b_w - 0.5 * duct_diameter
    else:
        b_w = b_w
    f_ctd = f_ctk_005 / gamma_c
    N_Ed = P_m_inf
    sigma_cp = N_Ed / A_c

    V_Rd_c = (I_c * b_w / S_c) * math.sqrt(f_ctd**2 + alpha_1 * sigma_cp * f_ctd)

    return V_Rd_c

def calculate_V_Rd_c_II(t_web, d_p, f_ck, A_p, P_m_inf, A_c, f_cd, gamma_c, k_1):
    """
    Parameters:
    d_p: Distance from top fiber to prestressing centroid in mm
    A_p: Cross section area of the prestressing in mm²
    P_m_inf: Long-term prestressing force in N
    f_cd: Compressive concrete strength in MPa
    gamma_c: Safety factor for the concrete
    k1: Empirical factor for shear resistance

    Returns: Shear resistance in Region II.
    """
    b_w = t_web
    C_Rd_c = 0.18 / gamma_c
    k = min(1 + math.sqrt(0.2 / d_p), 2.0)
    rho_l = A_p / (b_w * d_p)

    # Calculate sigma_cp and limit it to 0.2 * f_cd
    N_Ed = P_m_inf
    sigma_cp = N_Ed / A_c
    sigma_cp = min(sigma_cp, 0.2 * f_cd)

    term_1 = (100 * rho_l * f_ck)**(1/3)
    V_Rd_c = (C_Rd_c * k * term_1 + k_1 * sigma_cp) * b_w * d_p

    # Ensure V_Rd_c is greater than or equal to the minimum shear resistance
    v_min = 0.035 * k**(3/2) * math.sqrt(f_ck)
    V_Rd_c_min = (v_min + k_1 * sigma_cp) * b_w * d_p

    return max(V_Rd_c, V_Rd_c_min)
```

C.7.2. Shear resistance with shear reinforcement

Listing C.10: Shear resistance with shear reinforcement.

```python
def calculate_V_Rd_s(t_web, d_s, tan_theta, cot_theta, A_sw, s, f_yd, P_m_inf, A_c, f_cd, f_ck):
    """
    Parameters:
    d_s: Distance from top fiber to ordinary reinforcement in mm
    A_sw: Area of shear reinforcement in mm²
    s: Spacing of shear reinforcement in mm
    f_yd: Design yield strength of steel in MPa
    P_m_inf: Long-term prestressing force in N
    f_cd: Design compressive strength of concrete in MPa

    Returns: Shear resistance using shear reinforcement
    """
    b_w = t_web
    z = 0.9 * d_s

    # Calculate V_Rd,s
    V_Rd_s = (A_sw / s) * f_yd * z * cot_theta

    sigma_cp = P_m_inf / A_c / 1000

    # Calculate alpha_cw based on sigma_cp
    if 0 < sigma_cp < 0.25 * f_cd:
        alpha_cw = 1 + sigma_cp / f_cd
    elif 0.25 * f_cd <= sigma_cp < 0.5 * f_cd:
        alpha_cw = 1.25
    else:  # 0.5 * f_cd <= sigma_cp < 1.0 * f_cd
        alpha_cw = 2.5 * (1 + sigma_cp / f_cd)

    # Calculate v_1 based on f_ck
    if f_ck <= 60:
        v_1 = 0.6
    else:
        v_1 = 0.6 * (1 - f_ck / 250)

    # Calculate the denominator
    denominator = tan_theta + cot_theta

    # Calculate V_Rd,max
    V_Rd_max = (alpha_cw * b_w * z * v_1 * f_cd * 10**3) / denominator

    # Return the minimum shear resistance
    return min(V_Rd_s, V_Rd_max)
```

C.8. Bending moment resistance

Listing C.11: Bending moment resistance.

```
# Height of the compressive zone is estimated
# Assumed the reinforcement steel is yielding and prestressing steel is in plastic state
def calculate_xu(f_ck, f_pd, f_yd, A_p, A_sl, w_flange, f_cd):
    if f_ck <= 50:
        eta = 1.0
        lambda_ = 0.8
    elif 50 < f_ck <= 90:
        eta = 1.0 - (f_ck - 50) / 200
        lambda_ = 0.8 - (f_ck - 50) / 400
    else:
        raise ValueError("f_ck must be less than or equal to 90 MPa.")

    x_u = (A_p * f_pd + A_sl * f_yd) / (0.75 * w_flange * f_cd)
    return eta, lambda_, x_u

# Check whetther the height of the compressive zone meets the requirements
def calculate_f(f_pk, sigma_p_inf, A_p, f_yd, A_sl):
    # Calculate f using the provided formula
    f = ((f_pk / 1.1 - sigma_p_inf) * A_p + f_yd * A_sl) / (A_p + A_sl)
    return f

def check_compressive_zone_height(f, x_u, d, f_ck):
    if f_ck <= 50:
        condition = x_u <= d * (1 - f / (500 + f))
        return condition
    else:
        raise ValueError("f_ck must be less than or equal to 50 N/mm².")

def calculate_MRd(x_u, f_cd, t_flange, w_flange, f_yd, A_sl, d_s, centroid_y, A_p, sigma_p_inf, d_p, P_m_inf,
                  epsilon_cu, f_pd, E_p, epsilon_uk, f_pk2, tolerance=100, max_iterations=999):

    iteration = 0
    sigma_c_flange = 0  # Initialize for safety
    previous_x_u = x_u  # Store the initial value of x_u

    while iteration < max_iterations:
        # Calculate strains
        epsilon_s = epsilon_cu * (d_s / x_u - 1)
        epsilon_p = epsilon_s + sigma_p_inf / E_p

        # Calculate prestressing steel stress
        sigma_pu = f_pd + (epsilon_p - (f_pd / E_p)) / (epsilon_uk - (f_pd / E_p)) * (f_pk2 - f_pd)

        # Calculate N (total force from reinforcement and prestressing)
        N_s = A_sl * f_yd
        delta_N_p = A_p * (sigma_pu - sigma_p_inf)
        N = N_s + delta_N_p

        # Compression flange
        if x_u <= t_flange:
            N_c = w_flange * x_u * f_cd
        else:
            epsilon_c_flange = - epsilon_cu * (x_u - t_flange) / x_u
            sigma_c_flange = epsilon_c_flange * E_c
```

```
            N_flange = w_flange * t_flange * f_cd
            N_web = 0.5 * (x_u - t_flange) * (w_flange + t_web) * sigma_c_flange
            N_c = N_flange + N_web

        # Check convergence based on relative difference
        relative_difference = abs((x_u - previous_x_u) / previous_x_u)
        if relative_difference < 0.01:  # If relative difference < 1%
            x_u = (x_u + previous_x_u) / 2  # Take the average of the two
            break

        # Check convergence based on force balance
        if abs(N + P_m_inf - N_c) < tolerance:
            break

        # Update x_u
        previous_x_u = x_u
        if N + P_m_inf > N_c:
            x_u *= 0.99  # Smaller step for reduction
        else:
            x_u *= 1.01  # Smaller step for increase

        iteration += 1

        # Safeguard against non-physical values
        if x_u <= 0 or x_u > (t_flange + d_s):
            raise ValueError(f"x_u out of physical limits: {x_u:.2f}")

    if iteration == max_iterations:
        raise ValueError("Maximum iterations reached without convergence for x_u."
            )

    # First term: compressive force in the flange
    term1 = 0.75 * w_flange * x_u * f_cd * (centroid_y - 0.39 * x_u)

    # Second term: compressive force in the web (triangular distribution)
    term2 = 0.5 * (x_u - t_flange) * (w_flange - t_web) * sigma_c_flange * (
        centroid_y - t_flange - (x_u - t_flange) / 3)

    # Third term: tensile force in reinforcing steel
    term3 = A_sl * f_yd * (d_s - centroid_y)

    # Fourth term: tensile force in prestressing steel
    term4 = A_p * (sigma_pu - sigma_p_inf) * (d_p - centroid_y)

    # Total bending moment resistance
    M_Rd = term1 - term2 + term3 + term4

    return M_Rd
```

C.9. Corrosion

Listing C.12: Corrosion of the reinforcement.

```python
def calculate_initiation_time(t_cov, Cth, Cs, Dc):
    t_ini = t_cov**2 / (4 * Dc) * 1 / (erfinv(1 - Cth / Cs))**2
    return t_ini

def calculate_i_corr(t, w_c, t_cov, t_ini):
    if t <= t_ini:
        return 0  # Corrosion does not start before t_ini
    term1 = 37.5 * (1 - w_c)**(-1.64)
    term2 = (t - t_ini)**0.29
    i_corr = 0.85 * term1 / t_cov * term2
    return i_corr

def calculate_p_t(R, i_corr, t, t_ini):
    if t <= t_ini:
        return 0
    p_t = 0.0116 * (t - t_ini) * i_corr * R
    return p_t # Radius of the pit in reinforcement

def calculate_remaining_area(d_0, p_t):
    if p_t == 0:
        A_r = 0.25 * np.pi * d_0**2

    elif p_t <= (math.sqrt(2) / 2) * d_0:
        a = 2 * p_t * math.sqrt(1 - (p_t / d_0) ** 2)
        theta_1 = 2 * math.asin(a / d_0)
        theta_2 = 2 * math.asin(a / (2 * p_t))

        A1 = 0.5 * (theta_1 * (d_0 / 2) ** 2 - a * (d_0 / 2 - (p_t ** 2) / d_0))
        A2 = 0.5 * (theta_2 * p_t ** 2 - a * (p_t ** 2) / d_0)

        A_r = (math.pi * (d_0 ** 2) / 4) - A1 - A2

    elif (math.sqrt(2) / 2) * d_0 < p_t < d_0:
        a = 2 * p_t * math.sqrt(1 - (p_t / d_0) ** 2)
        theta_1 = 2 * math.asin(a / d_0)
        theta_2 = 2 * math.asin(a / (2 * p_t))

        A1 = 0.5 * (theta_1 * (d_0 / 2) ** 2 - a * (d_0 / 2 - (p_t ** 2) / d_0))
        A2 = 0.5 * (theta_2 * p_t ** 2 - a * (p_t ** 2) / d_0)

        A_r = A1 - A2

    else:  # p_t == 0
        A_r = 0.25 * np.pi * d_0**2

    return A_r

def calculate_percentage_area_loss(A_0, A_r):
    A_loss = ((A_0 - A_r) / A_0)
    return A_loss

alpha_corr = 0.0054
def calculate_reinforcement_strength_loss(alpha_corr, percentage_area_loss, f_y):
    strength_loss = (1 - 100 * alpha_corr * percentage_area_loss) * f_y
    return strength_loss
```

C.10. Loss of pre-stress

Listing C.13: Loss of pre-stress.

```
def calculate_prestress_loss(t, rho_1000, mu, sigma_p):
    t_hours = t * 365 * 24  # Convert time to hours
    loss_factor = 6.6 * rho_1000 * np.exp(9.1 * mu) * ((t_hours / 1000) ** (0.75 *
        (1 - mu)))
    prestress_loss = sigma_p * loss_factor * 1e-6
    return prestress_loss
```

C.11. Reliability for shear

Listing C.14: Reliabilty for shear, FORM.

```
# Arrays to store results
beta1_values = []

for i in range(len(t1)):
    # Pitting corrosion and area loss
    i_corr = calculate_i_corr(t1[i], w_c, t_cov, t_ini)
    p_t = calculate_p_t(R, i_corr, t1[i], t_ini)
    A_sl = n_sl * calculate_remaining_area(d_s, p_t)
    percentage_area_loss = calculate_percentage_area_loss(A_sl_0, A_sl)
    f_y = calculate_reinforcement_strength_loss(alpha_corr, percentage_area_loss,
        f_y)

    # Loss of prestress
    P_m_inf = P_m_inf - calculate_prestress_loss(t1[i], rho_1000, mu, sigma_p) *
        A_p

    # Applied loads
    V_Ed_g = V_Ed_g_i * (1 + load_increase_rate * t1[i])
    V_Ed_q = V_Ed_q_i * (1 + load_increase_rate * t1[i])

    # Shear resistance
    V_Rd_c = shear_resistance_concrete(t_web, d, f_ck, A_sl, P_m_inf, A_c)
    V_Rd_s = shear_resistance_stirrups(A_sw, f_y, d, s, cot_theta)

    # Reliability calculation
    beta = calculate_reliability(
                                V_Ed_g, 0.10,
                                V_Ed_q, 0.18,
                                A_sl, 0.05,
                                f_ck, 0.10,
                                A_c, 0.10,
                                d_s, 0.15,
                                sigma_p, 0.12,
                                V_Rd_c, V_Rd_s, 0)

    if beta <= beta_threshold:
        break  # Exit loop once threshold is crossed

    EoL_1 = t1[i]

    beta1_values.append(beta)
```

C.12. Reliability for bending

Listing C.15: Reliabilty for bending, FORM.

```
# Arrays to store results
beta1_values = []

for i in range(len(t1)):
    # Pitting corrosion and area loss
    i_corr = calculate_i_corr(t1[i], w_c, t_cov, t_ini)
    p_t = calculate_p_t(R_penetration, i_corr, t1[i], t_ini)
    A_sl = n_rebars_sl * calculate_remaining_area(rebar_diameter_sl, p_t)

    percentage_area_loss = calculate_percentage_area_loss(A_sl_0, A_sl)
    f_y = calculate_reinforcement_strength_loss(alpha_corr, percentage_area_loss,
        f_y)

    # Loss of prestress
    sigma_pm_inf = sigma_p_m0 - calculate_prestress_loss(t1[i], rho_1000, mu,
        sigma_p_m0)
    P_m_inf = sigma_pm_inf * A_p

    # Applied loads
    M_Ed = M_Ed_i * (1 + load_increase_rate * t1[i])

    eta, lambda_, x_u = calculate_xu(f_ck, f_pd, f_y, A_p, A_sl, w_flange, f_ck)
    f = calculate_f(f_pk, sigma_p_m0, A_p, f_y, A_sl)

    # Bending resistance
    M_Rd = calculate_MRd(x_u, f_ck, t_flange, w_flange, f_y, A_sl, d_s, centroid_y
        , A_p, sigma_pm_inf, d_p, P_m_inf,
                    epsilon_cu, f_pd, E_p, epsilon_uk, f_pk2, tolerance=100,
                        max_iterations=999) * 1.75

    beta = calculate_reliability(
                                M_Ed, 0.10,
                                A_sl, 0.15,
                                A_p, 0.05,
                                sigma_pm_inf, 0.12,
                                M_Rd, 0)

    if beta <= beta_threshold:
        break  # Exit loop once threshold is crossed

    EoL_1 = t1[i]

    beta1_values.append(beta)
```

C.13. Deterioration of external prestressing

Listing C.16: Deterioration of external prestressing.

```
# Arrays to store results
beta2_EP_values = []

for i in range(len(t2)):
    # Pitting corrosion and area loss of External Prestressing
    i_corr_EP = calculate_i_corr(t2[i], w_c, t_cov, t_protection)
    p_t_EP = calculate_p_t_EP(R, i_corr_EP, t2[i], t_protection)
    A_p_EP = n_p_EP * calculate_remaining_area_EP(d_p_EP, p_t_EP)
    P_m_inf_EP = P_m_inf_EP - calculate_prestress_loss_EP(t2[i], rho_1000, mu,
        sigma_p_EP) * A_p_EP
    sigma_p_EP =  P_m_inf_EP / A_p_EP

    # Pitting corrosion and area loss
    i_corr = calculate_i_corr(t2[i]-20, w_c, t_cov, t_ini)
    p_t = calculate_p_t(R, i_corr, t2[i]-20, t_ini)
    A_sl = n_sl * calculate_remaining_area(d_s, p_t)
    percentage_area_loss = calculate_percentage_area_loss(A_sl_0, A_sl)
    f_y = calculate_reinforcement_strength_loss(alpha_corr, percentage_area_loss,
        f_y)

    # Loss of prestress
    P_m_inf = P_m_inf - calculate_prestress_loss(t1[i], rho_1000, mu, sigma_p) *
        A_p

    # Applied loads
    V_Ed_g = V_Ed_g_i * (1 + load_increase_rate * t2[i])
    V_Ed_q = V_Ed_q_i * (1 + load_increase_rate * t2[i])

    # Shear resistance
    V_Rd_c = shear_resistance_concrete(t_web, d, f_ck, A_sl, P_m_inf, A_c)
    V_Rd_s = shear_resistance_stirrups(A_sw, f_y, d, s, cot_theta)
    V_Rd_EP = V_s_arch(A_p_EP, sigma_p_EP, alpha_EP) + V_arch_shear(nu_EP, f_ck,
        t_web, d, a_EP, z)

    beta_EP = calculate_reliability(
                                V_Ed_g, 0.10,
                                V_Ed_q, 0.18,
                                A_sl, 0.05,
                                f_ck, 0.10,
                                A_c, 0.10,
                                d_s, 0.15,
                                sigma_p, 0.12,
                                V_Rd_c, V_Rd_s, V_Rd_EP)

    if beta_EP <= beta_threshold:
        break

    beta2_EP_values.append(beta_EP)
```

C.14. Deterioration of memory-steel

Listing C.17: Deterioration of memory-steel.

```
beta2_MS_values = []

for i in range(len(t2)):
    # Loss of prestress
    P_m_inf = P_m_inf - calculate_prestress_loss(t2[i], rho_1000, mu, sigma_p) *
        A_p

    # Applied loads
    V_Ed_g = V_Ed_g_i * (1 + load_increase_rate * t2[i])
    V_Ed_q = V_Ed_q_i * (1 + load_increase_rate * t2[i])

    # Shear resistance
    V_Rd_c = shear_resistance_concrete(t_web, d, f_ck, A_sl, P_m_inf, A_c)
    V_Rd_s = shear_resistance_stirrups(A_sw, f_y, d, s, cot_theta)
    V_Rd_MS = calculate_V_Rd_MS(sigma_p_inf_MS, loss_factor_MS, A_MS_sw, s_MS,
        z_MS, cot_theta_MS) - 0.0001 * (t2[i] - EoL_1)**6

    beta_MS = calculate_reliability(
                                V_Ed_g, 0.10,
                                V_Ed_q, 0.18,
                                A_sl, 0.05,
                                f_ck, 0.10,
                                A_c, 0.10,
                                d_s, 0.15,
                                sigma_p, 0.12,
                                V_Rd_c, V_Rd_s, V_Rd_MS)

    if beta_MS <= beta_threshold:
        break

    beta2_MS_values.append(beta_MS)
```

C.15. Deterioration of CFRP

Listing C.18: Deterioration of CFRP.

```
beta2_CFRP_values = []

for i in range(len(t2)):
    # Loss of prestress
    P_m_inf = P_m_inf - calculate_prestress_loss(t2[i], rho_1000, mu, sigma_p) *
        A_p

    # Applied loads
    V_Ed_g = V_Ed_g_i * (1 + load_increase_rate * t2[i])
    V_Ed_q = V_Ed_q_i * (1 + load_increase_rate * t2[i])

    l_eff = calculate_l_eff(E_CFRP, t_CFRP, f_ctm)
    f_fdd = calculate_f_fdd(gamma_fd, E_CFRP, f_ck, f_ctm, t_cFRP)
    f_fed = calculate_f_fed_u(f_fdd, l_eff, beta, d, h_web)

    V_Rd_c = shear_resistance_concrete(t_web, d, f_ck, A_sl, P_m_inf, A_c)
    V_Rd_s = shear_resistance_stirrups(A_sw, f_y, d, s, cot_theta)
    V_Rd_CFRP = calculate_V_Rd_FRP(gamma_Rd, d, f_fed, t_CFRP, cot_theta, cot_beta
        ) - 0.001 * (t2[i] - EoL_1 - 20)**5

    beta_CFRP = calculate_reliability(
                                V_Ed_g, 0.10,
                                V_Ed_q, 0.18,
                                A_sl, 0.05,
                                f_ck, 0.10,
                                A_c, 0.10,
                                d_s, 0.15,
                                sigma_p, 0.12,
                                V_Rd_c, V_Rd_s, V_Rd_CFRP)

    if beta_CFRP <= beta_threshold:
        break

    beta2_FRP_values.append(beta_CFRP)
```

C.16. Deterioration of UHPC

Listing C.19: Deterioration of UHPC.

```
beta2_UHPC_values = []

for i in range(len(t2)):
    # Loss of prestress
    P_m_inf = P_m_inf - calculate_prestress_loss(t2[i], rho_1000, mu, sigma_p) *
        A_p

    # Applied loads
    V_Ed_g = V_Ed_g_i * (1 + load_increase_rate * t2[i])
    V_Ed_q = V_Ed_q_i * (1 + load_increase_rate * t2[i])

    V_Rd_c = shear_resistance_concrete(t_web, d, f_ck, A_sl, P_m_inf, A_c)
    V_Rd_s = shear_resistance_stirrups(A_sw, f_y, d, s, cot_theta)
    V_Rd_UHPC = calculate_V_Rd_UHPC(f_c_UHPC, t_UHPC, h_web)

    beta_UHPC = calculate_reliability(
                                V_Ed_g, 0.10,
                                V_Ed_q, 0.18,
                                A_sl, 0.05,
                                f_ck, 0.10,
                                A_c, 0.10,
                                d_s, 0.15,
                                sigma_p, 0.12,
                                V_Rd_c, V_Rd_s, V_Rd_UHPC)

    if beta_UHPC <= beta_threshold:
        break

    beta2_UHPC_values.append(beta_UHPC)
```

D

Appendix | Structural decay functions

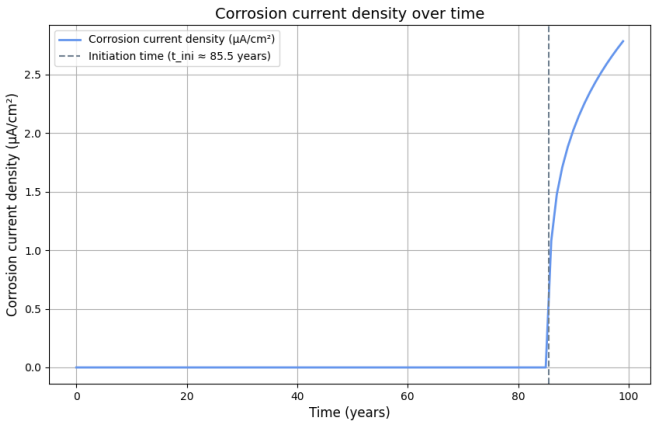

Figure D.1: Corrosion current density over time.

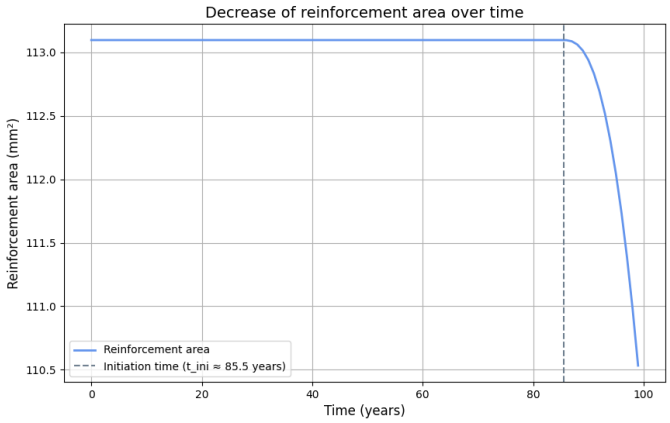

Figure D.2: Decrease of reinforcement area over time.

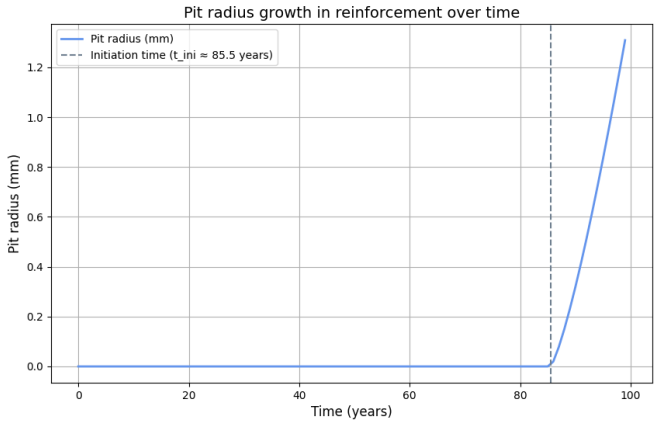

Figure D.4: Decrease of reinforcement area over time.

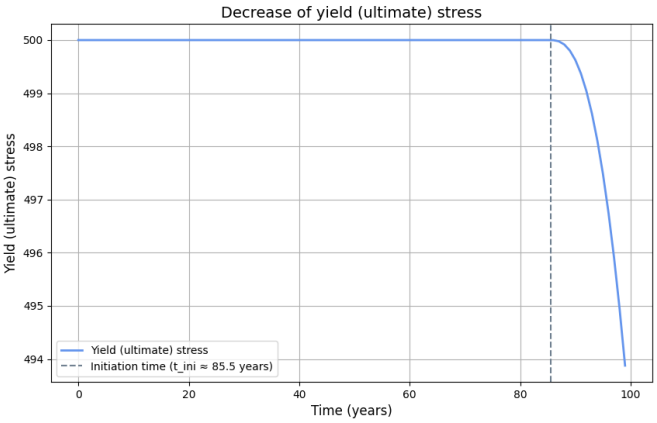

Figure D.3: Decrease of yield stress.

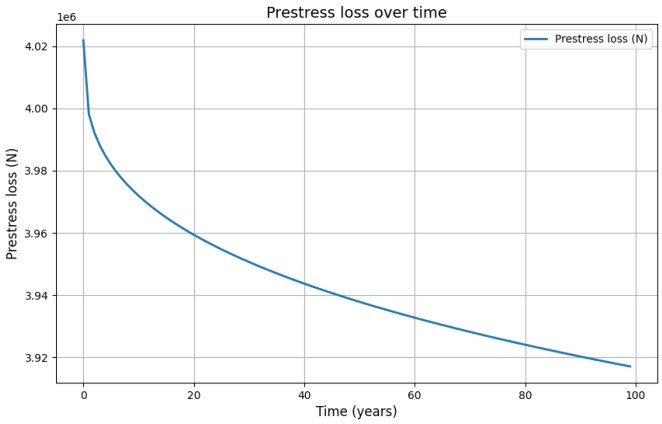

Figure D.5: Prestress loss over time.

E

Appendix | Case study Hamersbrug

E.1. Reinforcement lay-out

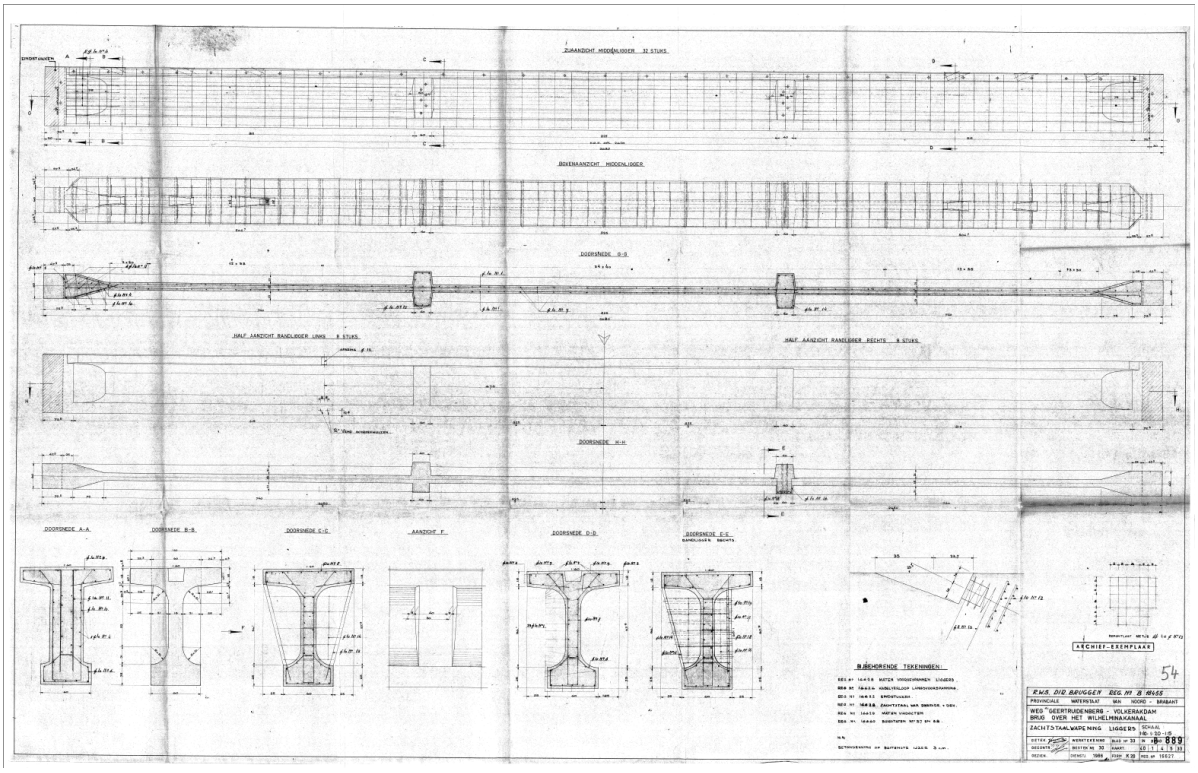

Figure E.1: Lay-out of reinforcement, Hamersbrug.

E.2. Prestressing lay-out

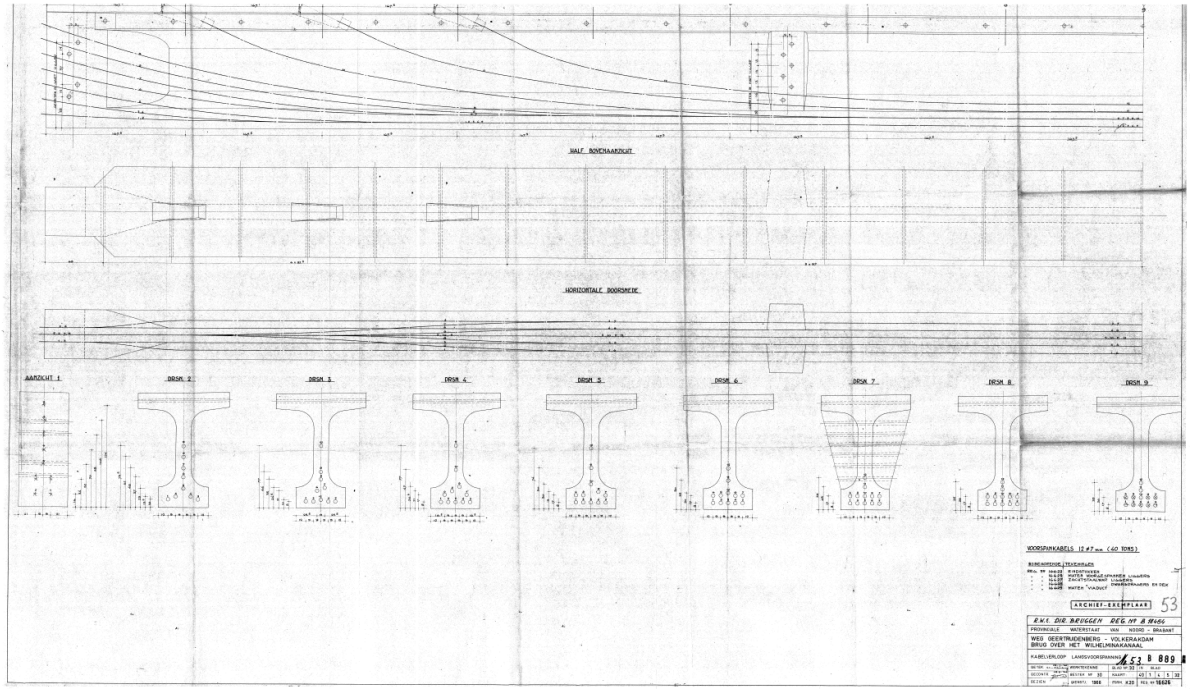

Figure E.2: Lay-out of prestressing cables, Hamersbrug.